INVESTIGATION INTO THE EFFECT OF GROOVE GEOMETRY ON GRINDING PERFORMANCE IN CREEP-FEED GRINDING

by

Alexandre Watters Riebel

Submitted in partial fulfilment of the requirements
for the degree of Master of Applied Science

at

Dalhousie University
Halifax, Nova Scotia
August 2019

TABLE OF CONTENTS

LIST OF TABLES

LIST OF FIGURES

ABSTRACT

This work investigates the effects of different groove depths and groove widths on grinding performance in creep-feed grinding using circumferentially grooved grinding wheels. Using two constant-width diamond tools having widths of 3.2 mm and 1.7 mm, respectively, square-shaped grooves were cut into the surface of two separate grinding wheels. The initial groove depths were determined from surface topography scans and subsequent groove depths were estimated by subtracting the dressing amounts. Force, power, and surface roughness data was acquired for each creep-feed grinding experiment. It was found that the grinding forces and spindle power decrease with respect to groove depth with diminishing reductions in forces and power as groove depth increases. For the experimental conditions of this research, it was found that there is little benefit in grooving deeper than ~400 µm. There was not a significant difference in results observed for the two different groove widths of 3.2 mm and 1.7 mm. Groove depth did not appear to influence workpiece surface roughness because the uncut chip thickness is not influenced by groove depth except at groove depths much shallower than those used in this research. The changes in grinding performance observed at different groove depths could then be attributed to changes in coolant flow. It was discovered that the coolant-induced force resulting from hydrodynamic pressure generation in the grinding zone decreased with respect to groove depth up until a certain groove depth. This groove depth was found to be ~400 µm which is consistent with the results observed for forces and power vs groove depth. The decrease in coolant-induced force signifies an increase in useful flow rate which is responsible for the improved grinding performance observed at different groove depths. However, the decrease in coolant-induced force could also signify a reduced ability of the coolant to fill the pores at the surface of the grinding wheel.

LIST OF SYMBOLS USED

α	-	Helix angle
a	-	Depth of cut
A_o	-	Total grinding wheel surface area
A_G	-	Total grooved area on grinding wheel surface
b_d	-	Dressing tool width
b_g	-	Groove width
d	-	Groove depth
d_s	-	Grinding wheel diameter
e_c	-	Specific energy
f_d	-	Dressing feed per revolution of the grinding wheel
F_n	-	Normal Force
F_t	-	Tangential Force
h_m	-	Maximum uncut chip thickness
L	-	Cutting edge spacing
l_c	-	Contact length
L_m	-	Length of surface roughness sample
η	-	Groove factor
N_g	-	Number of grooves
p	-	Groove pitch
P	-	Spindle power
R_a	-	Workpiece surface roughness
R_{MR}	-	Material removal rate
T	-	Grinding temperature
U_d	-	Dressing overlap ratio
v_s	-	Grinding wheel peripheral velocity
v_w	-	Workpiece feed rate
w	-	Workpiece width

ACKNOWLEDGEMENTS

To all the people that helped me along the way:

To my supervisors Robert Bauer and Andrew Warkentin, thank you so much for everything that you have done for me. Thank you for giving me this opportunity to further my education and to grow, not only as an engineer but as a person too. Your expertise, guidance, and availability are what made this work possible. I am sure that not all graduate students are as fortunate as I was to have supervisors that are so engaged and accessible, and for that I am very grateful.

To my family, especially my parents, if I could think of words to express how grateful I am for your everlasting love and support, I would put them here. But, I'm an engineer not a poet so I'll just say: thanks a bunch, I owe you one (or more…). Thanks to my beautiful girlfriend Kathleen for all your love and support along this journey. I am so happy to have you in my life.

To the techs, Jon, Peter, Angus, Mark, and Albert, thanks for being there when I needed to borrow a tool, when I needed to find a little extra elbow grease, or when I needed to brainstorm a solution to some problem I was having. I have learned a lot from you guys. Also, a big thanks to Craig and Frank from Pratt & Whitney for coming to our aid when the grinding machine was on the fritz.

To my grinding colleagues and friends, Akshay and Mokhtar, it has been a pleasure learning the grinding process with you, and from you. Thank you for being there when I wanted to talk about grinding, or when I needed assistance in the lab. You have both helped me immensely and I will always have fond memories of the time we spent at Dalhousie.

CHAPTER 1: INTRODUCTION

Since the time of the prehistoric man, abrasives have been used for shaping objects. Thousands of years ago, humans used sandstone, a natural abrasive, to sharpen stone tools and weapons [1]. Nowadays, one of the most important abrasive machining processes is grinding: a term used to describe machining by use of an abrasive wheel rotating on a shaft at very high speeds. Grinding is a major machining process that is used to produce accurate dimensions and very fine surface finishes in a part [2]. Another important application for grinding is the machining of materials which cannot be effectively shaped by other methods due to their high hardness or brittleness. Such materials include ceramics, glasses, and cemented carbides, to name a few. Nearly everything that is currently manufactured has been influenced by the grinding process in one way or another; either the manufactured item was ground directly, or it was very likely manufactured by use of machines whose parts were ground. Even now, after thousands of years of abrasive tool use, there is still much research needed to fully understand and optimize the grinding process [1].

1.1 MOTIVATION

Grinding is a very energy-inefficient machining process; nearly all the energy input in grinding is converted to heat due to friction. In many other machining processes, most of the heat generated is carried off in the discarded chips. However, in grinding, most of the heat remains in the ground surface which results in very high workpiece surface temperatures. These high temperatures can cause workpiece surface burns and cracks, undesirable softening of the workpiece surface, and residual stresses which may decrease the fatigue strength of the ground part [2]. Temperature increases are related to material removal rate, depth of cut, feed rate, and wheel speed, so there is a limited range of achievable values for these parameters before workpiece thermal damage will occur.

It has been shown that an effective way to reduce the risk of workpiece thermal damage is to use grooved grinding wheels [3], which are grinding wheels that have had parts of their surface area removed. This reduced surface area means that there are fewer

abrasive grains that come into contact with the workpiece which results in less friction between the wheel and the workpiece [3]. This reduced friction leads to decreased temperatures, forces, power consumption, and specific energy. It has also been shown that the grooves facilitate the flow of coolant into the grinding zone. Greater material removal rates, depths of cut, feed rates, and wheel speeds are thus achievable by using grooved grinding wheels before there is a risk of workpiece thermal damage [3].

There has been plenty of research demonstrating the advantages of grooved grinding wheels over conventional grinding wheels for a variety of different grinding wheels, grinding processes, and types of workpiece materials [4]. However, there has been very little research into how the geometry of the grooves affects grinding performance. This work provides an experimental investigation into the effects of groove depth and groove width on grinding performance in creep-feed grinding.

1.2 OBJECTIVES

The main objectives of this work are to:

- Determine whether it is possible to cut a groove into a grinding wheel whose width does not change relative to depth, allowing groove depth to be studied independently of groove width.
- Experimentally investigate the effect of various groove depths on grinding performance in creep-feed grinding experiments.
- Experimentally investigate the effect of different groove widths on grinding performance in creep-feed grinding experiments.
- Provide explanations on why different groove geometries produce different results.

1.3 THESIS OUTLINE

The content of this thesis is organized into seven chapters, excluding the introductory chapter. Chapter 2 presents the background information pertaining to the grinding process that is necessary to understand the results presented in this thesis. Chapter 3 is a review of the research publications and other relevant literature pertaining to groove geometry in grooved grinding wheels. Chapter 4 discusses the equipment and methods used throughout this research to perform the grinding experiments, groove the grinding wheels, and acquire data. Chapter 5 introduces a method of computing the groove geometry for a grinding wheel by analyzing surface topography scans. Chapter 6 presents the results obtained during creep-feed grinding experiments for wheels having different groove geometries. Chapter 6 also includes an analysis and discussion of the results obtained from the experiments. Chapter 7 presents an analysis on the reasons why different groove geometries yield different results. Finally, Chapter 8 presents the conclusions of this research.

CHAPTER 2: BACKGROUND

This chapter introduces the background material pertaining to grinding that is necessary to understand the content of this thesis. Grinding wheel composition is the first topic discussed in this chapter. Next, the important process parameters in grinding as well as a discussion of the creep-feed grinding process are presented. Then, an explanation of material removal in grinding is introduced, followed by an examination on the modes of abrasive grain interaction and temperatures in grinding. Finally, the chapter concludes with a discussion of the dressing process and workpiece surface roughness.

2.1   GRINDING WHEELS

The volume of a grinding wheel consists of abrasive grains, bonding material, and air gaps also known as "pores". Grinding wheels can be described by the following five parameters [2]:

- *Abrasive Material:* The abrasive material must be hard, wear resistant, tough, and friable. Friability is the tendency of an abrasive material to fracture when the cutting edge of the grain becomes dull, thus exposing a sharp new cutting edge. The most common abrasive materials used in grinding wheels nowadays, listed in order of increasing hardness, are aluminum oxide, silicon carbide, cubic boron nitride (CBN), and diamond [2].

- *Grain Size:* The size of the abrasive grains is important in determining the achievable surface finish and material removal rate. Small, or "fine", grain sizes produce better surface finishes, whereas large, or "coarse", grain sizes can achieve higher material removal rates. Grain sizes range from >1 mm (very coarse) to <20 μm (very fine) [2].

- *Bonding Material:* The bonding material determines the structural integrity of the wheel and thus must be able to withstand the high centrifugal forces, shock loads, and temperatures experienced during grinding. The bonding material must be able to hold the grains rigidly in place to achieve cutting while allowing worn grains to be pulled out so that new grains can be exposed. Bonding materials used in grinding wheels include vitrified, silicate, rubber, resinoid, shellac, and metallic [2].

- *Wheel Structure:* Wheel structure is a measure of the volume of pores in a grinding wheel and is measured on a scale that ranges from "open" to "dense". An open structure has fewer grains and more pores per unit volume than a dense structure, and vice versa. Dense structures have the advantage of providing better surface finish and dimensional control, whereas open structures should be used when clearance for chip flow is required [2].

- *Wheel Grade:* Wheel grade is a measure of the ability of a grinding wheel to retain abrasive grits during grinding and is dependent on the amount of bonding material present in the wheel structure. Wheel grade is measured on a scale that ranges from "soft" to "hard", where soft wheels easily lose grains and hard wheels retain their grains. Soft wheels are best suited for grinding hard materials at low material removal rates, whereas hard wheels are best suited for grinding soft materials at high material removal rates [2].

2.2 GRINDING PARAMETERS & CREEP-FEED GRINDING

There are three main user-controlled parameters in grinding: depth of cut, wheel speed, and feed rate. Depth of cut a is the vertical distance between the bottom dead center position of the grinding wheel and the height of the workpiece surface. It can simply be defined as the commanded vertical height of workpiece material being removed in a single pass of the grinding wheel. Wheel speed v_s is the grinding wheel peripheral velocity. Feed rate v_w is the speed at which the workpiece is fed into the grinding wheel. Two other important parameters in grinding are wheel diameter d_s and contact length l_c. Contact length is defined as the length of the area of contact between the wheel and the workpiece where the grinding action occurs and is determined by the wheel diameter and the depth of cut, as shown in Equation 2.1 [1]. As a result of the grinding action, forces are developed between the wheel and the workpiece. For straight surface grinding, the force vector can be separated into a tangential component F_t and a normal component F_n. The spindle power P is the product of the tangential force and wheel speed, as shown in Equation 2.2 [1]. The parameters discussed above are illustrated in Figure 2.1.

$$l_c = \sqrt{ad_s} \qquad\qquad (2.1)$$

$$P = F_t v_s \qquad\qquad (2.2)$$
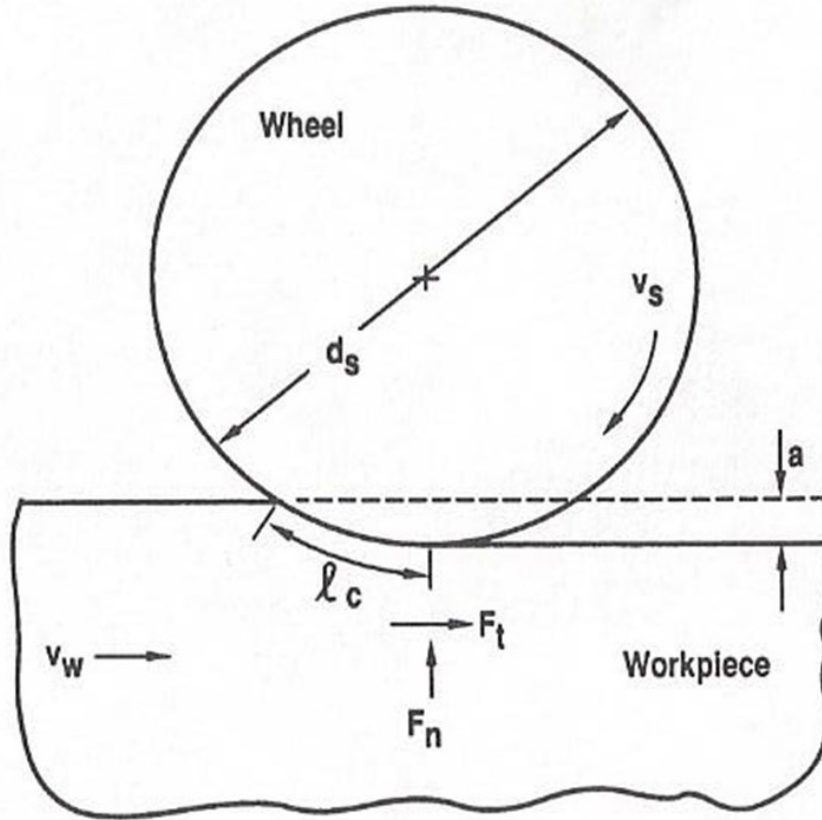
Figure 2.1: Illustration of grinding parameters. Adapted from [1].

The grinding operation used for this research is known as creep-feed grinding. Creep-feed grinding is characterized by very large depths of cut and very slow feed rates compared to conventional surface grinding which typically has low depths of cut and high feed rates. In creep-feed grinding, the workpiece material is typically removed in one very slow and very deep pass of the grinding wheel. In surface grinding, the workpiece material is removed in several quick and shallow reciprocating passes of the grinding wheel. Typical feed rates and depths of cut in creep-feed grinding range from $1 - 4$ mm/s and $500 - 10000$ μm, respectively. In conventional surface grinding, typical feed rates and depths of cut range from $500 - 2000$ mm/s and $5 - 15$ μm, respectively [2]. The advantage of creep-feed grinding is that productivity and material removal rate are increased compared to conventional surface grinding; in surface grinding, the reciprocating motion of the grinding

wheel results in significant lost time during each stroke, whereas in creep-feed grinding, the wheel is continuously cutting [2]. Recall from Equation 2.1 that contact length in grinding is related to depth of cut. Since depths of cut in creep-feed grinding are very large, the contact lengths in creep-feed grinding are quite large as well [1]. This large contact length means that there is increased heat generation during creep-feed grinding operations compared to surface grinding operations since a greater area of the grinding wheel is in contact with the workpiece. Thus, the proper application of cutting fluid in the creep-feed grinding process is very important to avoid workpiece thermal damage.

2.3 GRINDING MATERIAL REMOVAL & SPECIFIC ENERGY

Material removal in grinding occurs when the grinding wheel's abrasive grains come into contact with a workpiece. Like turning and milling, grinding is a machining process in which material is removed in the form of chips. However, the chips formed during grinding are typically much smaller than those formed in milling and turning [2]. Kinematically, the chip thickness h_m in grinding is related to the grit size, cutting edge spacing L, wheel speed v_s, feed rate v_w, depth of cut a, and wheel diameter d_s [1]. Figure 2.2 illustrates many of these parameters and Equation 2.3 shows the formula for uncut chip thickness [1].

$$h_m = 2L(\frac{v_w}{v_s})\sqrt{\frac{a}{d_s}}$$
(2.3)
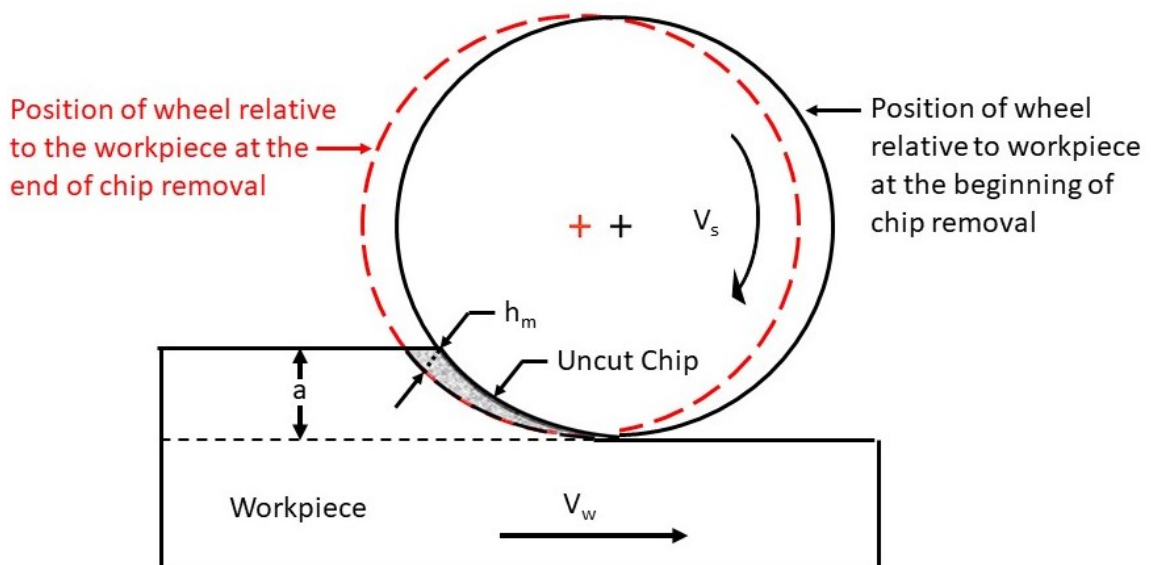
Figure 2.2: Uncut chip thickness

The size effect theory states that the chip size in machining is inversely related to the amount of energy required per unit volume of material removed, also known as the specific energy [1]. Since the chip sizes in grinding are very small, specific energies in grinding are much higher than in other machining processes. In fact, specific energies for grinding steels are typically bigger than the specific melting energies of steel, meaning that grinding is a very energy-inefficient machining process [1]. Most of the energy input in grinding is converted to heat for reasons which will be explained shortly. Thus, specific energy is regarded as a measure of the efficiency of the grinding process since a lower specific energy indicates that a lower percentage of the energy input is converted to heat and a higher percentage of the energy input is used for cutting. Specific energy can be calculated by dividing the spindle power P by the material removal rate R_{MR}, as shown in Equation 2.4 [2]. Material removal rate is the product of workpiece feed rate v_w, depth of cut a, and workpiece width w, as shown in Equation 2.5 [2].

$$U = \frac{F_t v_s}{v_w w a} = \frac{P}{R_{MR}} \qquad (2.4)$$

$$R_{MR} = v_w w a \qquad (2.5)$$

2.4 GRAIN INTERACTION & GRINDING TEMPERATURE

The grinding literature agrees that there are three ways in which abrasive grains interact with the workpiece that are responsible for the energy expenditure in grinding: rubbing, plowing, and cutting [2]. These modes of grain interaction are illustrated in Figure 2.3. Rubbing occurs when a grain contacts the surface of the workpiece but does not penetrate deep enough to remove any material. Plowing occurs when a grain penetrates deep enough into the workpiece to displace material, but not deep enough to form a chip and remove material. Cutting occurs when a grain penetrates deep enough into the workpiece to form a chip and remove material. It has been shown that a very small percentage of grains that pass through the grinding zone, known as the "cutting edges", succeed in cutting and that most of the grains rub, plow, or miss the workpiece entirely [5]. In both plowing and rubbing, energy is expended with no material removal and heat is generated as a result of the friction between the abrasive grain and the workpiece. Therefore, since most of the

grains are simply rubbing or plowing, most of the energy input in grinding is converted to heat which results in very high temperatures at the workpiece surface [1].
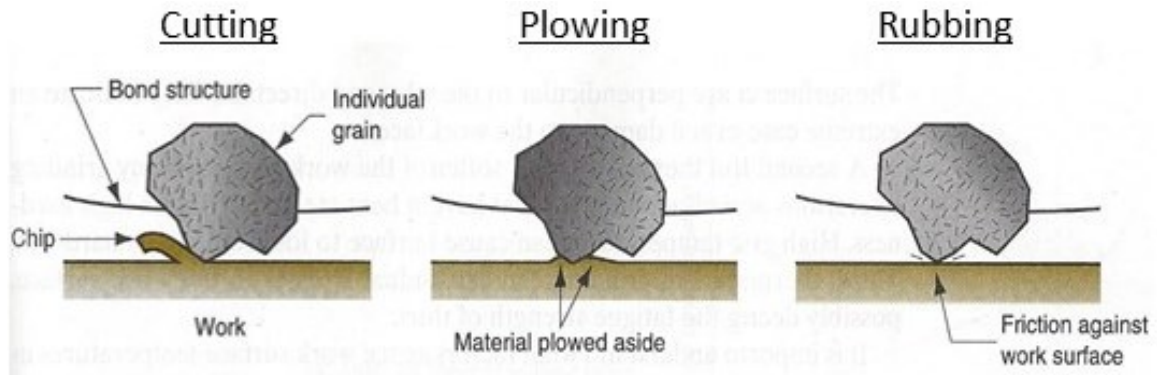
Figure 2.3: Modes of abrasive grain interaction. Adapted from [2].

The high workpiece temperatures in grinding can have multiple damaging effects on the ground surface such as softening of the workpiece surface, unwanted residual stresses, and workpiece burn [2]. Workpiece burn occurs when the temperature at the surface of the workpiece gets so high that the workpiece material is damaged. Workpiece material may even melt and bond itself to the grinding wheel [1]. Workpiece burn can occur in small, localized areas or it can spread across the entire grinding area. This grinding area burning is a process failure because it destroys the workpiece, results in a huge spike in spindle power which can damage the spindle motor if the grinding operation is not aborted, and is harmful to the grinding wheel as a result of the workpiece material becoming bonded to it [1]. When burn occurs, the grinding operation must be aborted, the workpiece must be discarded or re-ground, and the wheel must be dressed (sharpened) to remove the damaged portion of the grinding wheel. Therefore, to maximize productivity in an industrial setting, workpiece burn must be avoided at all costs due to the setbacks associated with it. Figure 2.4 shows an image of a workpiece that suffered workpiece burn during grinding. Note that near the left side of the workpiece shown in Figure 2.4, there are a couple of smaller burn marks that occurred at the beginning of the grinding operation but did not propagate to the full width of the workpiece. However, about halfway through the grinding operation, the full grinding area began to burn, and the grinding operation had to be aborted.

Figure 2.4: Workpiece burn

The most effective way to reduce the temperature at the workpiece surface during grinding is to use a cutting fluid [2]. The cutting fluid, or "coolant", has three functions: 1) cooling, 2) lubrication, and 3) transport of debris from the grinding area [6]. Lubrication via the cutting fluid greatly reduces the friction, and, consequently, the heat generated during grinding. The cutting fluid further reduces grinding temperatures by heat transfer from the workpiece to the coolant [7]. Proper application of a cutting fluid can increase the achievable material removal rates, provide a better work surface quality, and lengthen the tool life of the grinding wheel [6]. There are many different types of cutting fluids and of coolant application methods. The cutting fluid delivery system used in this research will be discussed in Chapter 4. Another way to reduce the temperature at the workpiece surface during grinding is to use a grooved grinding wheel [4]. Grooved grinding wheels are the focus of this thesis and will be discussed extensively in Chapter 3.

2.5   DRESSING & SURFACE ROUGHNESS

Grinding wheels are a type of cutting tool, and, like other cutting tools, grinding wheels wear during cutting. A worn grinding wheel will experience reduced cutting efficiency, higher grinding forces, and higher grinding temperatures compared to a sharp wheel [1]. To regenerate the surface of a worn grinding wheel, a procedure known as "dressing" is performed. Dressing consists of running a diamond tool along the surface of the grinding

wheel while the wheel is rotating which removes a small amount of material from the wheel diameter. The diamond tool breaks off the dulled grits along the periphery of the wheel to expose fresh, sharp grains and to remove chips that have become clogged in the wheel [1].

The two most important parameters during the dressing process are the number of spark-out passes and the overlap ratio. A spark-out pass is a pass of the dressing tool that is done at the end of the dressing process with no infeed with the objective of obtaining a smoother wheel topography [8]. The overlap ratio is a measure of how much the dressing tool will retrace the same area on the surface of the grinding wheel during a dressing pass. Overlap ratio U_d can be calculated by dividing the dressing tool width of penetration into the grinding wheel b_d by the dressing feed per revolution of the grinding wheel f_d, as shown in Equation 2.6 [8]. These parameters are illustrated in Figure 2.5. The dressing feed per revolution of the grinding wheel depends on the wheel diameter, the wheel speed, and the dressing tool traverse federate, as shown in Equation 2.7 [8].

$$U_d = \frac{b_d}{f_d} \tag{2.6}$$

$$f_d = \frac{\pi d_s v_w}{v_s} \tag{2.7}$$
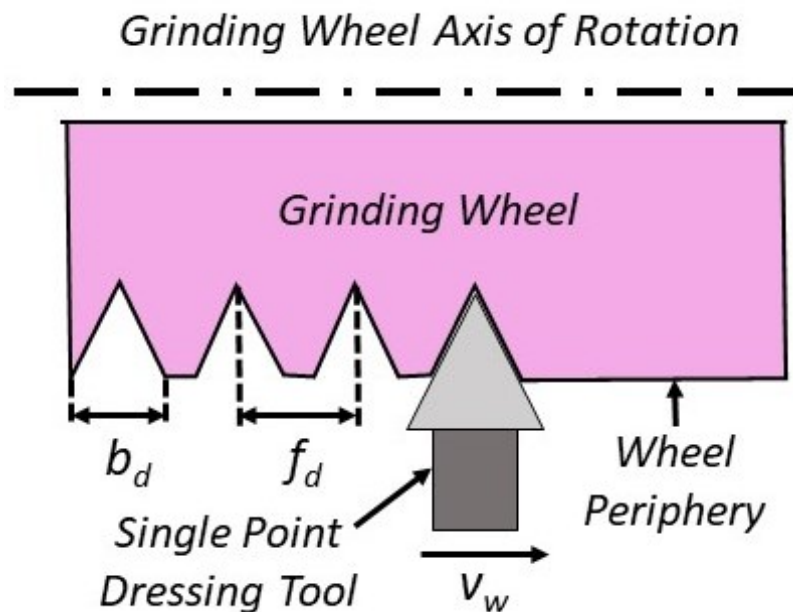
Figure 2.5: Dressing parameters

A smoother wheel topography can be obtained by increasing the number of spark-out passes and/or the overlap ratio, and a coarser wheel topography can be obtained by doing the opposite. A smoother wheel topography will result in duller grains which will increase the spindle power and grinding forces due to reduced cutting efficiency and reduced chip thickness [8]. Contrarily, a coarser wheel topography will have sharper grains, reduced spindle power and grinding forces, and increased chip thickness. Furthermore, a coarser wheel will result in a coarser workpiece surface finish whereas a smoother wheel will result in a smoother workpiece finish. It is also important to point out that chip thickness is proportional to workpiece surface roughness, where larger chip sizes result in a coarser workpiece surface, and vice-versa [8].

One of the main objectives of most grinding operations is to impart a specific surface roughness to a workpiece. Figure 2.6 illustrates the parameters used to calculate surface roughness. To measure the average surface roughness R_a, it is necessary to discretize the specified surface length L_m into n points. Then, the surface roughness is calculated by summing the vertical deviations from the nominal surface y_i at each point and dividing by n, as shown in Equation 2.8 [2]. Since chip thickness is proportional to workpiece surface roughness, the parameters that influence workpiece surface roughness the most are the same parameters that influence chip thickness the most; namely, grit size, cutting edge spacing, wheel speed, feed rate, depth of cut, and wheel diameter [1].

$$R_a = \sum_{i=1}^{n} \frac{|y_i|}{n} \tag{2.8}$$
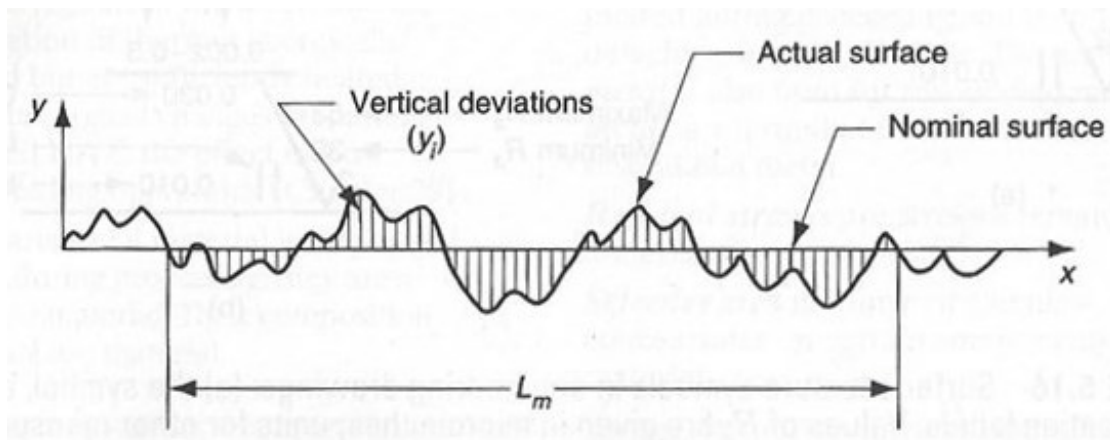
Figure 2.6: Surface roughness. Adapted from [2].

CHAPTER 3: LITERATURE REVIEW

This chapter presents a thorough discussion of the research publications related to grooved grinding wheels. First, the different types of textured grinding wheels, grooving methods, and the parameters used to describe a grinding wheel's groove geometry are introduced. Following this is a review on the effects of grooved grinding wheels on grinding performance. A table-form summary of the grinding parameters, groove geometries, and findings of each publication studying grinding with grooved wheels is then provided. Finally, there is a discussion of the findings in the literature on how groove geometry affects grinding performance. The chapter concludes by identifying gaps in the literature that should be subject to further investigation.

3.1 TEXTURED GRINDING WHEELS

In 2016, Li and Axinte [3] published a comprehensive review paper on the topic of textured grinding wheels. This paper defined textured grinding wheels as "those (grinding wheels) that have both specially-designed active and passive grinding areas on their geometrically active surfaces." Active and passive grinding areas refer to the areas on the surface of the grinding wheel that do and do not participate in the material removal process, respectively. The review went on to classify textured grinding wheels into the following categories:

- *Slotted/Grooved Grinding Wheels:* Conventional grinding wheels that have had grooves or slots cut into them by means of various material removal methods.
- *Segmented Grinding Wheels:* Grinding wheels that are produced by assembling individual abrasive segments onto wheel hubs by using fasteners or adhesives.
- *Grinding Wheels with Internal Coolant Supply Structures:* Grinding wheels that use grooves paired with internal coolant chambers and passages to facilitate coolant flow into the grinding zone.
- *Engineered Grinding Wheels:* Grinding wheels in which abrasive grains are specially arranged in pre-defined patterns, typically with large gaps between adjacent arrays of grains that are regarded as passive areas.

The passive areas on the grinding wheels used for this research were created by removing wheel material by means of abrasive contact between a diamond dressing tool and the wheel surface. Therefore, these wheels belong to the first category of textured grinding wheel presented above: "slotted/grooved grinding wheels" and will simply be referred to as "grooved grinding wheels" for this thesis.

3.2 GROOVING METHODS

Grinding researchers have employed a variety of methods to create grooved grinding wheels. In 2017, Forbrigger *et al.* [4] presented a review on vitrified bond grooving processes. These grooving methods are summarized below:

- *Molded Grooves:* This method produces grooved grinding wheels by incorporating the groove geometry into the mold used to manufacture the grinding wheel [9].
- *Machined Grooves:* This method employs machining operations, such as milling or grinding, to cut grooves into conventional grinding wheels [10-12].
- *Crushing Roll Dresser:* This method uses a carbide or diamond crushing roll dresser to crush grooves into a grinding wheel [13-15].
- *Single-Point Electromagnetic Shaker:* This method uses an electromagnetic shaker to actuate a single-point diamond dressing tool in the direction of the wheel's radius while the tool moves along the width of the grinding wheel [16,17].
- *Single-Point Servo Dresser:* This method creates a groove by moving a single-point diamond dressing tool along the width of a grinding wheel. The tool is mounted on a linear stage driven by a servo motor [18-21].
- *Laser Ablation:* This method uses a high intensity laser to vaporize material at the surface of a grinding wheel [22-25].
- *Water Jet Cutting:* This method uses a very high-pressure water jet to create grooves by removing material at the surface of a grinding wheel [26].

The methods discussed above each have advantages and disadvantages that were summarized by Forbrigger *et al.* [4] in the review paper which can be referenced for more information. It is important to note that grooves created via laser ablation may perform differently than grooves formed using other methods. The reason for this different behavior

is that, for grooves created by abrasive contact between a high hardness grooving tool and a grinding wheel, the wheel wear can be categorized into grain fracture, bond fracture, and attritious wear [2]; however, for grooves created by laser ablation, grinding wheel material is removed by vaporization which may produce a smooth area of melted material on the surface of the grinding wheel [4]. This melted area can lead to increased grinding forces until it is worn away. Deng and He [23] also suggested that when the width of the laser beam is smaller than the grain diameter, the groove created by laser ablation may create an additional cutting edge by splitting a grain in half. A greater number of cutting edges could then lead to reduced workpiece surface roughness. This mechanism of generating extra cutting edges would only be possible with laser grooving because other methods would cause the grains to fracture or to be pulled out. The point of this discussion is that the grooving method should be taken into consideration when comparing the results of different publications on grinding with grooved wheels.

3.3 GROOVE GEOMETRY

For this thesis, the following parameters are used to define the groove geometry of a grooved grinding wheel:

- *Helix Angle α:* Helix angle is the angle of the groove measured relative to the grinding wheel's axis of rotation, as shown in Figure 3.1. There are three main types of helical groove patterns: "Circumferentially-grooved grinding wheel" is the term used to describe a grinding wheel having a single very high helix angle ($85° - 90°$) groove that encircles the grinding wheel multiple times [18]. "Axially-grooved grinding wheel" is the term used to describe a grinding wheel having grooves that are parallel to the wheel's axis of rotation (i.e. $\alpha = 0°$). "Helically-grooved grinding wheel" will be the term used in this thesis to describe a grinding wheel having angled grooves that does not fit into either of the other two categories. These three types of groove patterns are shown in Figure 3.1.

- *Groove Pattern:* Groove pattern is the pattern that the grooves make along the width of the wheel. The most prevalent pattern in the literature is a helical groove pattern owing to its simplicity. However, some recent publications have explored more

intricate patterns thanks to the flexibility of laser grooving. Some examples of different groove patterns that have been studied are shown in Figure 3.1.

HELICAL GROOVE PATTERNS

Grinding Wheel Axis of Rotation

Circumferential   Axial   Helical

EXAMPLES OF OTHER GROOVE PATTERNS

Cross-Helix   Zigzag   V-Shape   W-Shape   Elliptical Holes
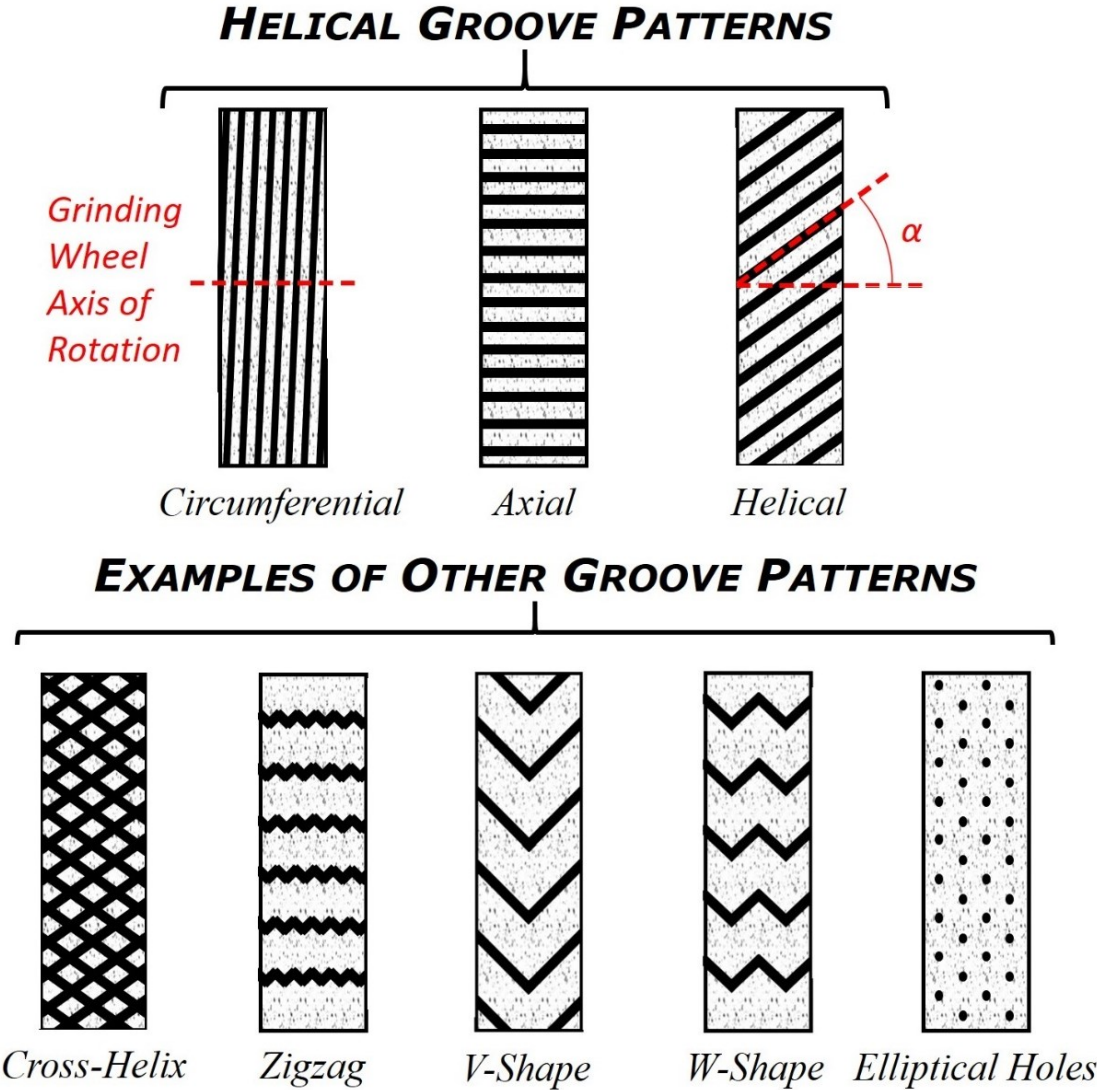
Figure 3.1: Helical groove patterns and examples of other groove patterns

- *Number of Grooves N_g:* One groove is defined as the area between where the grooving tool starts and stops removing material from the surface of the grinding wheel. Typically, the tool begins removing material at one edge along the circumference of the wheel and ends at the other edge of the wheel after traversing the width of the wheel, but this is not always the case.

- *Groove Width b_g:* Groove width is the distance from one groove edge to the other, as shown in Figure 3.2. Groove width is measured normal to the groove direction.

16

- *Groove Pitch p:* Groove pitch is the distance between two adjacent grooved areas and is measured perpendicularly from the groove edges, as shown in Figure 3.2. For non-helical groove patterns, such as the V-shape or W-shape patterns from Figure 3.1, groove pitch can be considered to be the distance between repeated patterns along the circumference of the wheel. Groove pitch cannot be defined for certain groove patterns, such as the elliptical holes pattern from Figure 3.1.

- *Groove Depth d:* Groove depth is measured as the radial distance between the outer radius of the wheel and the bottom of a groove, as shown in Figure 3.2.
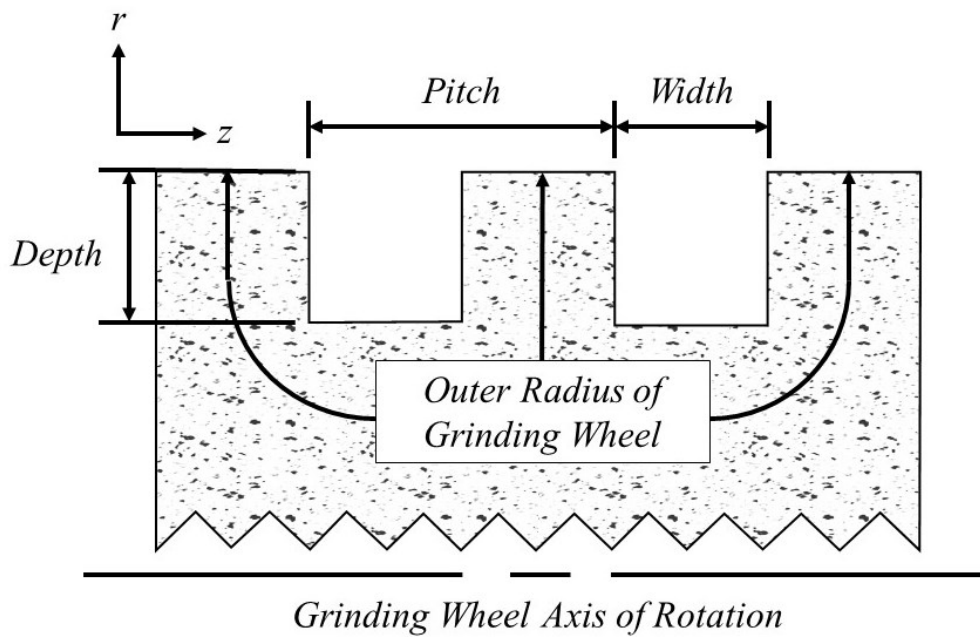
Figure 3.2: Illustration of grinding wheel groove depth, pitch, and width

- *Groove Factor η:* A term coined by Verkerk [27] in his 1979 paper, groove factor is the relationship between the grooved area (A_G) and the total surface area (A_O) of a grinding wheel. It is a number between 0 and 1, or a percentage between 0 and 100%, where a groove factor of 100% would indicate that the wheel is not grooved. A groove factor of 70%, for example, would indicate that 30% of the surface of the wheel has been removed. Groove factor has also been referred to as "intermittent ratio" [9] or "land ratio" [14]. Groove factor can be calculated using Equation 3.1.

$$\eta = \frac{A_O - A_G}{A_O} \tag{3.1}$$

- *Groove Cross-Sectional Shape:* The shape of the groove cross-section can be considered in both the z-r plane, as in Figure 3.2, and the x-y plane, as in Figure 3.3. The shape of the groove's cross-section in the z-r plane is determined by the shape of the cutting tool or mold used to fabricate the groove. Possible shapes include a "U", a "V", a trapezoid, or a square, to name a few. The shape of a grooved wheel's cross section in the x-y plane is determined by the number of grooves, the helix angle, the groove width, and the groove depth. A comparison of the x-y plane cross-sections of a circumferentially grooved grinding wheel and an axially grooved grinding wheel is shown in Figure 3.3. Although these wheels both have 50% groove factors and groove widths of 10 mm, their cross-sections are very different, and this should be considered when analyzing why different groove geometries yield different results.

$$\eta = 50\% \qquad \eta = 50\%$$
$$N_g = 1 \qquad N_g = 63$$
$$b_g = 10 \text{ mm} \qquad b_g = 10 \text{ mm}$$
$$\alpha = 89.9° \qquad \alpha = 0°$$
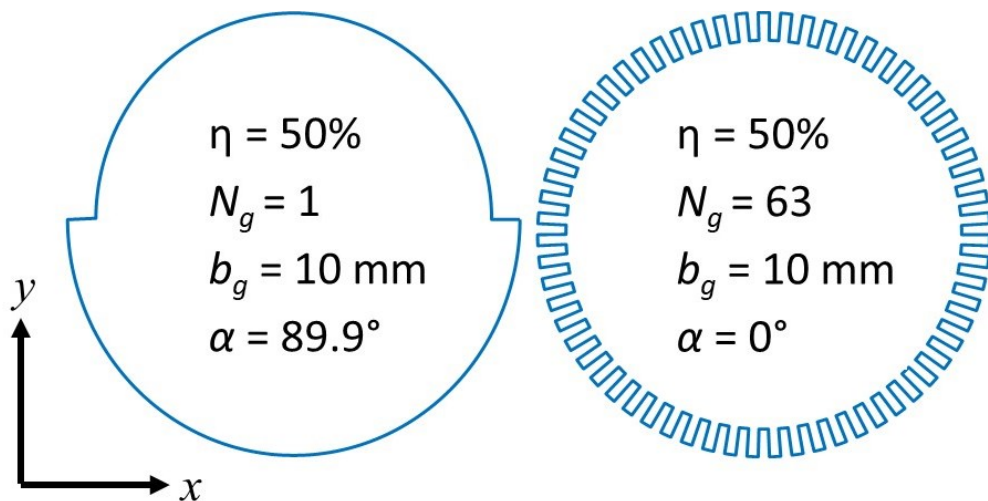
Figure 3.3: Cross-sections of circumferentially and axially grooved wheels

3.4 EFFECTS OF GROOVED WHEELS ON GRINDING PERFORMANCE

Many researchers have provided explanations as to why grooved grinding wheels affect grinding performance. The most recounted reason is the reduction in the number of grains that contact the workpiece [3]. By reducing the number of active grains, the average space between grains L is increased and thus the average chip thickness is increased as per Equation 2.3 [21]. Chip thickness is related to specific energy through the size effect; as chip thickness increases, specific energy decreases, which means that there is less energy

input needed to remove a volume of material compared to a conventional grinding wheel. A lower energy input means that power consumption, temperature, and forces will also be reduced [2].

Another advantage of using grooved grinding wheels that has been discussed extensively in the literature is increased coolant flow into the grinding zone [3]. The grooves act as channels through which the cutting fluid can easily flow directly onto the workpiece, contrarily to using conventional grinding wheels which offer very limited space between the wheel and the workpiece for coolant flow [39]. Two publications attempted to study the effect of using a grooved wheel on coolant flow. The first study was by Denkena *et al.* [34] in 2015 who collected the coolant passing through the grinding zone into a specially designed coolant bin. By measuring the resulting coolant volume, they found that grooved grinding wheels increase the coolant flow rate through the grinding zone compared to conventional grinding wheels. The second study was by Mohamed *et al.* [21] in 2016 who performed dry and wet grinding experiments. It was found that the specific energy dropped by 30.6% and 41.3% when using a grooved wheel compared to a conventional wheel for dry and wet grinding, respectively. The 10.7% difference between these two values was then attributed to the enhanced cooling and lubrication obtained as a result of the increased coolant flow through the grooved areas of the wheel. This publication also presented a study that found that using a grooved wheel could increase coolant flow through the grinding zone by up to 56.5%.

An additional advantage of using grooved grinding wheels that is often brought up in the literature is improved chip disposal from the grinding zone [3]. Intuitively, this concept makes sense: the grooves provide space through which the cut material can easily be washed away by the coolant jet, free of obstructions. However, the effect of improved chip flow in grooved grinding wheels has not been quantified or studied by anyone. Consequently, more research is needed to determine whether improved chip flow is a factor in the increased performance of grooved grinding wheels.

Grooved grinding wheels have also been shown to be an effective, low cost method to impart specific textures onto the workpiece surface. Research by Oliveira *et al.* [17] proved that the grinding wheel groove pattern can be transferred to the workpiece during

plunge grinding operations for several different groove patterns. Silva *et al.* [16] found that using a grooved grinding wheel with a certain groove geometry can easily and efficiently produce lubrication pockets in hydrodynamic bearings. These pockets can lead to improved lubrication. In 2017, Mohamed *et al.* [40] showed that it is possible to accurately predict the workpiece surface texture obtained from using circumferentially grooved grinding wheels by considering the groove geometry and the grinding parameters.

3.5 LITERATURE SUMMARY

A chronological summary of the findings of the various publications pertaining to grooved grinding wheels is provided in Table 3.1 and Table 3.2. These tables are split up into three sections: grinding parameters, groove geometry, and grinding performance.

The "grinding parameters" section lists the type of wheel, the grinding process, and the type of material that were used for each publication. The "groove geometry" section lists the number of grooves N_g, the groove factor η, the helix angle α, the groove width b_g, and the groove depth d for the grooved grinding wheels used in the research. Most publications use a type of helical groove pattern so groove pattern is not listed in the tables. The exceptions to this trend are the following publications which studied different types of groove patterns: [30, 22, 34, 35, 23, 41, 24, 25]. There is very little discussion regarding groove cross-sectional shape in the literature, so this parameter is also not included in the tables. Groove pitch is not included either because it can be calculated given the groove factor and groove width.

The "grinding performance" section lists the experimental findings of each publication on the effect of using a grooved grinding wheel compared to a conventional grinding wheel. This section includes specific energy e_c, grinding forces F, temperature T, wheel wear W, and surface roughness R_a. Up and down arrows are used to indicate whether using a grooved grinding wheel caused a value to increase or decrease compared to a conventional grinding wheel. Circles are used to indicate that a publication stated that using a grooved grinding wheel did not have any influence on a certain value compared to a conventional grinding wheel. Dashes are used to indicate that a publication did not report on that item.

Table 3.1: Summary of publications on grinding with grooved wheels (1/2)

Author	Year	Grinding Parameters			Groove Geometry					Grinding Performance				
		Wheel Type	Grinding Process	Workpiece Material	N_g	η (%)	α (deg)	b_g (mm)	d (mm)	e_c	F	T	W	R_a
Nakayama et al. [13]	1977	A46J6V	Surface	0.5% carbon steel	-	37 − 50	60	2 − 2.5	-	↓	↓	↓	●	↑
Verkerk [27]	1979	A100K7VA	Surface	100Cr6	225 − 545	69 − 81	22.5 − 67.5	1 − 1.2	>10	-	-	↓	↑	↑
Suto et al. [28]	1990	CBN, Diamond	Creep-Feed	Nickel-base alloys	120	47 − 70	0 − 45	1.6	-	↓	-	↓	-	●
Kim et al. [9]	1997	A60L7V	Surface	SM45C, copper, brass, A16061, SUS304	18 − 32	66 − 81	0 − 45	6 − 18	>10	-	-	↓	-	↓ ↓ ↓ ↓ ↑
Lee et al. [29]	2000	Diamond	Surface	Al₂O₃ based ceramics	40	64	0	-	>10	-	-	↓	↓	↑
Kwak & Ha [10]	2001	A100LMV	Surface	STD11 steel	6 − 24	78 − 94	0	6	-	-	↓	↓	-	↑
Tawakoli et al. [30]	2007	CBN	Surface (Dry)	100Cr6	-	25 − 75	60	0.6 − 1.5	0.03	↓	↓	↓	↑	↑
Piotr [31]	2007	A80K7V	Surface	Hard steel	1	35	>89	1.1	0.05	-	↓	-	↓	-
Nguyen & Zhang [32]	2009	CBN	Surface	AISI 4140	144	-	0	>2	-	↓	↓	↓	↓	-
Gavas et al. [33]	2011	EK60K6E30	Cylindrical	Brass, AISI 1010, AISI 1040, AISI 2080	1	50	89.5	5	3	-	-	-	-	↓ ↑ ↓ ↓
Uhlmann & Hochschild [12]	2013	CBN	Cylindrical	100Cr6	20 − 70	60 − 90	0 − 32	1.6 − 6.3	5	↓	↓	↓	↑	↓

Table 3.2: Summary of publications on grinding with grooved wheels (2/2)

Author	Year	Grinding Parameters			Groove Geometry					Grinding Performance				
		Wheel Type	Grinding Process	Workpiece Material	N_g	η (%)	α (deg)	b_g (mm)	d (mm)	e_c	F	T	W	R_a
Mohamed et al. [18]	2013	A60J5V1	Creep-Feed	AISI 4140	1	50	>89	0.5 – 1.1	0.1	↓	↓	-	●	↑
Walter et al. [22]	2014	CBN	Surface	100Cr6	-	63	0-30	0.12 – 0.14	0.05	-	↓	-	↑	↑
Koklu [11]	2014	Al$_2$O$_3$ (#60)	Cylindrical	AISI 1040, AISI 5140, AISI 8620, AISI 52100	24	-	15 – 45	2.6	3	-	-	-	-	↓ ↓ ↓ ↓
Aslan & Budak [15]	2015	SiC80J5V	Surface (Dry)	AISI 1050	1	65 – 82	89.3 – 89.8	1.1	0.1	↓	↓	↓	●	↑
Denkena et al. [34,35]	2015	Al$_2$O$_3$ (#80)	Surface, Cylindrical	X155CrVMo	-	57 – 90	0 – 90	0.5	0.1	-	↓	↓	↑	↑
Azarhoushang et al. [36]	2017	CBN	Cylindrical (Dry)	42CrMo4, 100Cr6	1	25 – 40	>89	0.3 – 0.35	0.005 – 0.015	↓	↓	↓	↑	-
Deng & He [23]	2017	Diamond	Surface	Cemented carbide	-	70	0 – 90	0.075	0.038	-	-	-	↓	↓
Zahedi et al. [41]	2017	CBN	Cylindrical (Dry)	100Cr6		85		0.08 – 0.18	0.3	-	↓	↓	↓	↑
Zhang et al. [24]	2018	Diamond	Surface	Al$_2$O$_3$	-	-	0 – 45	1.2	0.85	-	↓	-	↑	↑
Dewar et al. [37]	2018	A60J5V	Cylindrical	AISI 1045	1	50	89.9	0.9	0.1	↓	↓	-	-	↑
Forbrigger et al. [38]	2018	A60J5V	Surface	AISI 1018	1	61 – 64	89.9	0.97	0.1	↓	↓	-	-	↑
Zhang et al. [25]	2019	Diamond	Surface	Silicon nitride	-	-	0 – 30	0.9	0.75	-	↓	↓	↑	↑

It can be seen from Table 3.1 and Table 3.2 that every publication that reported on specific energy, forces, and temperature in grinding with grooved grinding wheels found that these values all decreased when compared to grinding with conventional grinding wheels. However, the results regarding grinding wheel wear and workpiece surface roughness are not as consistent. Eight publications found that wheel wear increased when using grooved wheels, four publications found that wheel wear decreased when using grooved wheels, and three publications found that using a grooved wheel does not affect wheel wear. Based on these results, it remains unclear if a grooved grinding wheel wears differently than a conventional grinding wheel.

Most researchers found that using grooved grinding wheels increases workpiece surface roughness. However, there are five publications [9, 33, 12, 11, 23] that found that using a grooved grinding wheel reduced workpiece surface roughness. To attempt to theorize why these researchers found reduced workpiece surface roughness, some observations on similarities between these publications are made. The paper by Deng & He [23] is not comparable to the other papers and will be excluded from the following analysis; this paper is unique in that the grooves were created by laser cutting and the groove width was smaller than the grain size, so they believed that the grooving process split the grains which created additional cutting edges.

- Three out of four publications that found reduced surface roughness were for cylindrical grinding operations [33, 12, 11].
- Some researchers found that while using a grooved grinding wheel may reduce surface roughness for certain materials, it can increase surface roughness for other materials [9, 33]. This inconsistency suggests that the material properties must be considered when attempting to understand how grooved grinding wheels influence workpiece surface roughness.
- The groove widths used in the publications that found reduced surface roughness were all relatively large; the smallest groove width used in a paper that reported reduced surface roughness was 1.6 mm [12], whereas most researchers have used groove widths that are less than 1 mm.

- The groove depths used in the publications that found reduced surface roughness were also all relatively large; the smallest groove depth used in a paper that reported reduced surface roughness was 3 mm [33]. Most researchers have used groove depths that are less than 1 mm.

The foregoing analysis simply provides some observations that can be made based on the literature summary presented in Table 3.1 and Table 3.2. More research is needed to validate whether there is any substance to these observations.

3.6 EFFECTS OF GROOVE GEOMETRY ON GRINDING PERFORMANCE

There has been some research into how the groove geometry of a grooved grinding wheel affects grinding performance. By far the most researched aspect of groove geometry is the effect of groove factor. Multiple researchers [10, 12, 14, 18, 20, 30, 34, 36] have found that as groove factor decreases, temperature, force, and specific energy decrease due to reduced active cutting edges which results in higher uncut chip thickness. Many of these same researchers and others [10, 18, 20, 27, 30, 34] found that surface roughness increases as groove factor decreases since surface roughness tends to increase relative to uncut chip thickness [2]. Verkerk [27] suggested that wheel wear increases as groove factor decreases since the effective metal removal rate per grain, and thus the force acting on each grain, increases as the active area of the wheel decreases. Similarly, Uhlmann and Hochschild [12] found that a CBN wheel with a 60% groove factor experienced much greater wear than wheels having groove factors of 75% and 90%. Likewise, Denkena *et al.* [34] and Azarhoushang *et al.* [36] found that wheel wear increases as groove factor decreases due to larger contact pressures and larger cutting forces per grain.

There have also been several studies on the effect of helix angle on grinding performance. Verkerk [27] was the first to suggest that grooves should be made at an angle to the wheel axis to keep grinding force fluctuations to a minimum. In 1997, Kim *et al.* [9] found that helically-grooved wheels experienced less wear on their leading edges than axially grooved wheels. This reduced wear was attributed to the helical grooves allowing the cutting edges to gradually contact the workpiece and thus reduce the impact forces on the grains. In 2013, Uhlmann and Hochschild [12] performed experiments with grooved grinding wheels having helix angles of 0° and 32°. They found that the axially-grooved

24

wheel led to a significant increase in vibration amplitudes which was attributed to a short loss of contact between the grinding wheel and the workpiece as the grooved section of the grinding wheel rotated through the grinding zone. These vibrations resulted in higher radial wheel wear and worse surface roughness since the vibrations caused an oscillating depth of cut. Grinding forces, however, were nearly identical for both cases. In 2014, Koklu [11] performed cylindrical grinding experiments with grooved grinding wheels having helix angles of 15°, 30°, and 45°. He found that the grooved grinding wheels reduced workpiece surface roughness and that helix angles of 30° and 45° produced the best workpiece surface roughness in low-hardness and high-hardness materials, respectively. In 2017, Deng and He [23] experimented with laser micro-structured coarse-grained diamond wheels having helix angles of 0°, 30°, 60°, and 90°. They remarked that when the helix angle is 0°, there is intermittent contact between the wheel and the workpiece which results in greater impact forces and increased vibrations which increases workpiece surface roughness. They also remarked that when the helix angle is 90°, ridges are left on the workpiece which result in a poor workpiece surface finish. The helix angles of 30° and 60° ensured a continuous grinding process but the grinding wheel with the 60° helix angle was found to provide the best surface finish.

There have been a few studies that have compared various groove patterns; however, all of these studies were for grinding wheels that were grooved with lasers. In 2014, Walter *et al.* [22] experimented with laser-structured CBN grinding wheels having helical (A), cross-helix (B), small zigzag (C), large zigzag (D), and axial (E) groove patterns but otherwise similar groove geometries. They found that these patterns can be ranked from lowest to highest forces and from highest to lowest surface roughness as follows: B, D, A, E, C. Deng and He [23] compared two laser-structured coarse-grained diamond grinding wheels having W-shaped and V-shaped groove patterns. They found that both grooved wheels reduced workpiece roughness compared to a conventional wheel, but that the wheel with the W-shaped groove pattern provided the best workpiece surface finish. In 2017, Zahedi and Azarhoushang [41] compared a grinding wheel having hundreds of 180 μm width elliptical holes (A) to a grinding wheel having multiple axial zigzag shaped grooves that were 80 μm wide (B). Both wheels had groove factors of 85%

and it was found that wheel B reduced forces more than wheel A, but that wheel A had greater wear resistance than wheel B.

There has only been one publication that studied the effect of groove width on grinding performance. Mohamed *et al.* [18] compared two grooved grinding wheels having groove widths of 0.5 mm (A) and 1.08 mm (B). They found that wheel A provided lower consumed power, forces, and specific energy than wheel B. However, it was found that wheel A produced a worse surface finish than wheel B, particularly at higher depths of cut. It should be noted that the main topic of the aforementioned paper was not the effect of groove width on grinding performance, so a thorough investigation on the effect of groove width was not provided. Nonetheless, the findings presented by this paper are interesting and highlight the need for more research on this subject. Another relevant publication by Fu *et al.* [42] suggested that groove spacing can be optimized by first calculating the space between effective grains based on the anticipated grinding parameters, then cutting grooves such that the distance between each leading edge is equal to this space. A study by Aurich and Kirsch [43] found that coolant is accelerated to flow out of the sides of the grooves and away from the contact zone if the groove width is larger than the workpiece width. There has only been one publication discussing the effect of the grooved grinding wheel cross-section on grinding performance. The paper by Mohamed *et al.* [40] found that the space between trailing and leading edges along the circumference of the cross-section of the grinding wheel is related to the height of ridges that are left over on the workpiece surface as a result of the groove. There has not been any research into the effect of groove depth on grinding performance.

3.7 CONCLUSIONS AND RECOMMENDATIONS

Although there has been a lot of research into the effects of groove geometry on grinding performance, there are still several aspects of groove geometry that require further investigation. The present author identified the following areas that require more research:

- The effect of groove depth on grinding performance.
- The effect of groove width on grinding performance.
- The development of a continuous grooving device that could be implemented in an industrial setting such that wheel grooving does not cause any down-time.

- A study comparing a wheel with a single circumferential groove to wheels with multiple helical grooves but otherwise similar groove geometries.
- In what situation grooved wheels may improve workpiece surface roughness.
- In what situation grooves may increase or decrease grinding wheel wear.
- A study on whether the discarded chips flow differently between grooved grinding wheels and conventional grinding wheels.

The research presented in this thesis focuses on the effects of groove depth and groove width on grinding performance. From Table 3.1 and Table 3.2, it can be seen that groove depths in the range of 0.005 mm to >10 mm have been proven to be effective. Similarly, groove widths ranging from 0.075 mm to 18 mm have been shown to be effective. It remains unclear, however, what the effects of different groove depths or different groove widths might be. In order to study the effects of groove depth and groove width on grinding performance, it is necessary to be able to vary these parameters with minimal change to the other groove geometry parameters. The most important parameter to keep constant when comparing the results from different groove geometries is groove factor because it has been shown to have the greatest effect on grinding performance. However, it is not possible to vary groove width while maintaining a constant groove factor without adjusting at least one other groove geometry parameter; when varying groove width for a grinding wheel with multiple grooves, the number of grooves must be modified in order to maintain a constant groove factor. A circumferential groove pattern provides a good medium to study groove width; when varying groove width for a wheel with a single groove, it is simply a matter of slightly changing the helix angle to maintain a constant groove factor. Thus, circumferentially grooved wheels were used for the research presented in this thesis. Furthermore, since it has been shown that grooved wheels have less of a negative impact on workpiece surface roughness when using low feed rates [119, 40], thus creep-feed grinding was chosen as the grinding process for this investigation.

CHAPTER 4: EXPERIMENTAL SETUP

This chapter presents the equipment that was used throughout this research. The equipment can be broken down into three groups; first is the grinding setup which includes the grinding machine, grinding wheel, coolant delivery system, and workpieces. Next is the measurement equipment which includes the devices used to measure power, force, wheel surface topography, and workpiece surface roughness. Lastly is the grooving setup which pertains to the equipment used to groove a grinding wheel.

4.1 GRINDING SETUP

The grinding experiments performed for this research employed a Radiac Abrasives grinding wheel having the specification WRA-60-J5-V1 which represents a 60-grit, friable aluminum oxide grinding wheel with vitrified bonds. The dimensions and specifications of this grinding wheel are listed in Table 4.1. Prior to performing any grinding experiments, the grinding wheel was trued using a single point dressing tool, and then balanced.

Table 4.1: Grinding wheel specifications

Specification	Marking	Meaning
Grain Type	WRA	Friable Aluminum Oxide Mixture
Grit Size	60	Medium Grains (~250 µm diameter)
Grade	J	Medium Strength Bonds
Structure	5	Dense Grain Spacing
Bond Type	V1	Vitrified Bond
Diameter	16″	
Width	1″	
Hole Diameter	5″	

All grinding experiments were performed on a Blohm Planomat 408 grinding machine, which is shown in Figure 4.1. AISI 4140 steel workpieces were used for all the experiments. The workpiece dimensions were 4.5" x 0.25" x 2". The workpieces were positioned such that the 4.5" x 0.25" surface was being ground. For many experiments, two workpieces were clamped together and ground simultaneously such that the overall workpiece dimension was 4.5" x 0.5" x 2".

Figure 4.1: Picture of grinding machine

Prior to performing any grinding experiments, the coolant tank of the grinding machine was cleaned to ensure optimal grinding fluid quality. The tank was then filled with a mixture of water and CIMTECH 310 metal working fluid such that the mixture concentration was 5.1%, which is the minimum recommended concentration for grinding operations. The grinding fluid concentration was measured daily prior to performing any experiments using a refractometer to ensure a consistent mixture concentration. This measurement is important because the water in the mixture would evaporate which would increase the concentration of cutting fluid in the mixture requiring more water to be added.

The grinding fluid was delivered from an 8 mm diameter coherent jet nozzle that was positioned such that the maximum amount of grinding fluid flows into the grinding zone. The height of the coolant delivery nozzle was adjusted regularly to account for changes in the wheel radius; as the grinding wheel radius is reduced during dressing, the coolant nozzle must be raised by an amount equal to the reduction in wheel radius to ensure that the coolant jet is consistently striking the same area on the surface of the grinding wheel throughout the grinding experiments. The grinding fluid flow rate was measured using a flowmeter and was kept at a constant 10 gallons per minute. Experiments were performed such that the direction of the wheel feed was opposite to the direction of fluid flow, and that the direction of the wheel velocity at the grinding zone was the same as the direction of coolant flow to optimize cooling and lubrication during grinding experiments, as shown in Figure 4.2.
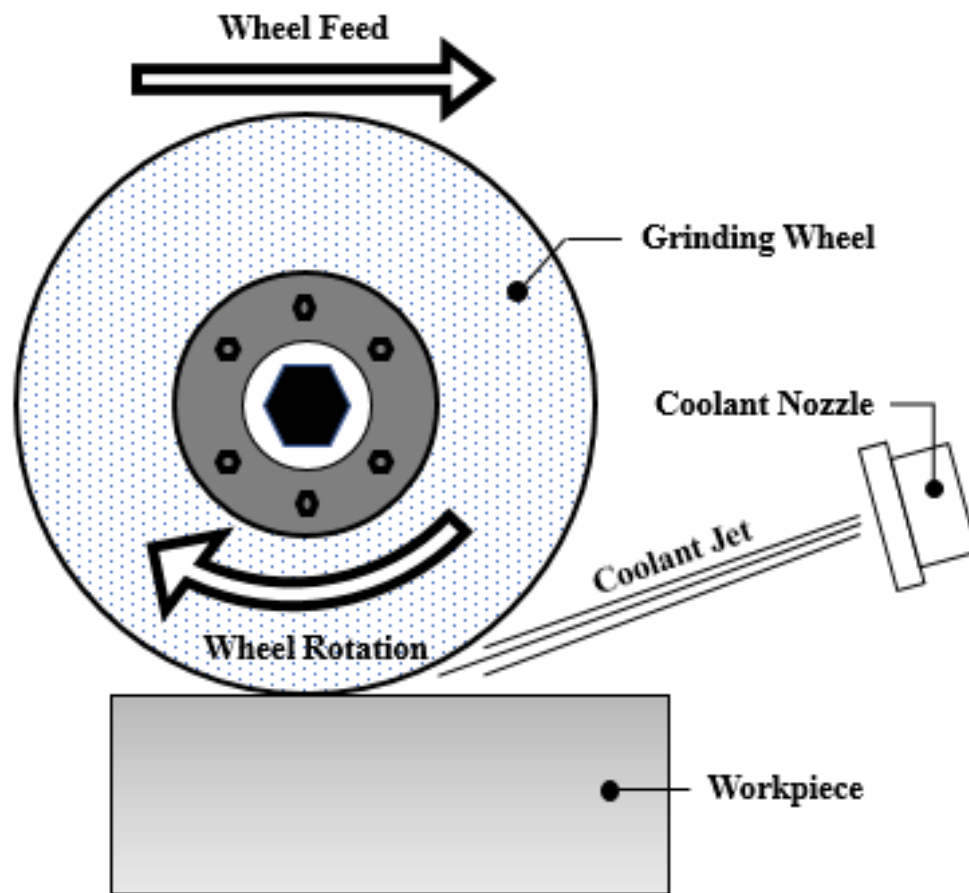
Figure 4.2: Coolant jet orientation

4.2 MEASUREMENT DEVICES

Many measurement devices were used throughout this research to collect data. Specifically, power and force data were collected during the experiments and surface roughness measurements were taken afterwards. Wheel topography scans were also taken prior to performing a set of experiments in order to record the grinding wheel's groove geometry. Workpiece topography scans were taken to validate surface roughness measurements and to verify the existence of patterns on the AISI 4140 workpiece surfaces. The following sections discuss the various measurement devices used to acquire data.

4.2.1   Power & Forces Data Acquisition

Grinding power was acquired using a power transducer that would measure the voltage and current supplied to the spindle motor. Grinding forces were measured using a dynamometer upon which the workpiece clamp was mounted, as shown in Figure 4.3. This dynamometer measured normal, tangential, and transverse forces. Table 4.2 lists all the hardware used to acquire force and power data. A LabVIEW program was used to control data acquisition.
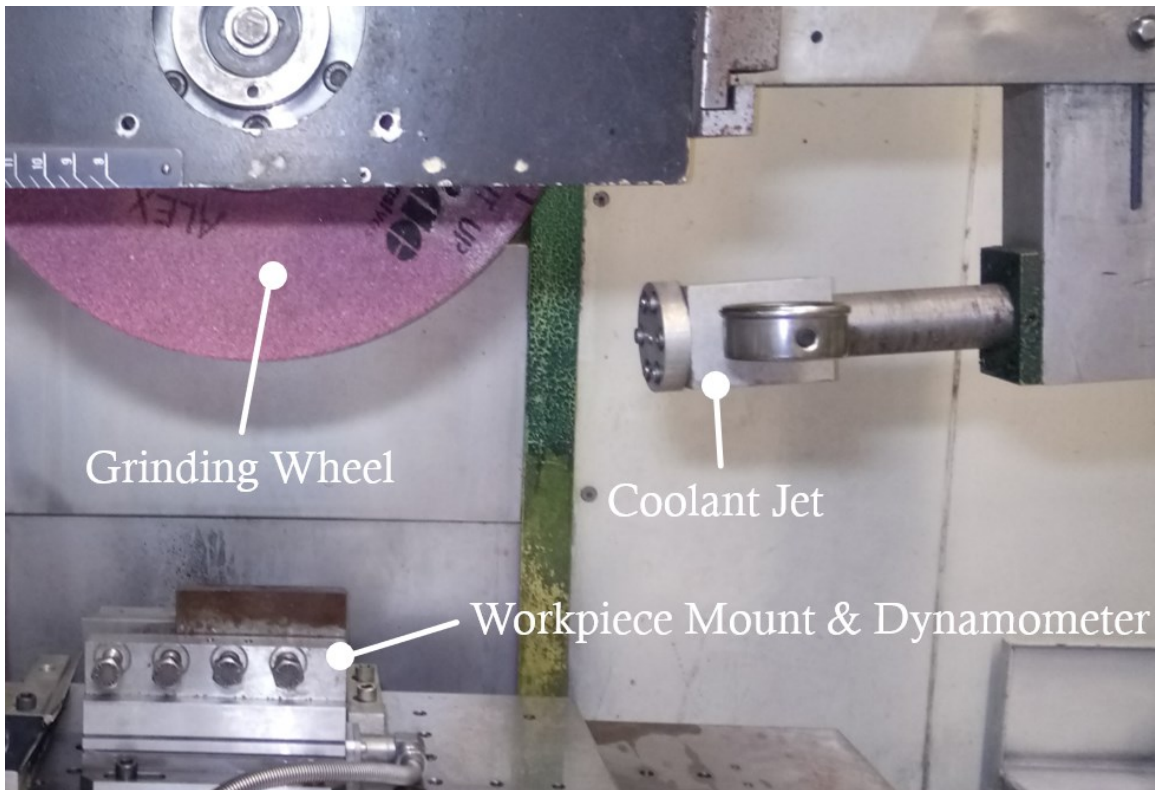
Figure 4.3: Equipment setup inside grinding machine

Table 4.2: Force and power data acquisition hardware

Item	Make & Model
Spindle Power Meter	Load Controls Inc. PH-3A Power Transducer
Force Dynamometer	Kistler Multi-Axis Force Dynamometer 9257B
Charge Amplifier	Kistler Multi-Channel Charge Amplifier 5019B
Connector Block	National Instruments BNC 2120
Data Acquisition Card	National Instruments PCI-MIO-16XE-10

4.2.2 Wheel Topography Measurements

The grinding wheel scanner developed by McDonald *et al.* [44] was used extensively throughout this thesis work to validate the various groove geometries that were used. This scanning system is shown in Figure 4.4 with the various components of the system identified. This system uses an optical measuring pen with a measurement range of 1200 μm to measure the surface topography of a grinding wheel. The wheel is set on a freely rotating vertical shaft. The optical pen is then held in a mount near the cutting surface of the grinding wheel and the pen position is adjusted until the grains are within the measuring range of the pen. A friction wheel is used to rotate the grinding wheel while a linear actuator is used to move the optical pen vertically along the width of the grinding wheel. These two degrees of freedom allow the height at any position on the cutting surface of the grinding wheel to be measured. National Instruments data acquisition hardware is used acquire the optical pen measurements, hub encoder data, friction wheel encoder data, and to drive the linear actuator as well as the friction wheel. LabVIEW programs are used to execute the scans and to record the data.
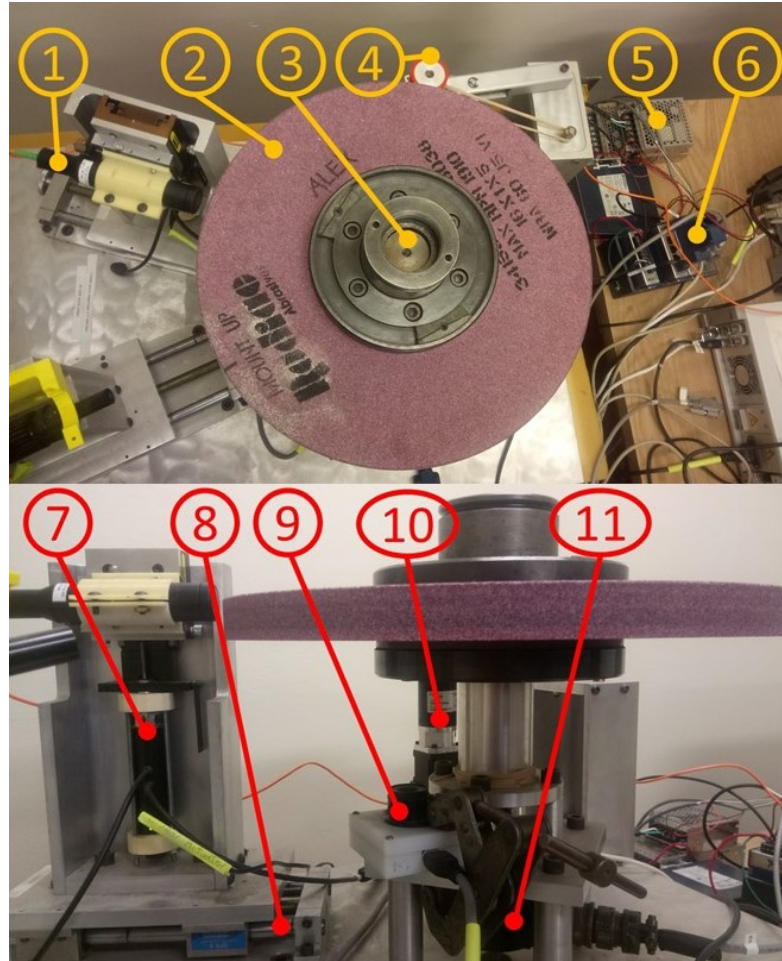
1	Optical pen	7	Linear actuator
2	Grinding wheel	8	Lead screw to move optical pen
3	Freely rotating shaft	9	Digital camera for homing
4	Friction wheel	10	Friction wheel motor & encoder
5	Power supplies	11	Hub encoder
6	DAQ hardware		

Figure 4.4: Grinding wheel scanning system

The grinding wheel scanner was programmed by McDonald *et al.* [44] primarily to take scans along the circumference of the grinding wheel and did not have the ability to simply scan the width of the grinding wheel without changing the angular position of the grinding wheel. Since it was important to know the groove geometry across the width of the grinding wheel for this research, the present author developed a LabVIEW program to scan the width of the grinding wheel.

A flowchart describing this LabVIEW program along with the user-controlled parameters are shown in Appendix A. This program begins with the linear actuator holding the optical pen in its lowest position. The actuator is then raised by the vertical step size, after which a height measurement is acquired. These two steps are then repeated until the actuator reaches the final scan height. The motor is then turned on to rotate the grinding wheel by the circumferential step size, and the pen is then incrementally lowered by the vertical step size while acquiring height measurements in between steps until the linear actuator reaches its starting position. This process is repeated until the desired number of profiles have been scanned. The data can then be processed to show a 3D image of the scanned area, or all the measured profiles can be averaged along the circumference of the grinding wheel to show a 2D figure of the width of the grinding wheel. An example of a scan of a grooved grinding wheel that was taken using this program is shown in Figure 4.5. This figure was achieved by scanning 50 profiles and averaging them. Each profile was spaced only 10 μm apart along the circumference of the wheel for this scan. It is helpful to take multiple profiles and average them to reduce measurement noise since individual profiles can be quite noisy. A picture of the grinding wheel from Figure 4.5 is shown in Figure 4.6 for reference.
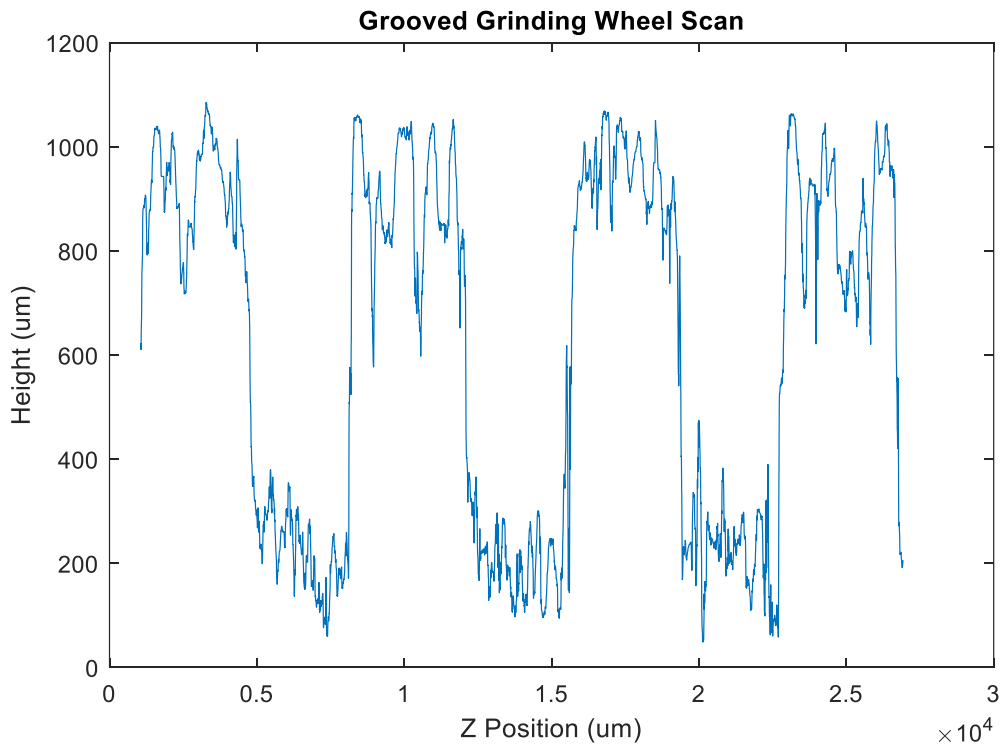
Figure 4.5: Grooved grinding wheel scan

Figure 4.6: Image of grooved grinding wheel

4.2.3 Surface Roughness Measurements

A Mahr Federal Pocket Surf, shown in Figure 4.7, was the primary device used to take surface roughness measurements due to its measurement speed, simplicity, and portability. The Pocket Surf is capable of measuring surface roughness at an accuracy of ±0.01 um. A Nanovea CHR 150 profilometer, shown in Figure 4.8, was also used to measure surface roughness and to scan the workpiece topography of the AISI 4140 steel workpieces. The profilometer is stationary and profilometer scans are more time consuming than Pocket Surf measurements. Therefore, the profilometer was mostly used to scan larger sections, to produce images of the workpiece surface, and to validate the measurements of the Pocket Surf. Approximately one in every five workpieces were scanned on the profilometer. It was found that the measurements from the profilometer agreed well with the measurements from the Pocket Surf.

Figure 4.7: Image of pocket surf
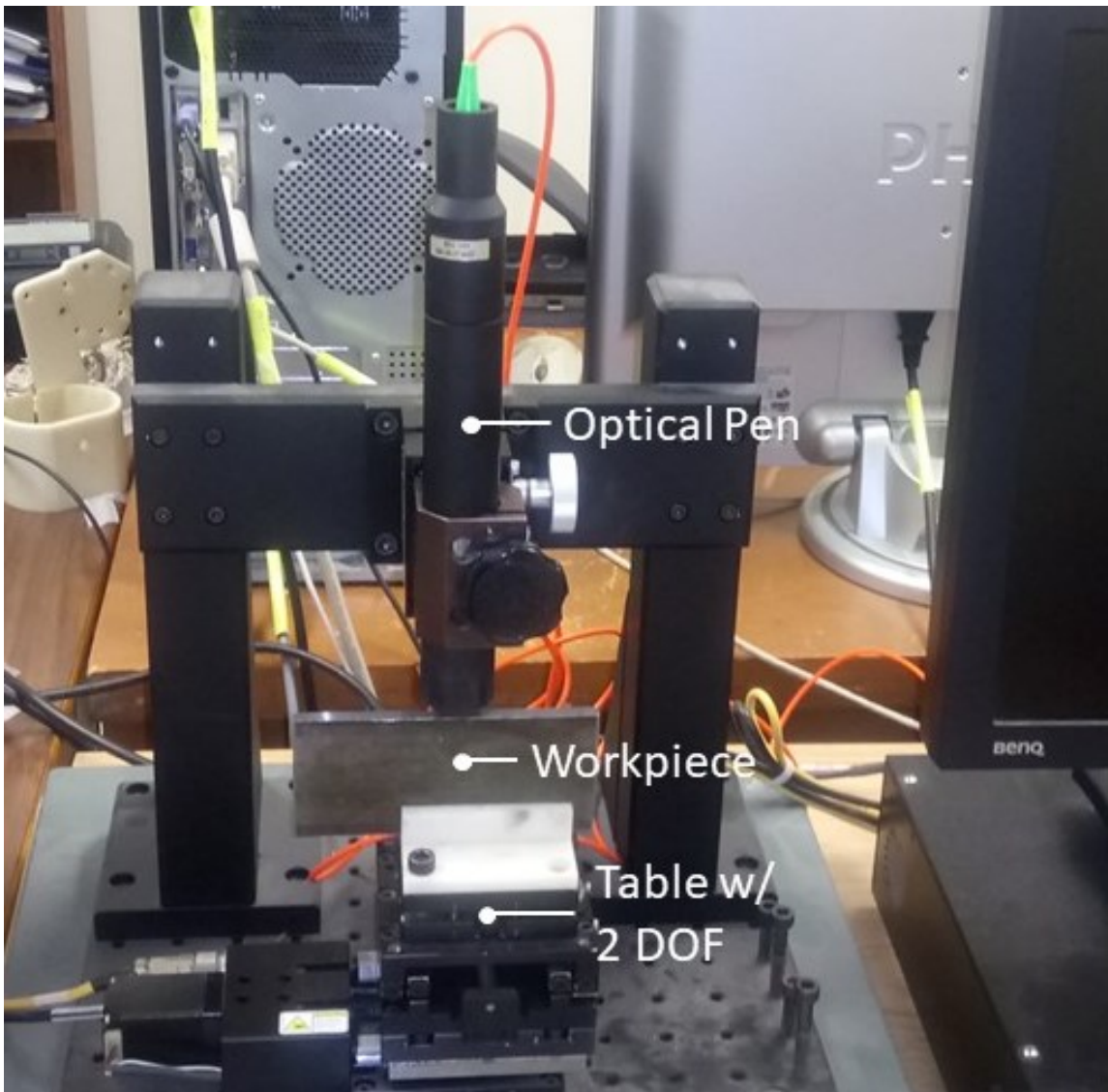
Figure 4.8: Image of Nanovea profilometer

4.3 GROOVING SETUP

A crucial part of this research was the ability to accurately and easily groove a grinding wheel. A grooving device had previously been developed to cut grooves into grinding wheels by means of abrasive contact between the grinding wheel and a diamond dressing tool [19]. The following sections discuss this grooving device, as well as the modifications that were made to the grooving process by the present author for this thesis work.

4.3.1 Grooving Device

The grooving device developed by Mohamed *et al.* [19] and Forbrigger *et al.* [38] ("the groover") was used to cut grooves into the grinding wheels used for this research. This device consists of a tool mount that sits upon a linear stage that is driven by a DC servo motor. A KFLOP motion controller is used to control the device; the KFLOP receives encoder data from the servo motor and calculates the error between the actual position and the desired position. This error is then processed through a PID controller which determines the voltage to supply to the motor.

The groover, shown in Figure 4.9, functions by moving a high hardness tool along the width of the grinding wheel in an axis parallel to the axis of rotation of the grinding wheel. The process is similar to a dressing process in that the tool moves across the width of the grinding wheel and removes grains from the surface of the grinding wheel. However, unlike a dressing process, the groover can retrace the same path along the surface of the grinding wheel at every pass of the cutting tool which creates a groove. This retracing is accomplished by monitoring the index pulse of the grinding wheel encoder through a C program executed on the KFLOP; when an index pulse is detected, the groover motion is triggered and the tool begins to move from its starting position to a final position at a desired speed. Provided that the wheel velocity, the starting position of the grooving tool, and the grooving speed are constant, the tool will retrace the same path every time it passes across the grinding wheel's surface.
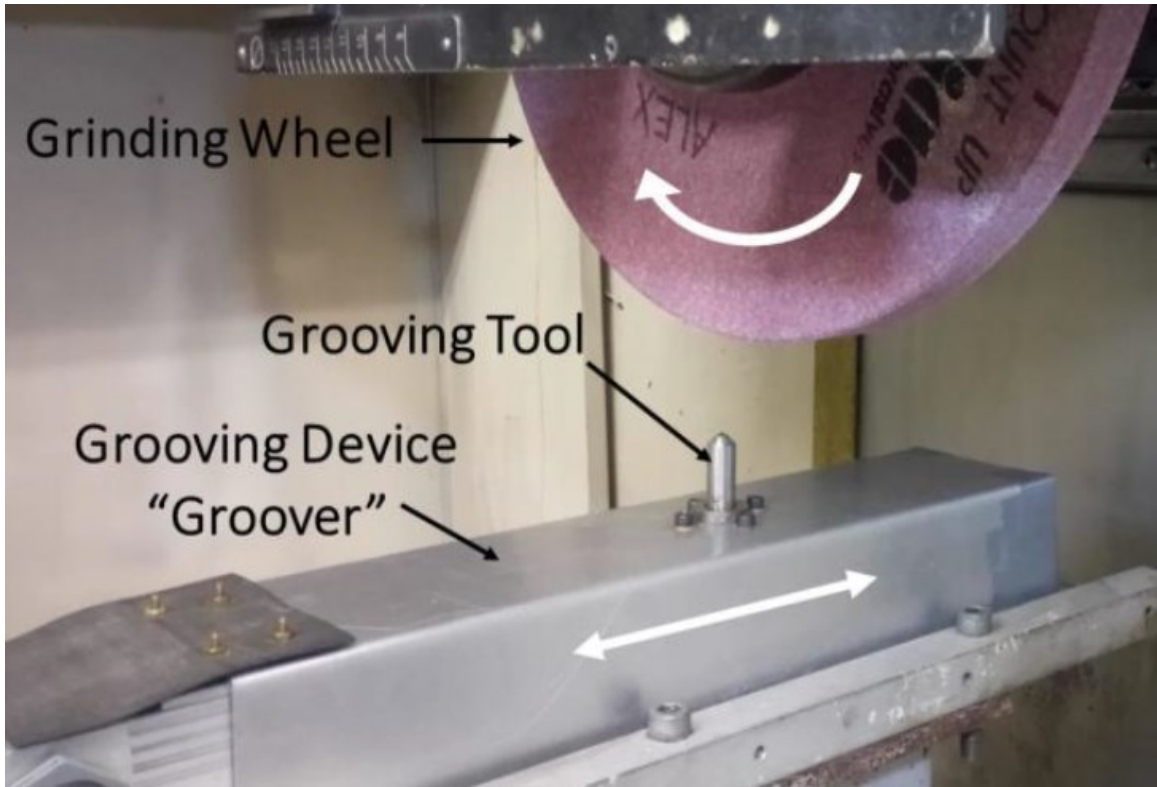
Figure 4.9: Grinding wheel grooving device
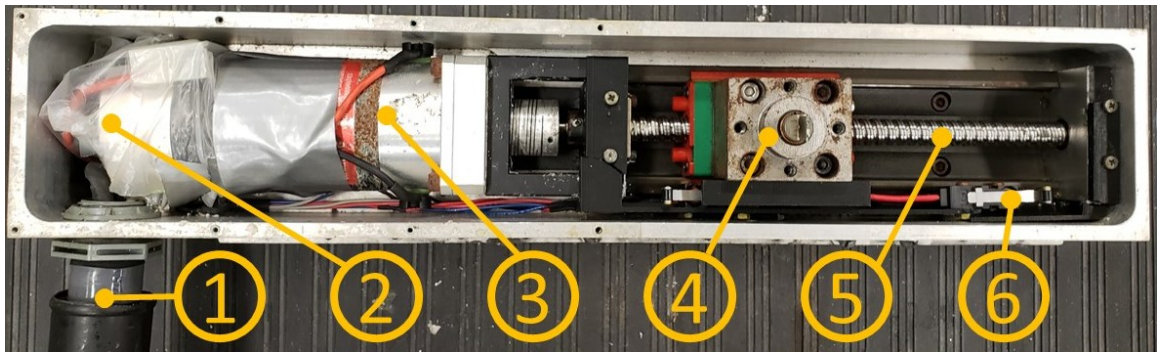
1	Protective Tubing for Cables	4	Tool Mount and Grooving Tool
2	Encoder	5	Linear Stage
3	Brushed DC Motor	6	Limit Switch

Figure 4.10: Components of grooving device

4.3.2 Grooving Process

The grooving system developed by Mohamed *et al.* [19] was originally used to cut a 0.1 mm deep groove in a single pass of the cutting tool. The grinding wheel would then be re-grooved in a single pass to maintain a consistent groove depth as the wheel wore. This process simply involved manually moving the grinding wheel to the correct position and then running the tool across it once as the wheel was rotating.

For this thesis work, grooves much deeper than 0.1 mm are investigated, and it is not possible to cut these deeper grooves in a single pass of the tool. Furthermore, it was decided that each tool pass would cut into the wheel by only 6.35 µm (0.00025") to reduce tool wear, since tool wear rate is proportional to depth of cut [2]. Over 150 cutting tool passes would be required to cut a 1 mm groove while feeding the tool into the wheel by 6.35 um per pass. Moreover, the wheel must be raised after every pass to allow the tool to return to its initial position, then lowered again for the next pass of the cutting tool. This repeated movement of the grinding wheel introduced a need for a more efficient way of controlling the positioning of the grinding wheel, since manually adjusting the position of the grinding wheel after every pass of the cutting tool would be very time-consuming.

To address this need, a G-code program was written for the Fanuc 18i-M grinding machine controller. A flowchart describing this program and the variables associated with this program are shown in Appendix A. This program starts by rotating the grinding wheel at a desired velocity, turning on the coolant jet, and moving the grinding wheel to a pre-set zero-position with a z-axis offset. This zero-position is set to be the point at which the bottom dead center point of the front-face of the grinding wheel touches the back edge of the top of the grooving tool. The wheel is offset in the z-axis so that the wheel is not in contact with the tool when the tool is at its initial position. With the grinding wheel and grooving tool at their respective initial positions, the C program controlling the groover motion can be executed. The tool will then run across the width of the grinding wheel and stop shortly after the back edge of the wheel. Afterwards, the wheel is raised by a pre-set amount and the grooving tool is returned to its initial position. Once the grooving tool is back in its initial position, the wheel is lowered to a height which is one depth of cut (typically 6.35 um) lower than the previous pass. This process is then repeated until the

desired groove depth is achieved. This G-code program must be operated in "Single Block" mode. This mode allows only one line of code to execute at a time when the operator presses the "Start" button. This method was determined to be the simplest way of timing the raising and lowering of the grinding wheel; the user simply has to execute the C program triggering the groover motion, then press "Start" on the Fanuc controller which moves the wheel up, then return the groover to its initial position using C code, then press "Start" on the Fanuc controller again to move the wheel down, and so on.

CHAPTER 5: GROOVE GEOMETRY ANALYSIS

This chapter presents an analysis of the groove geometries for the grinding wheels used in this research. First, the tools used to groove the grinding wheels are discussed. Then, methods of computing the groove depth and the groove width of a grinding wheel based on wheel topography scans are introduced.

5.1 GROOVING TOOLS

One of the challenges involved in researching the effect of groove depth on grinding performance was to find a way to vary the depth of a groove without changing the other groove parameters (such as groove width). Many of the grooves presented in the grooved grinding wheel literature are parabolic in shape [18, 19, 37, 38, 40]. Figure 5.1 shows an image of a single-point dressing tool which is a type of tool that is commonly used for grooving and would clearly result in a parabolic-shaped groove with sloped sides. For a parabolic-shaped groove, the groove width changes with respect to groove depth so this shape would not be suitable for this research.

Figure 5.1: Single-point dressing tool

This research requires tools that can cut grooves whose width does not change with depth meaning that the width of the tool itself must not increase with depth. A tool in the shape of a rectangular prism or a cylinder would meet this requirement. It was found to be very difficult to find a tool in these shapes made entirely of diamond; however, polycrystalline diamond tools with these shapes do exist. Two different polycrystalline diamond tools were used to groove the grinding wheels studied in this research. One of them is cylindrically shaped with a width of 3.2 mm, and the other has the shape of a rectangular prism whose 1.7 mm edge was used for grooving. Side views and top views of these tools are shown in Figure 5.2 and Figure 5.3. These tools were purchased from Abrasive Diamond Tool Co.
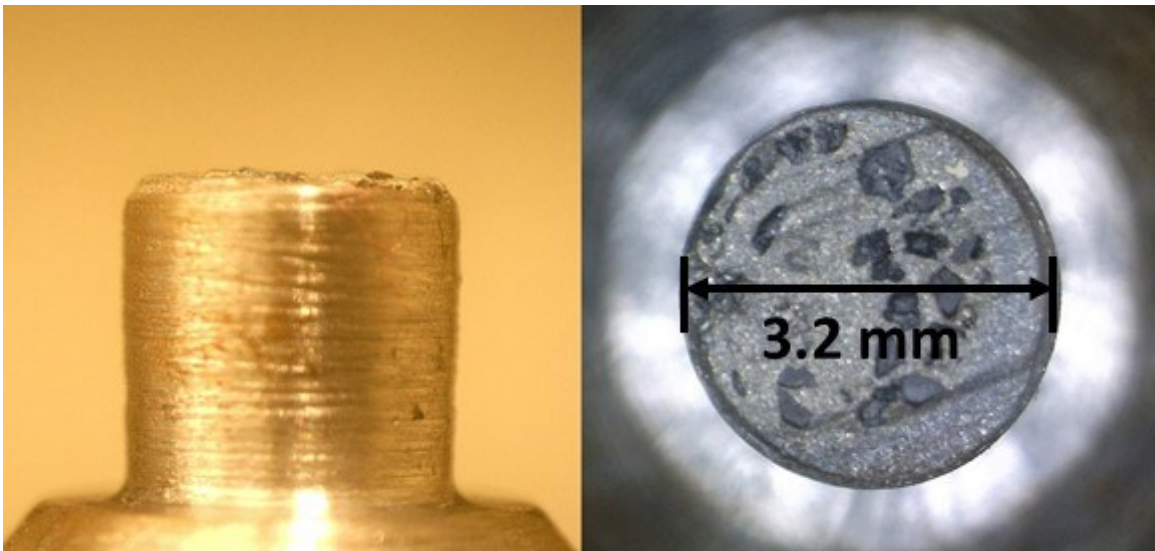
Figure 5.2: 3.2 mm wide cylindrical grit dressing tool used for grooving
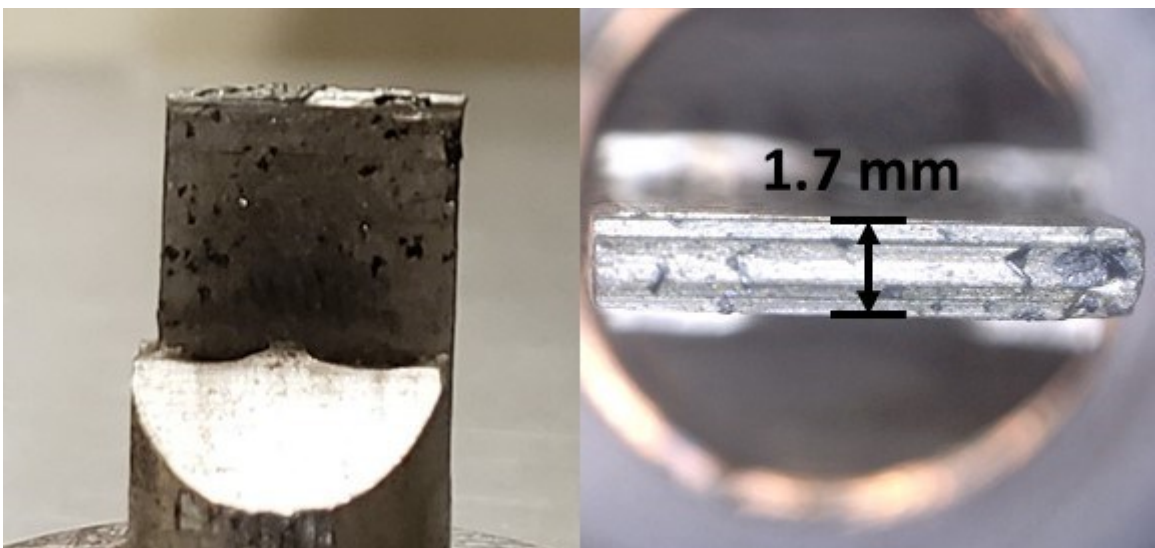
Figure 5.3: 1.7 mm wide shank grit dressing tool used for grooving

5.2 GROOVE DEPTH ANALYSIS

In the literature surrounding grinding with grooved wheels, no methods of measuring groove depth have been developed. Many researchers simply take the groove depth to be the commanded cutting depth of the groove when the groove is cut into the grinding wheel [3, 4]. The commanded groove depth, however, should not be taken as the actual groove depth for several reasons. The zero position of the grinding wheel is set by slowly lowering the grinding wheel until it first contacts the grooving tool, meaning that this point is the position at which the highest point in that area of the grinding wheel touches the highest point on the surface of the grooving tool. Therefore, when a groove is cut into the grinding wheel, the actual groove depth is slightly lower than the commanded depth because most of the cutting edges on the surface of the grooving tool lie slightly below the zero position, and most of the cutting edges on the surface of the grinding wheel lie slightly above the zero position. Essentially, the cutting surface of the grooving tool and the surface of the grinding wheel are not fully engaged when the tool is at the zero-position, which results in the actual groove depth being lower than the commanded groove depth. Furthermore, the height of the grooving tool changes as the tool wears, which results in a lower depth of cut than intended unless the zero position has been adjusted. Additionally, the grooving tool does not have a uniform surface. These factors result in error between the actual groove depth and the commanded groove depth and introduce a need for a method of measuring the groove depth.

To address this need, it was determined that the grooved grinding wheels should be scanned using the grinding wheel optical scanner, and that the groove geometry should be determined algorithmically using the scan data. Therefore, a grinding wheel was grooved with the groove parameters listed in Table 5.1.

43

Table 5.1: Grooving process parameters

Parameter	Value
Wheel speed (RPM)	150
Groover speed (µm/s)	18000
Number of wheel revs per pass	3.6
Commanded groove depth (µm)	900
Depth of cut per pass (µm)	6.35
Number of tool passes	140
Cutting tool width (µm)	3200

A scan of the grooved grinding wheel was then taken. This is the same scan that has been shown previously in Figure 4.5. Given this scan data, the next challenge was to find a way to process the data in such a way that ascertains the groove depth. It was decided that the groove depth would be defined as the difference between the position of the cutting edges at the surface of the wheel and the position of the cutting edges within the grooves. The positions of the cutting edges at the wheel surface and within the groove will be referred to as the "surface height" and the "groove height", respectively. Therefore, the groove depth would be the difference between the surface height and the groove height. The cutting edges are the collection of grains with the highest protrusion heights and these are the grains that participate in the material removal process. In order to maintain a constant groove factor, none of the grains within the grooves can be involved in the cutting process which is why this definition for groove depth was chosen; if the groove height was taken as a value lower than the cutting edge height, then it is possible that at low groove depths the grains within the grooves could be active in the cutting process in which case any changes in grinding performance could no longer be singularly attributed to changes in groove depth. Given this methodology, the problem then becomes: how does one determine the cutting edge height?

A few examples of methods that were considered to determine cutting edge height, as well as the approximated locations of potential cutting edges, are displayed in Figure

5.4. One method was to average all the points at the wheel surface and then average all the points within the grooves and take the difference between these two numbers to be the groove depth. Another suggested method was to take the difference between the highest point at the wheel's surface and the highest point within a groove as the groove depth. Taking the difference between the median of the points at the wheel's surface and the median of the points within a groove was also contemplated. Using these methods, the groove depth would be 703.9 um, 610.5 um, and 712.8 um respectively.
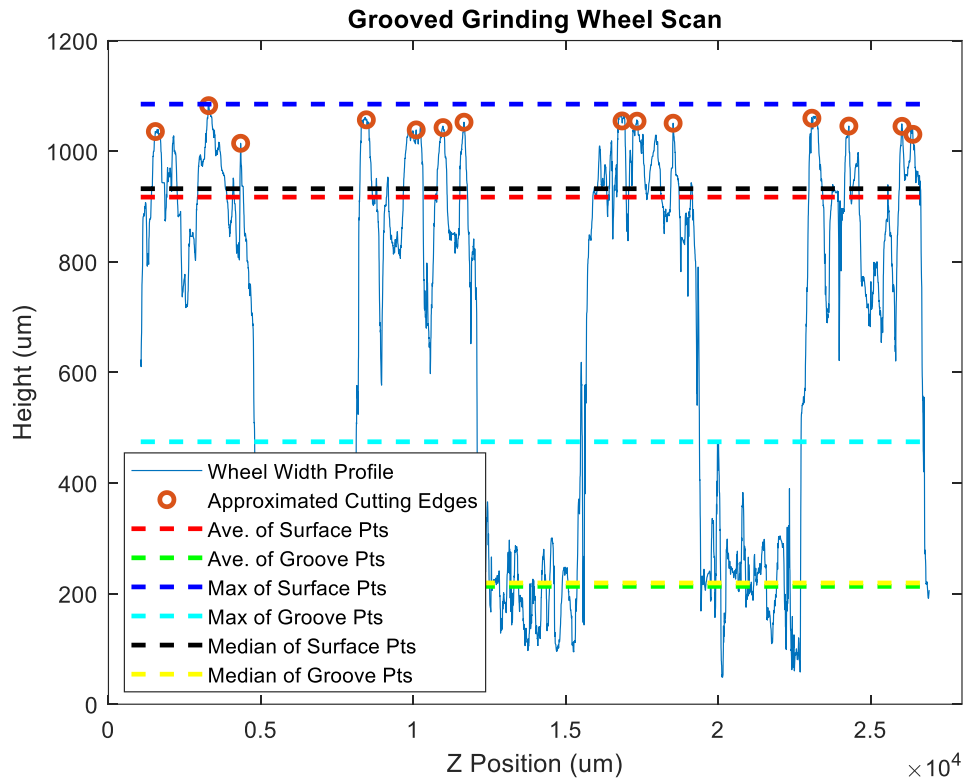
Figure 5.4: Wheel scan showing methods to determine cutting edge height

It is evident from Figure 5.4 that these methods are inadequate for determining the cutting edge height since the average and median lines are clearly well below where most of the cutting edges lie, and the maximum line is well above where the majority of the cutting edges lie. Therefore, the real cutting edge height is slightly below the maximum grain height. It was then decided that the cutting edge height would be taken as the 95th percentile of all points located at the wheel surface. The following methodology was then developed using MATLAB to compute the groove depth:

1) Manually choose boundaries of surface points and groove points, shown as the black and red lines respectively in Figure 5.5, to include as many points as possible while omitting the points at the groove edges.
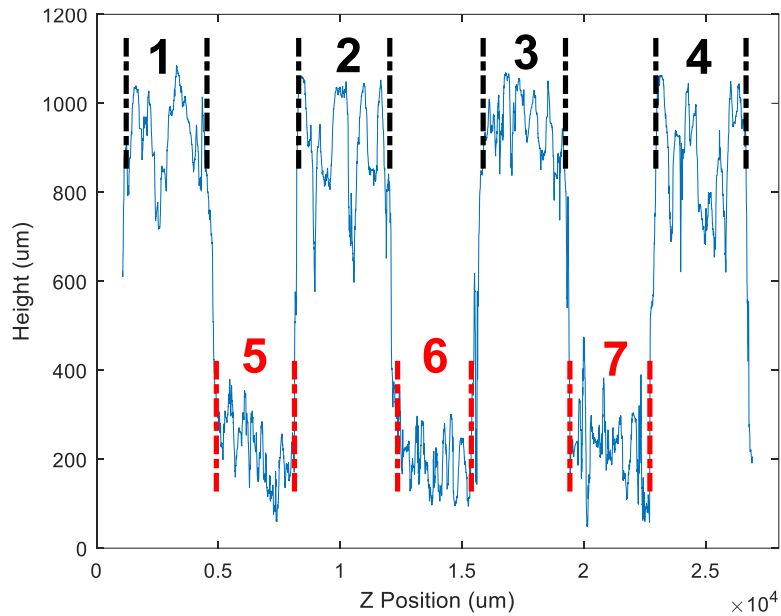
Figure 5.5: Wheel scan showing boundaries of surface and groove points

2) Concatenate the points within the boundaries into two separate arrays: one array for the points at the surface of the wheel and one array for the points inside the grooves. Figure 5.6 shows plots of these two arrays.
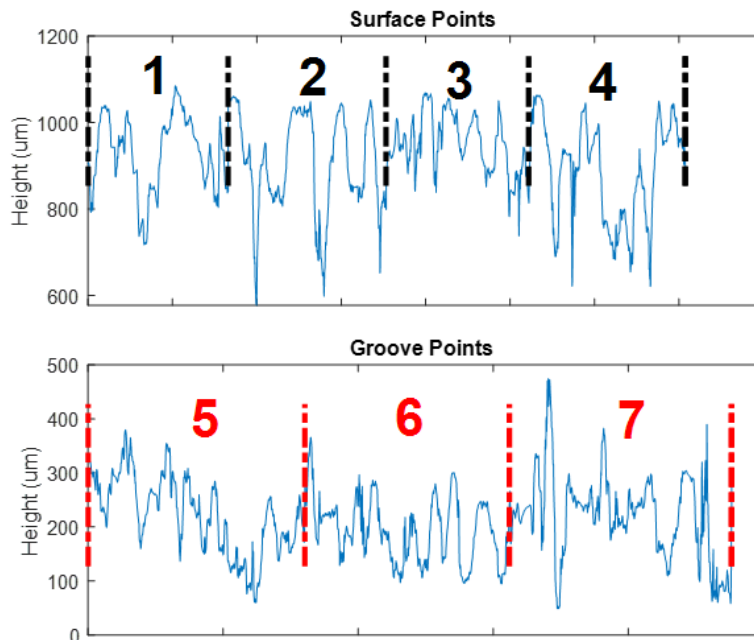
Figure 5.6: Arrays of surface points and groove points

3) Take the 95th percentile of both arrays to get the surface height and the groove height. In Figure 5.7, the surface height and the groove height are indicated by the black and red lines respectively.
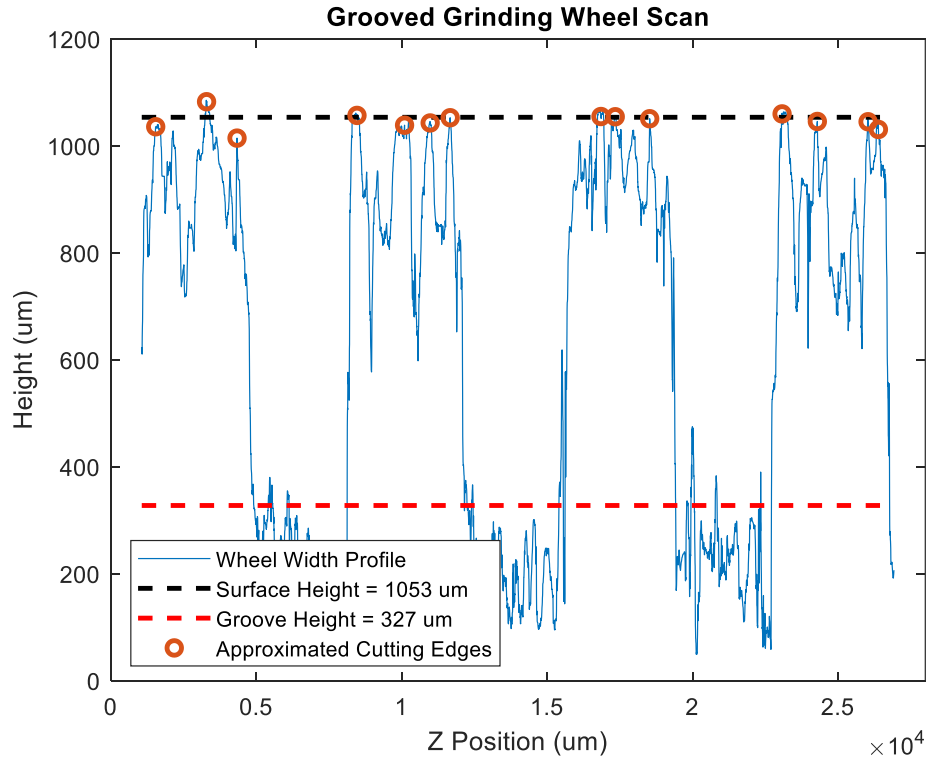
Figure 5.7: Wheel scan showing calculated surface height and groove height

4) Take the difference between the surface height and the groove height to get a representative value of the groove depth.

$$\text{Groove depth} = 1053 \ \mu\text{m} - 327 \ \mu\text{m} = \textbf{726 } \boldsymbol{\mu}\textbf{m}$$

Using this method, there is a 174 μm difference between the commanded groove depth of 900 μm and the measured groove depth of 726 μm for this example. Based on Figure 5.7, it is clear that this method of determining the cutting edge height is in much better agreement with the heights of the approximated cutting edges than the methods discussed previously. Now that a method of determining groove depth has been established, two other important parameters pertaining to groove geometry must be discussed: groove width and groove factor.

5.3 GROOVE WIDTH ANALYSIS

The previous section began by pointing out that many researchers assume that the groove depth is equal to the commanded depth of cut when the groove is cut and ended by showing that there is a fair bit of error between the measured groove depth and the commanded depth of cut. Similarly, many researchers assume that the groove width is equal to the width of the grooving tool [3, 4]. This section presents a method of measuring groove width and groove factor to determine how much these two values change with respect to groove depth. The measured groove width and groove factor are also compared with the estimated groove width based on the tool width, and the estimated groove factor based on the grooving parameters to verify the accuracy of these estimates.

Based on the grooving parameters listed in Table 5.1, it is possible to estimate the groove width and groove factor for this grinding wheel using the grinding wheel speed, the groover speed, and the tool width. It is estimated that the groove width is 3.2 mm (same as the tool width), and that the groove factor is 55.5%. The groove factor was obtained by calculating the time for the grooving tool to traverse the width of the grinding wheel using the groover speed and the wheel width. This time was then multiplied by the grinding wheel period to get the number of groove encirclements of the grinding wheel which was found to be about 3.6 for this wheel. This value was then multiplied by the tool width to get the total amount of wheel width that was grooved, and the resulting value was then used to get the groove factor by dividing it by the wheel width.

The groove width and the groove factor were also measured using the same scan data from Figure 4.5. Lines of best fit, shown in Figure 5.8 as black dash-dotted lines, were matched to the groove edges. The groove edges at the surface of the wheel were taken as the intersection points of the lines of best fit and the surface height line. Similarly, the groove edges at the base of the grooves were taken as the intersection points of the lines of best fit and the groove height line. The groove width was then taken to be the difference between adjacent groove edges. The resulting data for this example is shown in Table 5.2.
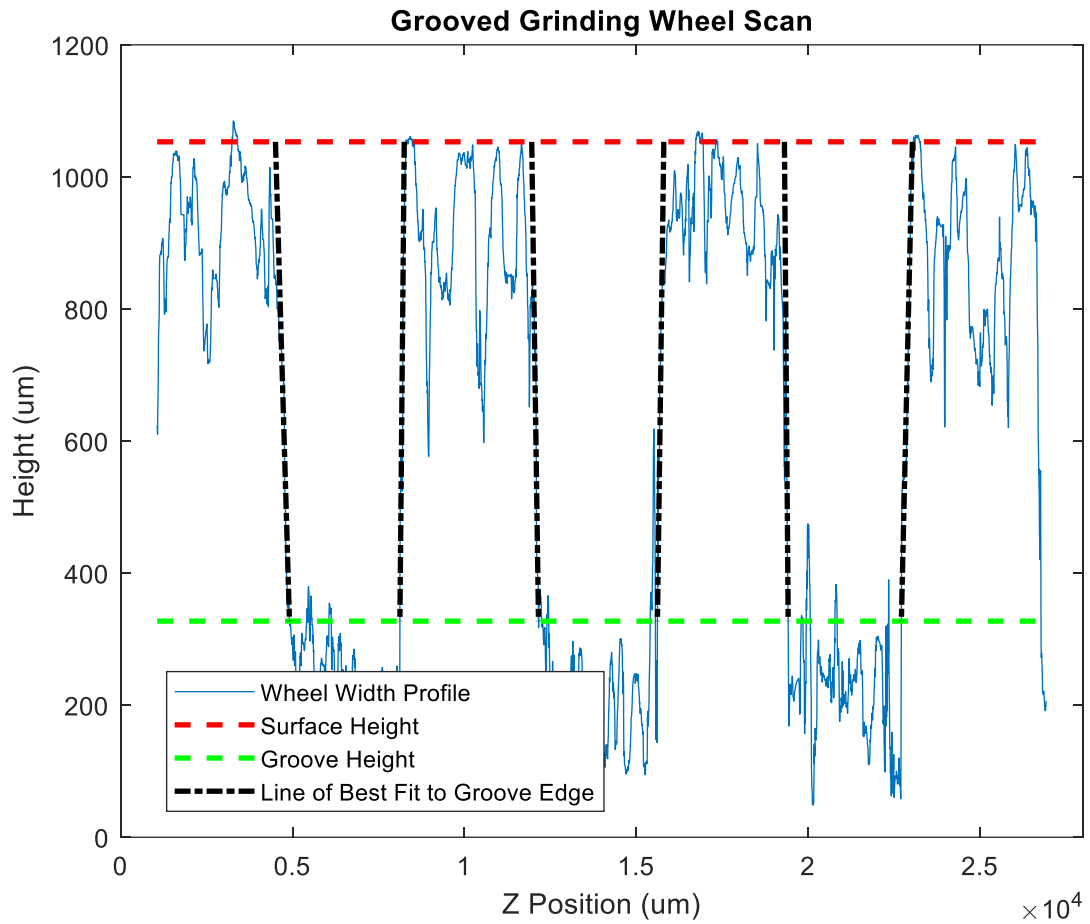
Figure 5.8: Wheel scan showing groove width lines

Table 5.2: Groove geometry parameters

Parameter	@ Wheel Surface	@ Base of Groove
Groove Width (um)	3770.6	3322.2
Est. Groove Width (um)	3200	3200
Groove Width Error (%)	15.1	3.7
Groove Factor (%)	47.6	53.9
Est. Groove Factor (%)	55.5	55.5
Groove Factor Error (%)	16.6	3.0

The grooves are roughly 450 μm wider at the surface of the wheel than at the base of the groove: a change of only 12%. This results in a 6.3% change in groove factor between the surface of the wheel and the base of the groove. Based on the tool geometry, the grooves should be perfectly square; however, they are in fact slightly trapezoidal. It is likely that the error between the tool geometry and the groove geometry are caused by small fluctuations in grinding wheel speed and groover speed during grooving, as well as minute inaccuracies in the triggering of the groover motion.

The measured groove width and groove factor at the bottom of the groove show good agreement with the same estimated values discussed at the beginning of this section. Between the estimated and measured values for groove width and groove factor there is 3.7% and 3.0% error, respectively. This result confirms that the grooving process is working as intended, and that the grooving tool is indeed retracing the same path on every tool pass with minimal error. However, the error between the estimated and measured values for the groove width and groove factor at the surface of the wheel is significant. At the surface of the wheel, there is 15.1% and 16.6% error between the estimated and measured values of groove width and groove factor, respectively.

These findings show that the error between the estimated groove geometry and the measured groove geometry at the wheel surface increases as the groove depth increases. Therefore, it may be acceptable to assume that the groove geometry is equal to the grooving tool geometry for shallow grooves (<100 μm). However, for grooves deeper than 100 μm, the present author recommends that the groove geometry be measured, and that the groove width and groove factor be determined from the measurements.

CHAPTER 6: RESULTS AND ANALYSIS

This chapter presents the results obtained throughout the grinding experiments performed for this research and provides analyses on the significance of these results. First, the results for preliminary proof of concept experiments will be presented. Then, the experimental procedure for the primary experiments will be discussed. Following this discussion, an analysis of the groove geometry for the grinding wheels used throughout the experiments will be presented. Finally, the main results for the primary experiments are introduced accompanied by a discussion on the meaning of these results.

6.1 PROOF OF CONCEPT

Up until now, there has not been any published research investigating the effect of groove depth on grinding performance. It is unknown whether groove depth is an important parameter to consider when grooving a grinding wheel. Before embarking on an extensive experimental study into the effects of groove depth in grinding, it was decided that a series of quick and simple proof of concept experiments would be performed to ensure that groove depth is a subject that is worthy of further investigation.

To test whether groove depth has any influence on grinding performance, multiple creep-feed grinding experiments were performed for wheels having various groove depths. Creep-feed grinding was chosen over surface grinding for these experiments since it has been shown that grooved grinding wheels tend to leave small ridges on the workpiece surface and that the height of these ridges is proportional to feed rate [40]. These ridges are generally undesirable since they increase the workpiece surface roughness. The higher the ridges, the greater the increase in workpiece surface roughness. In creep-feed grinding where the feed rate is very low, the height of the ridges caused by the grooved grinding wheel is also very low, so the adverse effects of the ridges on workpiece surface roughness are minimized. Therefore, creep-feed grinding seems like an excellent niche area for the application of grooved grinding wheels.

An example of the force data collected during a creep-feed grinding experiment is shown in Figure 6.1. This figure shows tangential, transverse, and normal force data. An example of the spindle power data collected during a creep-feed grinding experiment is shown in Figure 6.2. Force and power data sets such as these were collected for each experiment performed for this research. It can be seen from Figure 6.1 that the forces sharply increase when the grinding wheel comes into contact with the AISI 4140 workpiece, which occurs in Figure 6.1 at around 25 seconds into the experiment. Once the wheel is fully engaged in the workpiece, there is about 60 seconds of grinding. Then, at around 95 seconds into the experiment from Figure 6.1, the forces rapidly decline as the grinding wheel reaches the end of the workpiece. Subsequent sections show figures such as "force vs groove depth" or "power vs groove depth". The force and power data points for these graphs were obtained by averaging the middle 30 seconds of the grinding data for each experiment, as shown in Figure 6.1 and Figure 6.2. Doing this averaging yields single values that are representative of the average power and average forces for each grinding experiment.
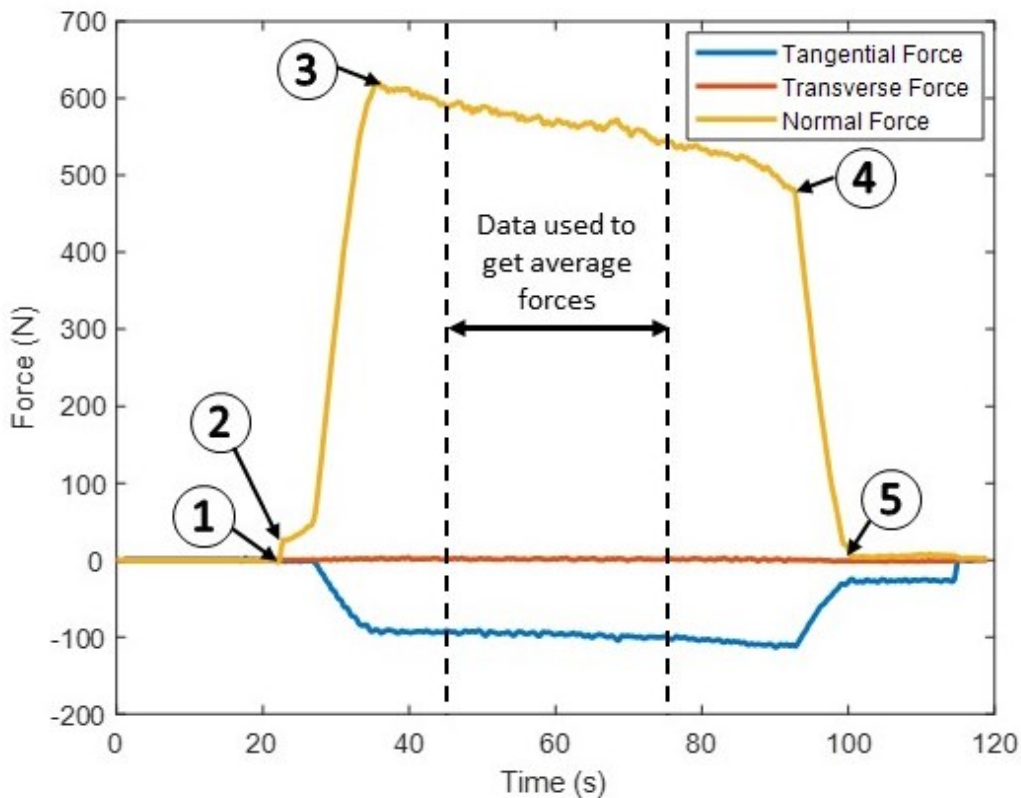
Figure 6.1: Forces vs time for a creep-feed grinding experiment
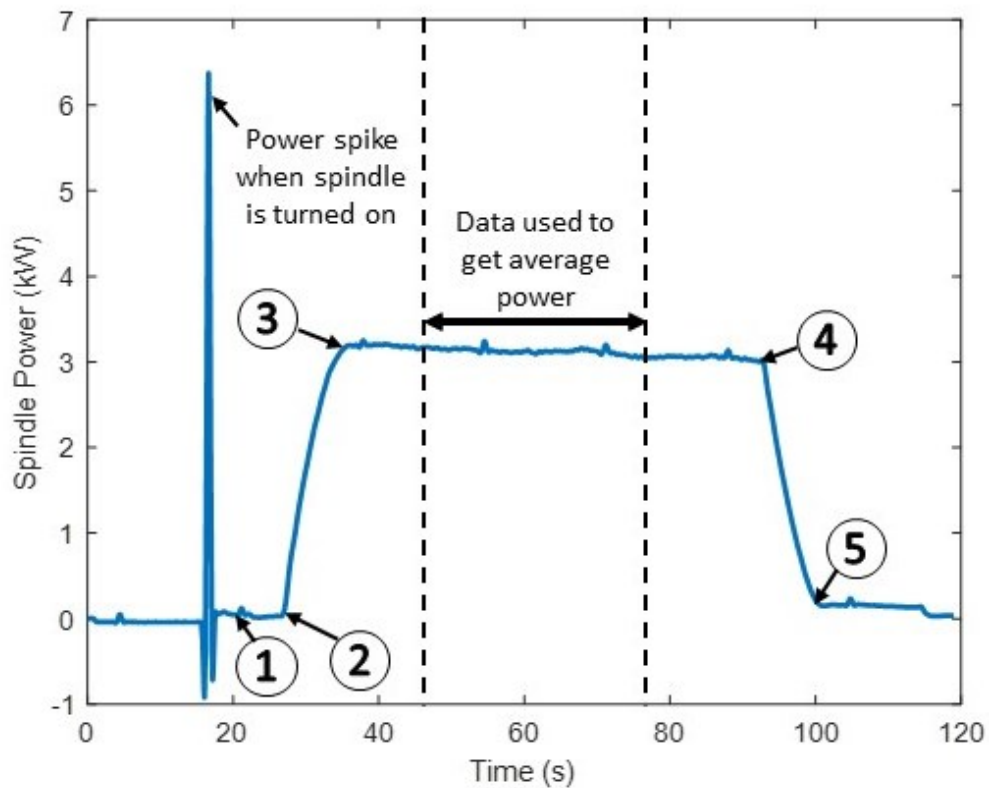
① Coolant jet begins to strike the workpiece

② Wheel makes contact with the workpiece and contact length begins to increase

③ Wheel is fully engaged in the workpiece and maximum contact length is achieved

④ Wheel approaches the end of the workpiece and contact lengths begins to decrease

⑤ Wheel is no longer in contact with the workpiece

Figure 6.2: Spindle power vs time for a creep-feed grinding experiment

For this set of proof of concept experiments, the same grinding wheel whose groove geometry was analyzed in Chapter 5 was used in a series of creep-feed grinding experiments. Groove depths of approximately 624, 312, 100, and 0 μm were tested, where a groove depth of 0 μm signifies a non-grooved wheel. The experiments proceeded in order of decreasing groove depth; the deepest groove depth was tested first, then the wheel was dressed to reduce the groove depth to the next desired value. The dressing process reduces the radius of the grinding wheel, which effectively reduces the groove depth. Two experiments were performed at each groove depth for a total of eight experiments. The grinding and dressing conditions for these experiments are listed in Table 6.1. Grinding

forces and spindle power data were collected for each experiment. Normal force, tangential force, and spindle power are plotted in Figure 6.3, Figure 6.4 and Figure 6.5, respectively. The markers in these figures correspond to the data from the individual experiments and the lines are plotted through the average value for the two experiments at each groove depth. A depth of cut of 0.5 mm was chosen for these experiments because it was found through a series of preliminary experiments that, for the selected grinding parameters and workpiece dimensions, a depth of cut greater than 0.5 mm would result in workpiece burn when using a non-grooved wheel.

Table 6.1: Grinding and dressing parameters for proof of concept experiments

Parameter	Value
Feed Rate (mm/s)	1.7
Depth of Cut (mm)	0.5
Wheel Speed (mm/s)	22400
Overlap Ratio	10
Dressing Amount (μm)	10
Spark Out Passes	5
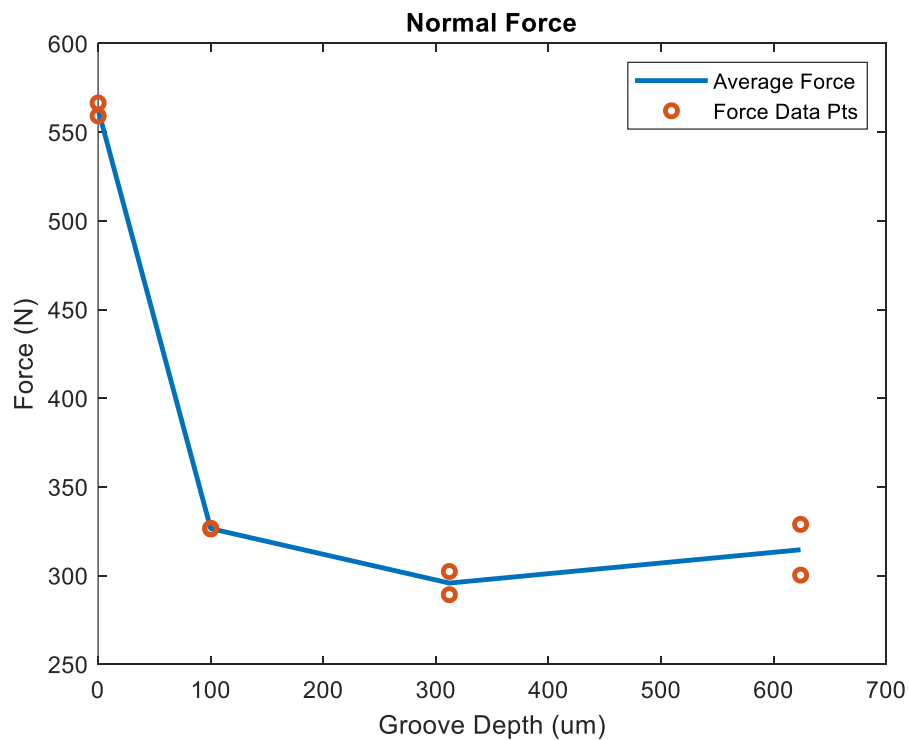
Figure 6.3: Normal force vs groove depth for proof of concept experiments
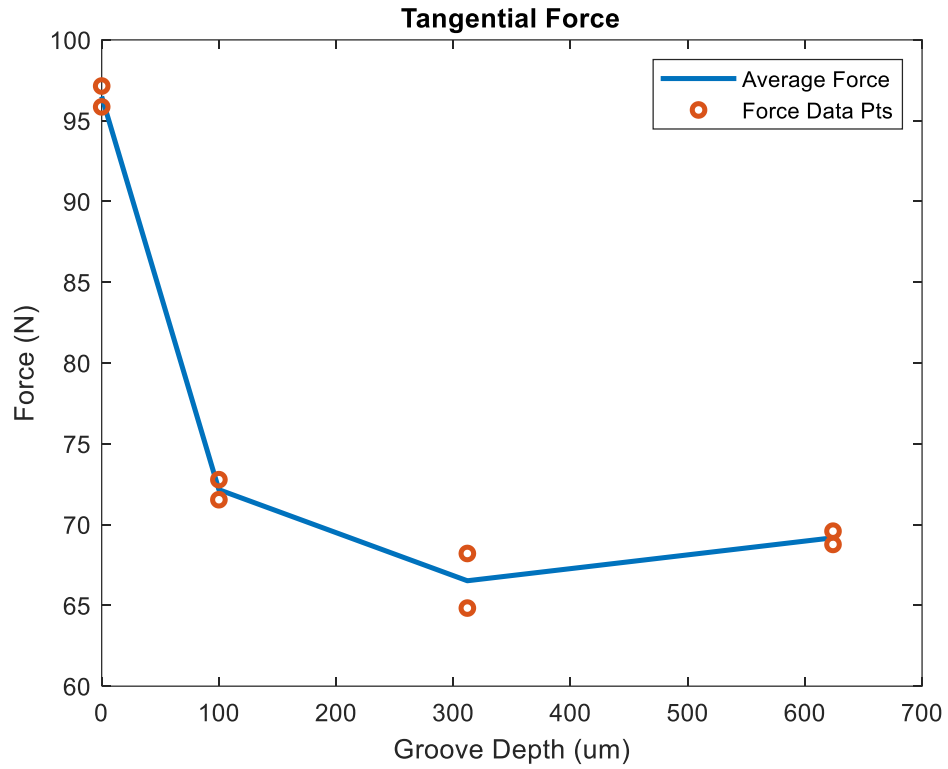
Figure 6.4: Tangential force vs groove depth for proof of concept experiments
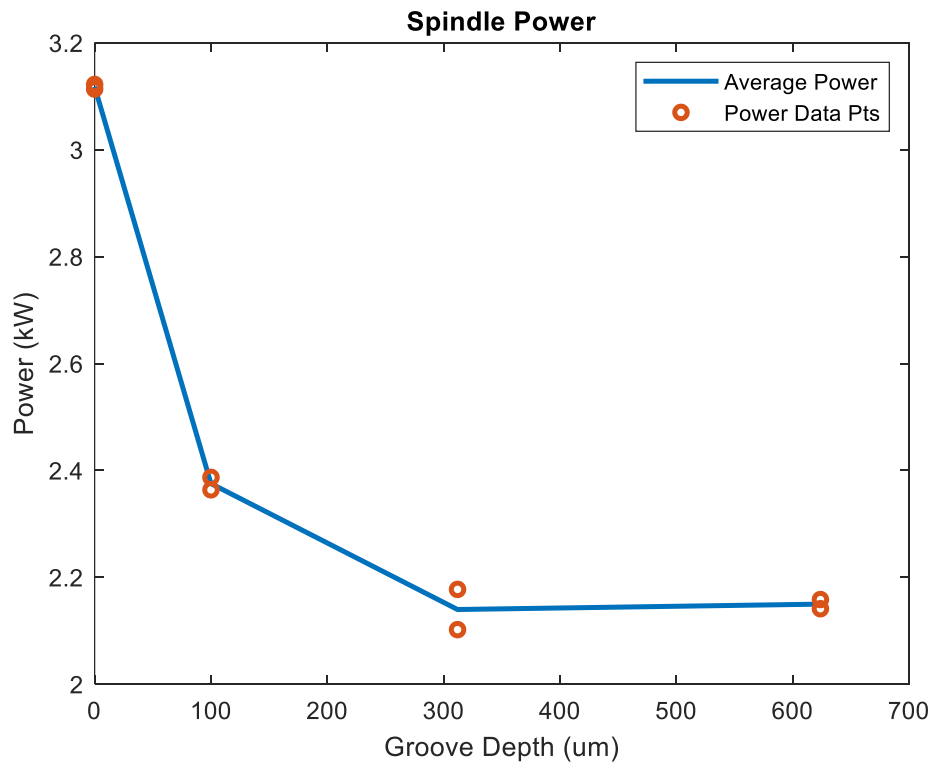
Figure 6.5: Spindle power vs groove depth for proof of concept experiments

55

As can be seen from Figure 6.3, Figure 6.4, and Figure 6.5, the power and forces experience a sharp decline between groove depths of 0 (non-grooved wheel) and 100 μm. This decline is expected since it is known that a grooved wheel performs much better than a conventional wheel. However, to reiterate the objective of this proof of concept, what is not known is how grooved wheels with different groove depths compare to each other. Interestingly, the power and forces continue to decline between groove depths of 100 and 312 μm. Between groove depths of 312 and 624 μm, there seems to be little change in power and forces.

These results seem to indicate that there exists a groove depth beyond which deeper grooves provide no additional reduction in power and forces. For the data presented above, this groove depth appears to be at 312 μm. However, not enough data was collected during these experiments to properly define the curve or to make any conclusive statements about what the data means. Nevertheless, this proof of concept was successful because it indicates that groove depth is a parameter that needs to be considered when designing grooved grinding wheels since different groove depths yield different results.

6.2 EXPERIMENTAL PROCEDURE

Following this proof of concept, the next step was to perform a more thorough investigation on the effects of groove depth by doing more grinding experiments with a greater number of different groove depths, and a larger range of groove depths. The AISI 4140 steel workpieces were also collected, and surface roughness measurements were taken to verify whether groove depth has any influence on workpiece surface roughness.

It was decided that groove depths ranging from 0 to about 1100 μm would be tested for the next series of experiments. This range of groove depths was chosen because the goal was to expand the range of groove depths tested in the proof of concept experiments, while still considering the time required for the grooving process. A 1100 μm deep groove requires a commanded groove depth of about 0.05" and each pass of the grooving tool penetrates into the wheel by 0.00025" more than the previous pass. Therefore, it takes 200 passes of the grooving tool to groove a wheel to a commanded groove depth of 0.05", so

this process can be quite time-consuming. Furthermore, based on the proof of concept experimental results, it appeared as though grooving deeper than 312 μm did not appear to have much of an effect on grinding performance meaning that grooving much deeper than this value may be unnecessary.

It was decided that a total of nine groove depths would be tested. For groove depths ranging between 500 – 1100 μm, three sets of experiments would be performed in which the groove depth decreases by about 200 μm for each set of experiments. For groove depths ranging between 0 – 500 μm, five sets of experiments would be performed in which the groove depth decreases by about 100 μm for each set of experiments. Then, one final set of experiments would be performed for a non-grooved wheel. Based on the proof of concept results, it appeared as though most of the changes in power and forces would occur for groove depths ranging between 0 – 500 μm and that there would not be much change in power and forces for groove depths ranging between 500 – 1100 μm. This reasoning is why more experiments are performed in the 0 – 500 μm range than the 500 – 1100 μm range.

It was also decided that three different depths of cut would be tested for these experiments to determine whether there is a relationship between groove depth and depth of cut. The idea here was that perhaps shallow grooves are sufficient for shallow depths of cut and that deep grooves may be necessary for larger depths of cut. Depths of cut of 0.5, 0.3, and 0.1 mm were tested for every groove depth. In total, 27 sets of experiments were performed which is the product of nine groove depths and three depths of cut. A minimum of two experiments were performed for each set of experiments. If the data from the first two experiments did not agree well with each other, then more experiments were performed to help ensure the repeatability of the results.

Two large series of experiments were performed following the procedure detailed above for two grinding wheels having different groove widths, but the same groove factor. The two series of experiments will be referred to as "experiment series A" and "experiment series B" throughout this thesis. For experiment series A, the grinding wheel that was used for every experiment had been grooved using the 3.2 mm polycrystalline diamond tool from Figure 5.2. For experiment series B, the grinding wheel that was used for every

experiment had been grooved using the 1.7 mm polycrystalline diamond tool from Figure 5.3. The purpose of doing the same series of experiments with two grinding wheels having different groove widths is to study whether different results are observed for the different groove widths. A total of 71 experiments were performed for experiment series A and a total of 63 experiments were performed for experiment series B.

Similarly to the procedure for the proof of concept experiments, the grinding wheels were initially grooved to the deepest groove depth. The groove depth was then gradually reduced between experiments by dressing the grinding wheel. From the beginning to the end of the experiments, the grinding wheel diameter was reduced by only ~1.4 mm which is a 0.4% change in wheel diameter. This reduction in wheel diameter results in a change in uncut chip thickness of only 0.2%. Therefore, the change in wheel diameter on grinding results is negligible. The grinding parameters and dressing parameters for these experiments are shown in Table 6.2. To transition from one range of groove depths to the next range of groove depths, it was necessary to dress off more than 10 μm of wheel radius. For example, upon completing the grinding experiments for a groove depth range of 700 – 900 μm, it is necessary to dress off a certain amount of wheel radius to get a groove depth in the next range of 500 – 700 μm. At these times, the wheel was roughly dressed down to a radius of 10 μm more than the desired groove depth at a dressing infeed of 6.35 μm. Then, the final 10 μm was dressed off using the fine dressing parameters listed in Table 6.2.

Table 6.2: Grinding and dressing parameters for grinding experiments

Parameter	Value
Feed Rate (mm/s)	1.7
Depth of Cut (mm)	0.5, 0.3, 0.1
Material Removal Rate (mm^3/s)	10.8, 6.5, 2.2
Wheel Speed (mm/s)	22400
Dressing Overlap Ratio	10
Dressing Amount (μm)	10
Dressing Infeed (μm)	5
Spark Out Passes	5

6.3 GROOVE GEOMETRY

6.3.1 Initial Groove Geometry

The first step in performing a series of grooved grinding wheel experiments is to groove a grinding wheel. The grinding wheels used for experiment series A (grinding wheel A) and experiment series B (grinding wheel B) were grooved using the 3.2 mm wide and 1.7 mm wide grooving tools, respectively. The grooving parameters used to groove the grinding wheels are listed in Table 6.3.

Table 6.3: Grooving parameters for grinding experiments

Parameter	Experiments A	Experiments B
Tool Width (mm)	3.2	1.7
Groover Velocity (mm/s)	18	10.125
Wheel Diameter (mm)	386.73	389.12
Wheel RPM	150	150
Commanded Groove Depth (µm / in)	1397 / 0.055	1270 / 0.050
Groover Infeed (µm / in)	6.35 / 0.00025	6.35 / 0.00025
# of Groover Passes	220	200

Once the grinding wheel was grooved, it was then removed from the grinding machine and scanned using the grinding wheel scanning system. The resulting scans were then analyzed following the procedure outlined in Chapter 5 to get an idea of the groove geometry for these grinding wheels. The grinding wheels were scanned in three separate places that were spaced roughly 120° apart along the circumference of the wheel. The groove geometry values were then computed separately for the three scans and averaged. An example of one of the topography scans that was taken for the grinding wheel used in experiments A and for the grinding wheel used in experiments B are shown in Figure 6.6 and Figure 6.7, respectively. The rest of the initial wheel topography scans can be found in Appendix B. Note that the red and green dashed lines shown in Figure 6.6 and Figure 6.7 represent the heights used to compute the groove depth for those scans. Similarly, the black dashed lines shown in Figure 6.6 and Figure 6.7 represent the lines used to calculate the

groove width for those scans. Figure 6.8 shows images of the two grinding wheels whose topography scans were shown in Figure 6.6 and Figure 6.7. Table 6.4 lists the groove geometry parameters for the two grinding wheels used in experiments A and B.
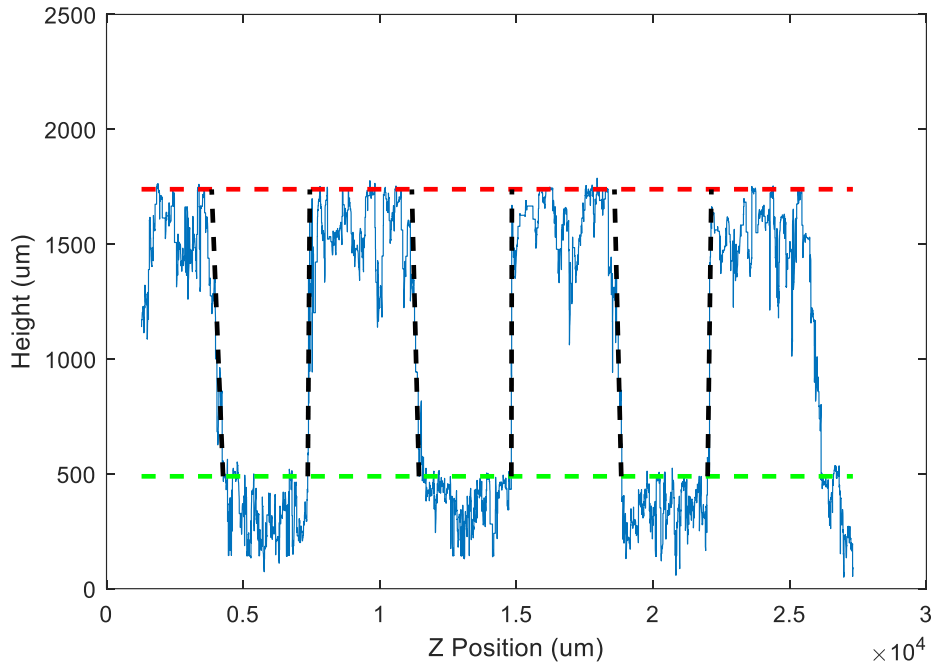
Figure 6.6: Initial topography scan of grinding wheel A (1/3)
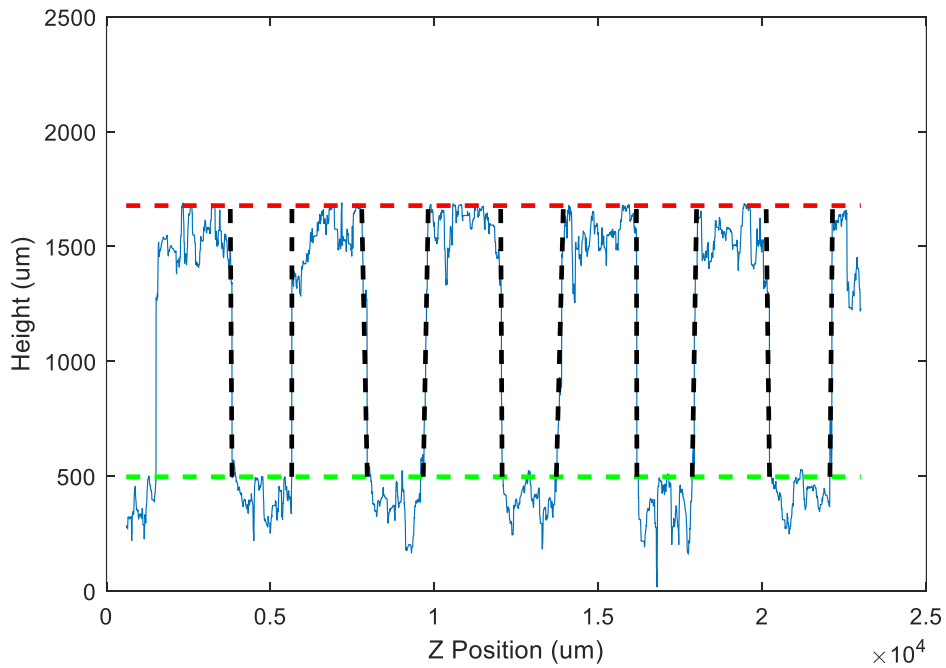
Figure 6.7: Initial topography scan of grinding wheel B (1/3)
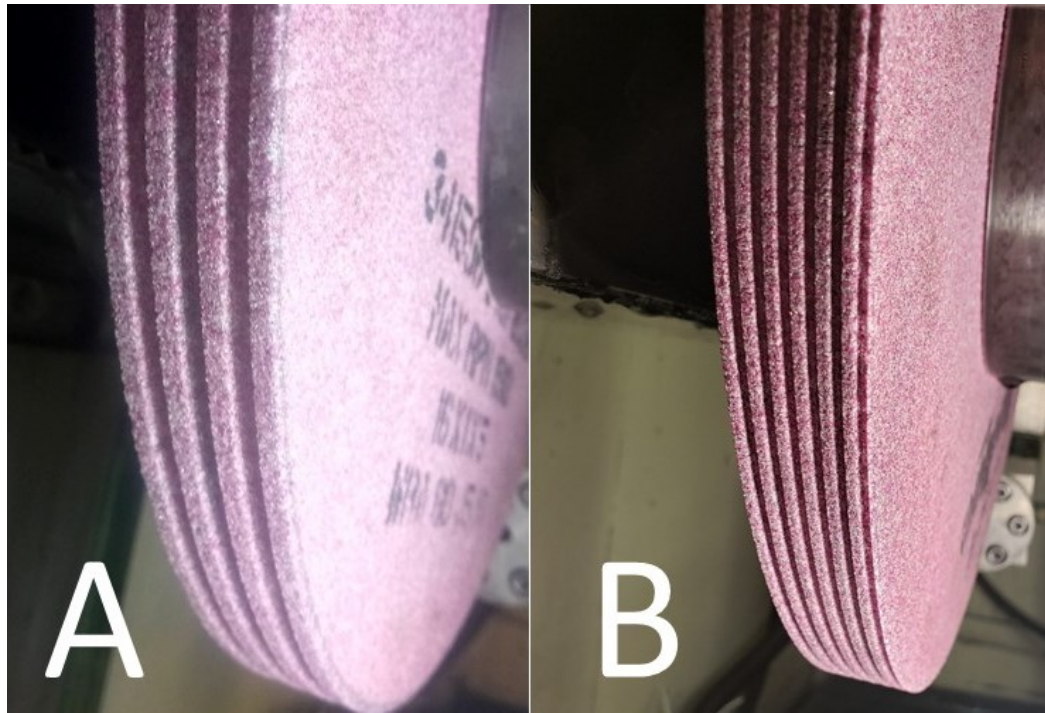
Figure 6.8: Images of the grinding wheels used for experiments A (left) and B (right)

Table 6.4: Groove geometry parameters based on initial scans

Parameter	Units	Wheel A	Wheel B
Commanded Groove Depth	µm	1397	1270
Groove Depth (Measured)	µm	1240.2	1187.6
Difference	µm	156.8	82.4
% Difference (Groove Depth)	%	11.2	6.5
Groove Width (Top)	µm	3738.5	1953.6
Groove Width (Bottom)	µm	3209.8	1708.2
% Difference (Groove Width)	%	14.1	12.6
Groove Factor (Top)	%	48.1	51.8
Groove Factor (Bottom)	%	55.4	57.8
Difference (Groove Factor)	%	7.3	6.0
Number of Grooves	-	1	1
Number of Encirclements	-	3.6	6.4
Helix Angle	°	88.9	89.4
Groove Pattern	-	Circumferential	Circumferential

As can be seen in Table 6.4, the measured groove depths are 156.8 µm and 82.4 µm less than the commanded groove depths for the grinding wheels used in experiments A and B, respectively. The higher error between commanded and measured groove depth for the grinding wheel used in experiment series A can likely be attributed to two things. First, the grooving tool used to groove wheel A likely wears faster than the tool used to groove wheel B. Second, the grooving tool used to groove wheel A has a rougher surface than the tool used to groove wheel B, so the wheel must descend further onto the tool for the full width of the tool to penetrate into the grinding wheel.

Another observation about the data presented in Table 6.4 is that the groove widths for grinding wheels A and B decrease by 14.1% and 12.6%, respectively, from the surface of the grinding wheel to the bottom of the groove. This decrease in groove width results in increases in groove factor of 7.3% and of 6.0% for grinding wheels A and B, respectively. As a result of this increase in groove factor, one might expect the power and forces throughout the grinding experiments to slightly increase as groove depth decreases. However, it remains to be seen whether this increase in groove factor will show itself in the experimental results. It is also interesting to note that the groove widths at the bottom of the grooves for both grinding wheels almost perfectly match the widths of the tools that were used to groove them; recall that the widths of the tools used were 3.2 mm and 1.7 mm for grinding wheels A and B, respectively. The grinding wheels used for these experiments had a circumferential groove pattern, meaning that they had a single groove that encircled the grinding wheel multiple times. The helix angles of the two grinding wheels only differed by 0.5°. The grooves for grinding wheels A and B encircled the wheels 3.6 and 6.4 times, respectively.

6.3.2   Intermediate Groove Geometry

Partway through each series of experiments, the grinding wheels were removed from the grinding machine and once again scanned using the grinding wheel scanning system. The purpose of doing these scans was to verify whether the grooves were maintaining their groove geometry after being subject to the grinding process. What one would hope to see

with these scans is that the measured groove geometry parameters are consistent with what one would expect them to be based on the initial scans presented in the previous section. It is important to ensure that the groove geometry is maintained so that the results of the experiments can be attributed solely to changes in groove depth and are not caused by changes in other groove geometry parameters.

The grinding wheels were removed after the first three sets of experiments. The groove depth at this point for each wheel lies in the 500 – 700 μm range. Once again, the grinding wheels were scanned in three separate places that were spaced roughly 120° apart along the circumference of the wheel and the groove geometry values were then computed separately for the three scans and averaged. An example of one of the intermediate topography scans that were taken for grinding wheel A and for grinding wheel B are shown in Figure 6.9 and Figure 6.10, respectively. The rest of the intermediate topography scans can be found in Appendix C. Table 6.5 lists the measured intermediate groove geometry parameters for the two grinding wheels used in experiments A and B.
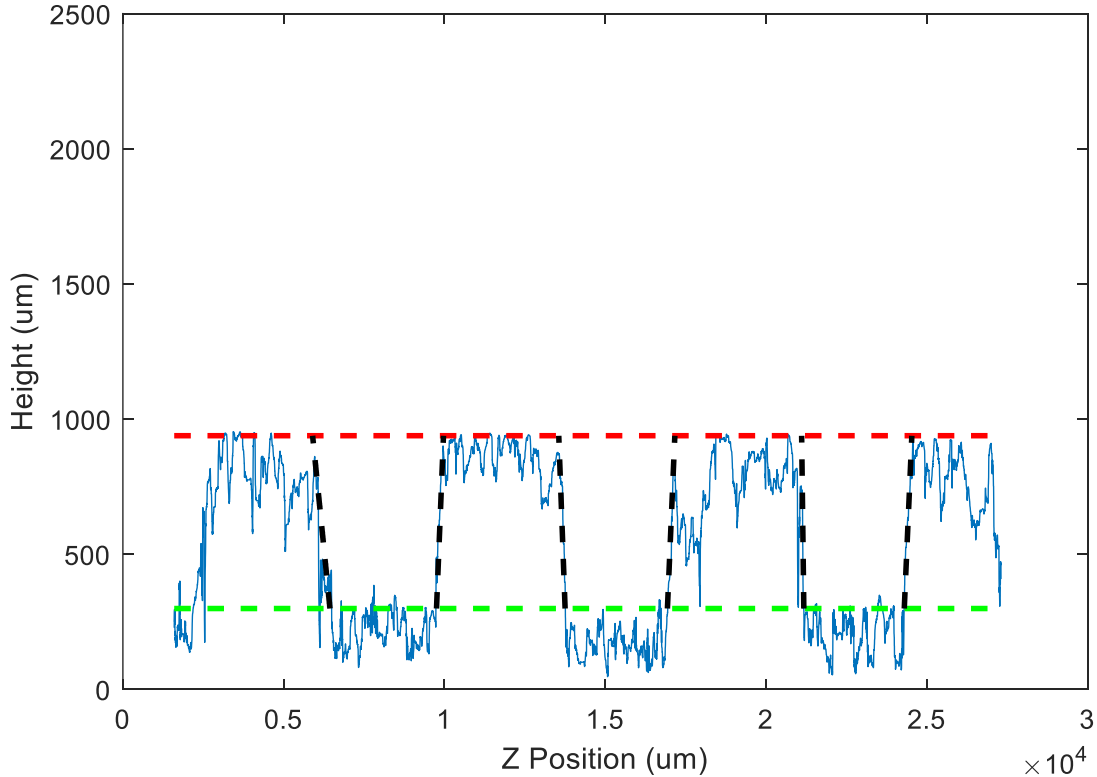
Figure 6.9: Intermediate topography scan of grinding wheel A (1/3)
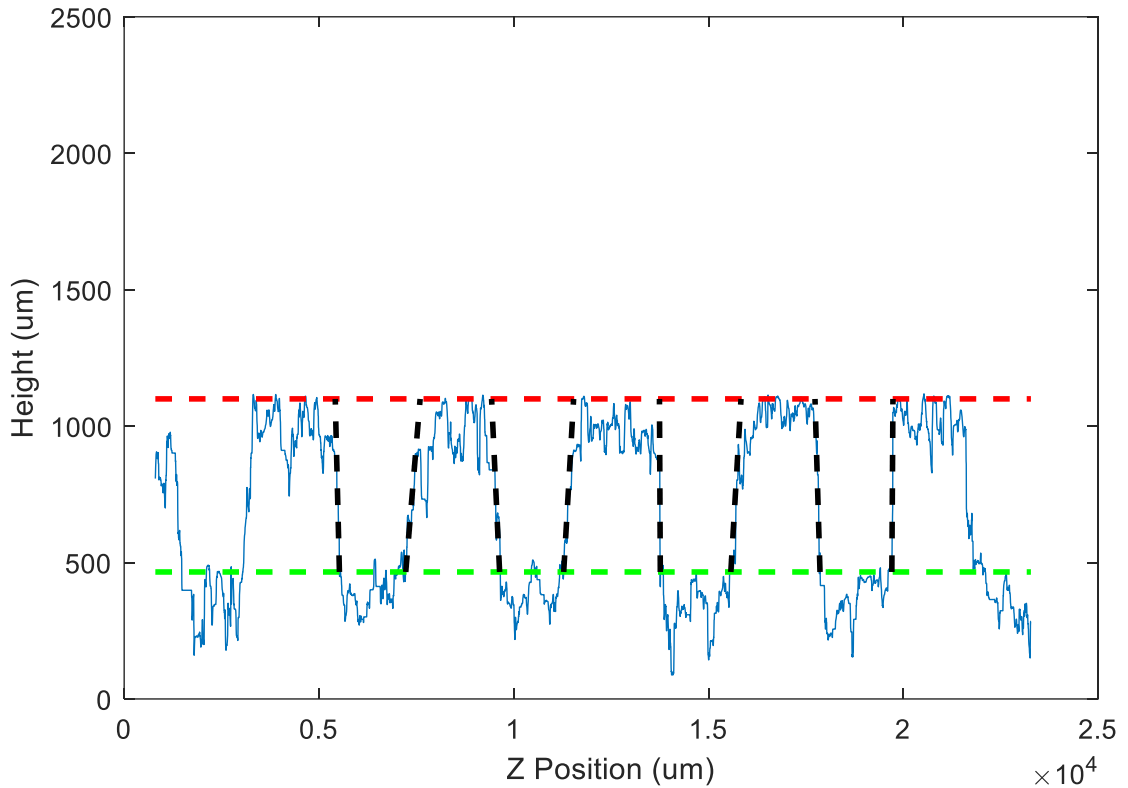
Figure 6.10: Intermediate topography scan of grinding wheel B (1/3)

Table 6.5: Groove geometry parameters based on intermediate scans

Parameter	**Units**	**Wheel A**	**Wheel B**
Groove Depth (Estimated)	μm	638.2	639.0
Groove Depth (Measured)	μm	625.5	634.1
Difference (Groove Depth)	μm	12.7	4.9
% Difference (Groove Depth)	%	2.0	0.8
Surface Groove Width (Estimated)	μm	3585.6	1839.9
Surface Groove Width (Measured)	μm	3655.3	1916.1
% Difference (Groove Width)	%	1.9	4.1
Groove Factor (Estimated)	%	50.2	54.5
Groove Factor (Measured)	%	49.2	52.7
Difference (Groove Factor)	%	1.0	1.8

Based on Figure 6.9 and Figure 6.10, it seems as though the grooves have succeeded in maintaining their geometry throughout the grinding process; the groove geometry appears to be very similar to that observed from the initial topography scans except with a shallower groove depth. In Table 6.5, the estimated groove depths were obtained by taking the measured groove depths from the initial topography scans and then subtracting the dressing amounts from these values. The measured groove depth values matched the estimated groove depth values very well; there is only 12.7 μm and 4.9 μm of error between the measured and estimated groove depths for grinding wheels A and B, respectively. This result means that the estimated values are off from the measured values by only 2.0% and 0.8% for grinding wheels A and B, respectively. This finding confirms that the method of subtracting the dressing amounts from the initial measured groove depth is quite accurate. Any error between the estimated and measured values of groove depth can be attributed to dressing tool wear and inaccuracies in setting the dressing tool's zero position.

The estimated groove widths shown in Table 6.5 were obtained using the initial topography scans and the estimated intermediate groove depths. Interestingly, the measured groove widths are slightly larger than the estimated groove widths for both grinding wheels A and B. This finding indicates that the grooves tend to get slightly wider during grinding probably due to wear along the edges of the groove. In fact, grinding wheels A and B are 1.9% and 4.1% wider than the estimated groove width values. This groove widening is good news for this research because it means that the groove width has actually changed less from the initial groove width than what was expected. This change in width also causes the change in groove factor to be less significant than what was expected. The measured grooved factors for wheels A and B are 49.2% and 52.7%, respectively. These results indicate that the groove factors for wheels A and B have only changed from their initial values of 48.1% (A) and 51.8% (B) by 1.1% and 0.9%, respectively, after having removed around 500 μm of groove depth. The whole purpose of these intermediate scans and the purpose of this discussion is to prove that the groove geometry (besides groove depth) is consistent throughout all the experiments, and to prove that the estimated groove depths for the experiments are accurate. The preceding discussion effectively proves this, and it can now assuredly be said that any changes in experimental results that are observed can be attributed solely to changes in groove depth.

6.4 EXPERIMENTAL RESULTS

6.4.1 Power & Forces

This section presents the experimental results from experiment series A and experiment series B. Spindle power, normal force, and tangential force are plotted against groove depth in Figure 6.11, Figure 6.12, and Figure 6.13, respectively. These graphs may seem cluttered and difficult to understand at first so what follows is an explanation of what these figures show. There are six curves in total on each graph: one curve for each of the three depths of cut for grinding wheel A (3.2 mm groove width) and one curve for each of the three depths of cut for grinding wheel B (1.7 mm groove width). The lines for the data collected during the experiments performed with grinding wheels A and B are solid and dashed, respectively. The markers show the data collected for each experiment that was performed. To obtain the values that the lines pass through, the data for each experiment that was performed at the same groove depth and at the same depth of cut were averaged.

The results for power and forces can also be seen on separate graphs for experiment series A and experiment series B in Appendix D. Some readers may find the power and forces graphs in the appendices easier to interpret than the graphs presented below; however, it was necessary to plot the results for experiment series A and experiment series B on the same graph for the body of this thesis. That way, the differences in results between experiment series A and experiment series B could be better compared and discussed. It should also be noted that all the results presented in this chapter can be viewed in table form in Appendix E.
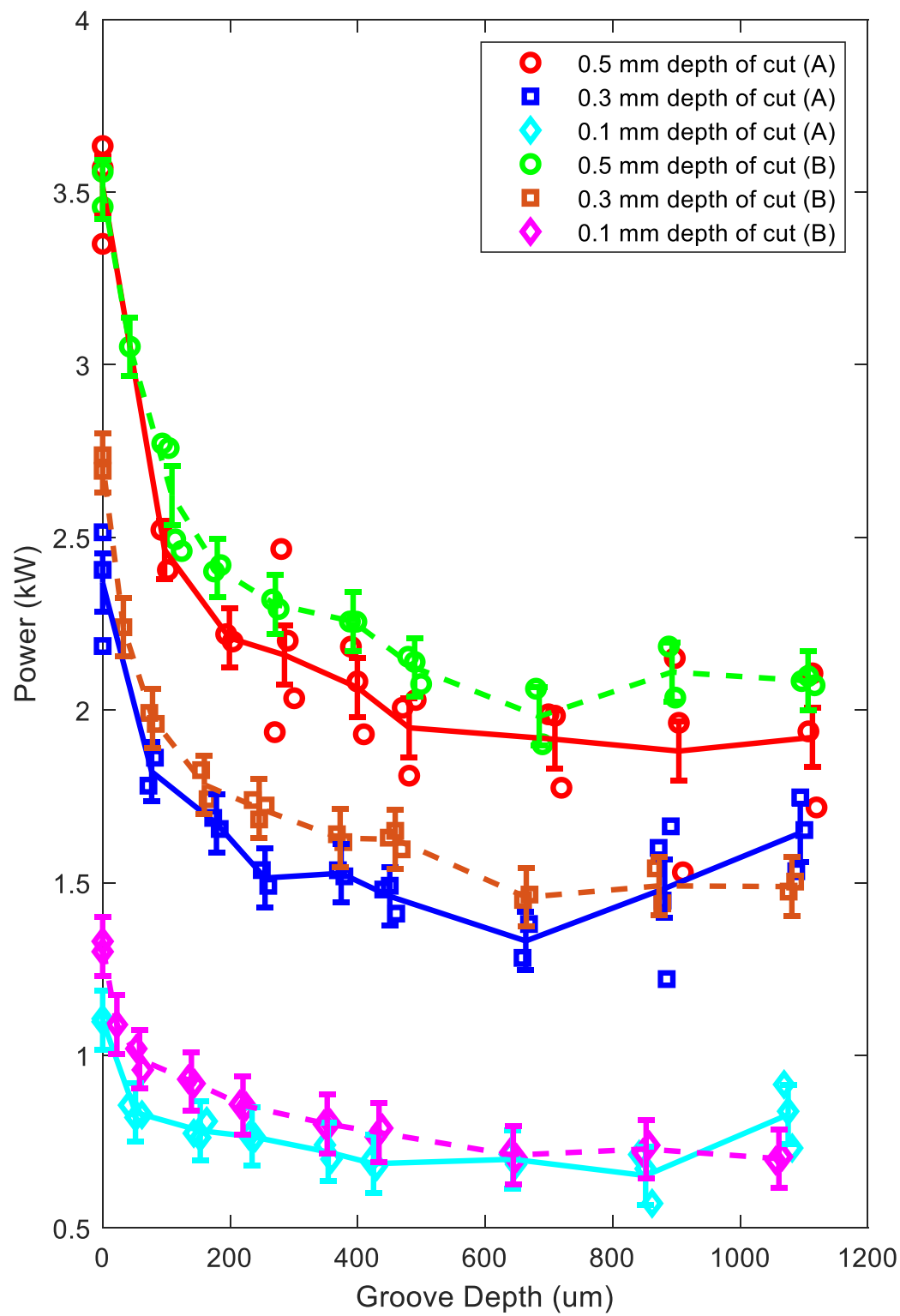
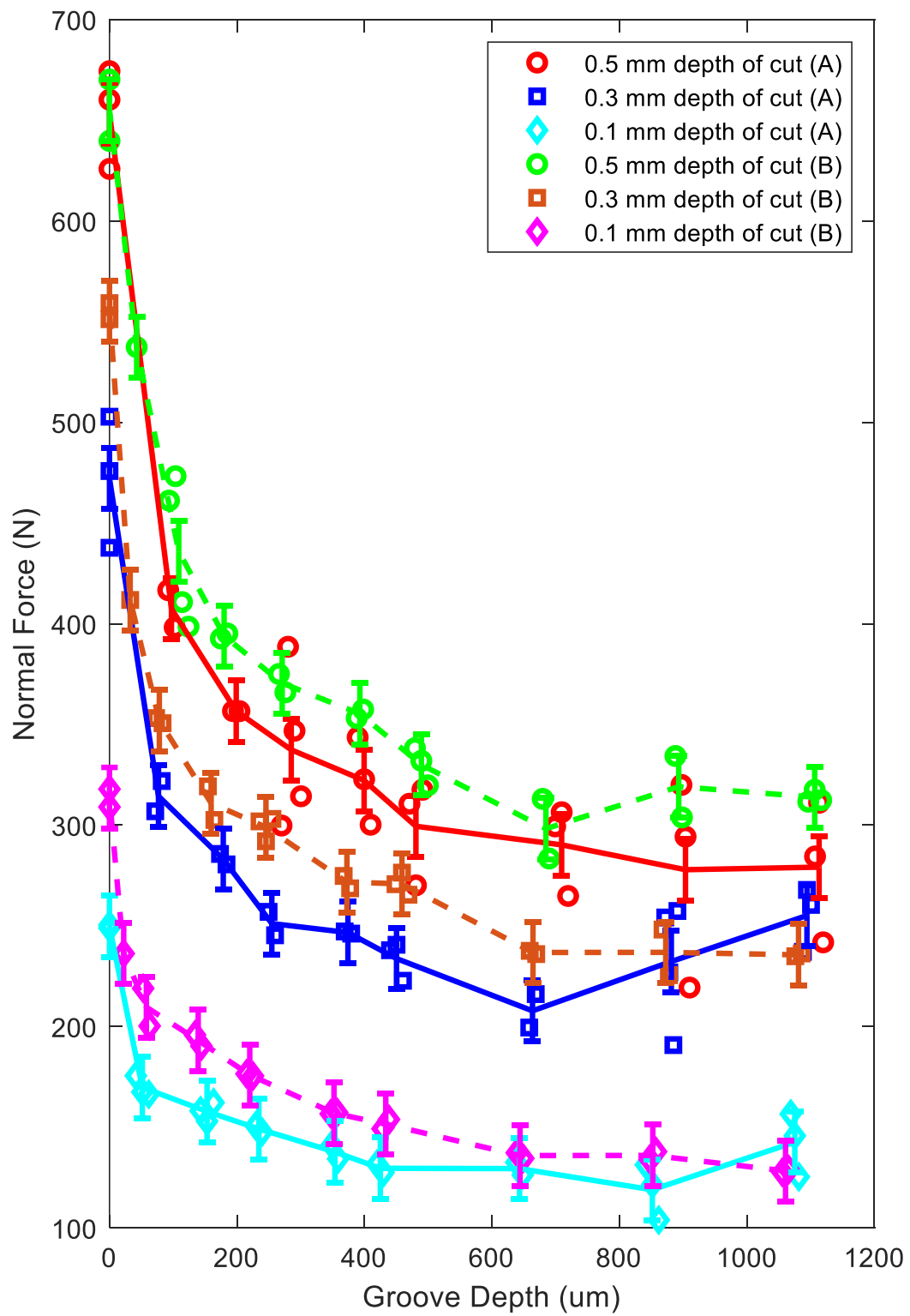Figure 6.11: Experimental results for spindle power vs groove depth

Figure 6.12: Experimental results for normal force vs groove depth
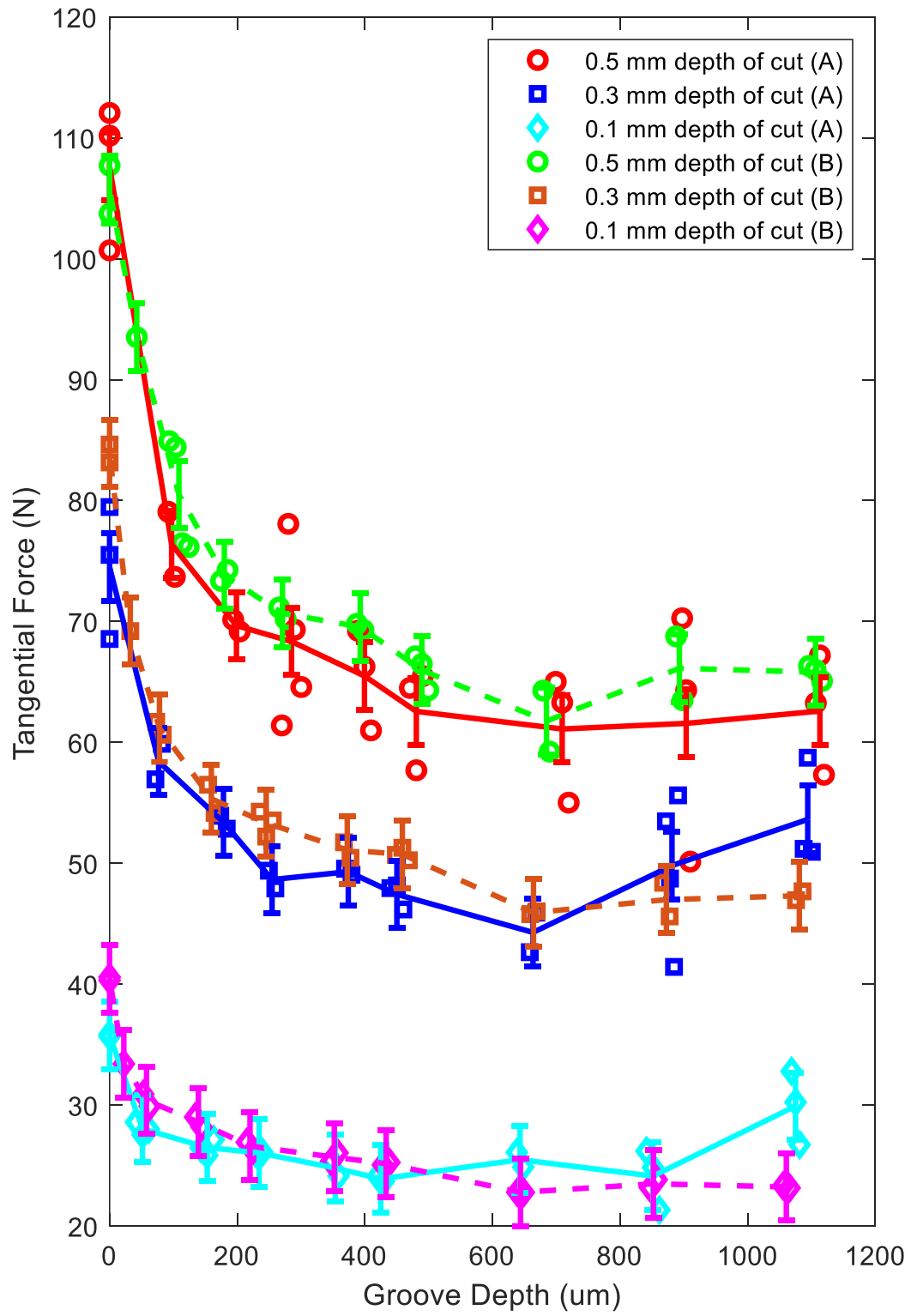
Figure 6.13: Experimental results for tangential force vs groove depth

It can be seen from Figure 6.11, Figure 6.12, and Figure 6.13 that the power and forces experience an initial sharp decline between a groove depth of 0 μm and the shallowest groove depth. Then, the power and forces continue to decrease as groove depth increases until a groove depth of roughly 400 μm. For groove depths greater than 400 μm, the results for power and forces do not decrease significantly. These results indicate that, for the conditions used in these experiments, it is unnecessary to groove deeper than 400 μm to achieve the full reductions in power and forces provided by using a grooved grinding wheel. The three figures presented above also show that the power and forces are highest and lowest for the experiments performed at depths of cut of 0.5 mm and 0.1 mm, respectively. This is expected, since higher material removal rates lead to higher forces and power. An interesting observation that can be made is that a grooved wheel that is grinding at a depth of cut of 0.5 mm has much lower forces and power that a non-grooved wheel that is grinding at a depth of cut of 0.3 mm. This impressive result shows that a grooved wheel can produce lower power and forces than a non-grooved wheel and yet still remove 1.67 times more material than a non-grooved wheel.

When comparing the results from experiment series A and experiment series B, it does not seem as though there are any significant differences between the results for the two different groove widths. The power and forces for experiment series B are consistently slightly higher than those for experiment series A. However, the power and forces experienced by the non-grooved wheels are also slightly higher for experiment series B than for experiment series A. Therefore, the higher forces and power experienced during experiment series B cannot be attributed to the difference in groove width, since the non-grooved wheels also experienced this offset in forces and power. Consequently, the higher forces and power in experiment series B can be attributed to inconsistencies in the experimental conditions between the two series of experiments. The biggest source of error between the two series of experiments is likely mismeasurement of the single point dressing tool which can lead to an inaccurate overlap ratio during dressing. Other sources of error include differences in wheel diameter and coolant jet alignment. To eliminate these sources of error in future experiments, one should ensure to measure the grinding wheel diameter as accurately as possible and to minimize dressing tool wear throughout the grinding experiments. Dressing tool wear can cause changes in dressing tool topography

which can change the dressing conditions and thus result in changes in grinding performance. The standard deviations throughout all the experiments for power, normal force, and tangential force are 0.085 kW, 15.2 N, and 2.8 N, respectively.

There are two main conclusions from the results presented in this section. First, that a groove depth of around 400 μm provides the maximum reduction in forces and power and that grooving deeper than this groove depth does not influence results significantly. Second, that there are no observable differences in forces and power for two grinding wheels having groove widths of 3.2 mm and 1.7 mm but having the same groove factor.

6.4.2 Normalized Results

Following the results presented in the previous section, it is still unclear whether there is any sort of connection between groove depth and depth of cut. It did not seem like there was any significant relationship between the two since each power and force curve appeared to decrease until a groove depth of roughly 400 μm, irrespective of the depth of cut. However, this section will investigate whether any relationship truly exists by presenting and analyzing the power and force results normalized for each depth of cut.

For each depth of cut, the power and forces during the non-grooved wheel experiments were averaged and the results for power and forces of each other experiment were then divided by the resulting value. The effect of doing this normalizing is that each data point becomes a value between 0 and 1, where a value of 1 represents the power and forces obtained from using a non-grooved wheel. The normalized spindle power results for experiment series A and B are presented in Figure 6.14 and Figure 6.15, respectively. The normalized normal force results for experiment series A and B are presented in Figure 6.16 and Figure 6.17, respectively. Note that the normalized tangential force curves have not been included in this section because they are essentially identical in shape to the normalized curves shown in Figure 6.14 and Figure 6.15. Thus, it was decided that including normalized tangential force as well would be redundant.
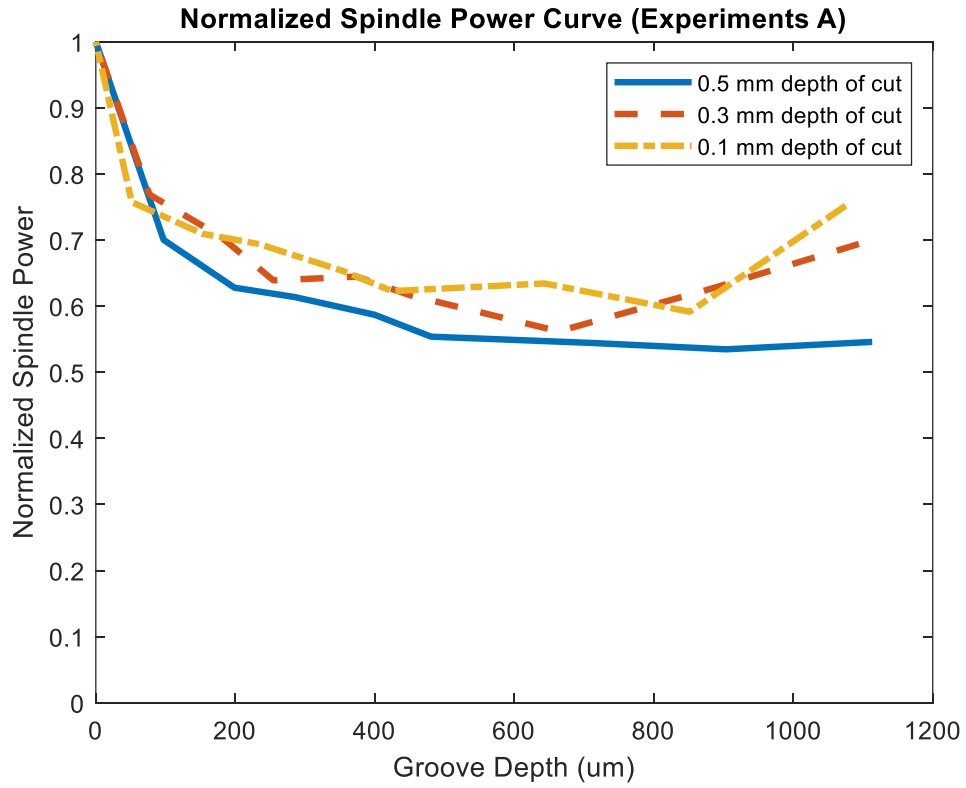
Figure 6.14: Normalized power curve for experiment series A
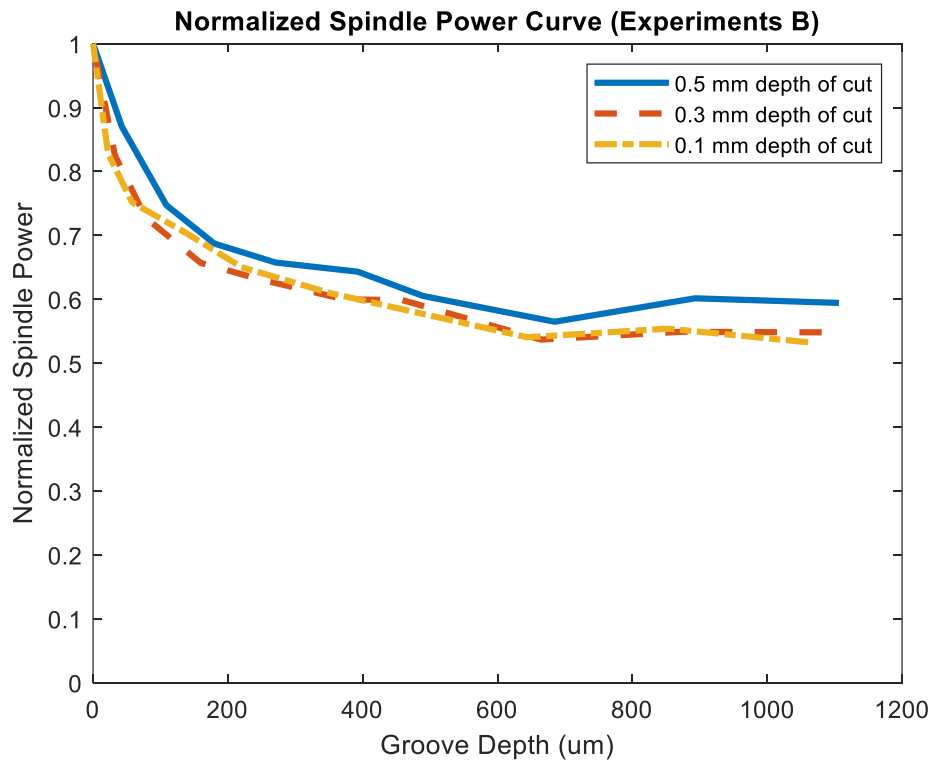
Figure 6.15: Normalized power curve for experiment series B

72
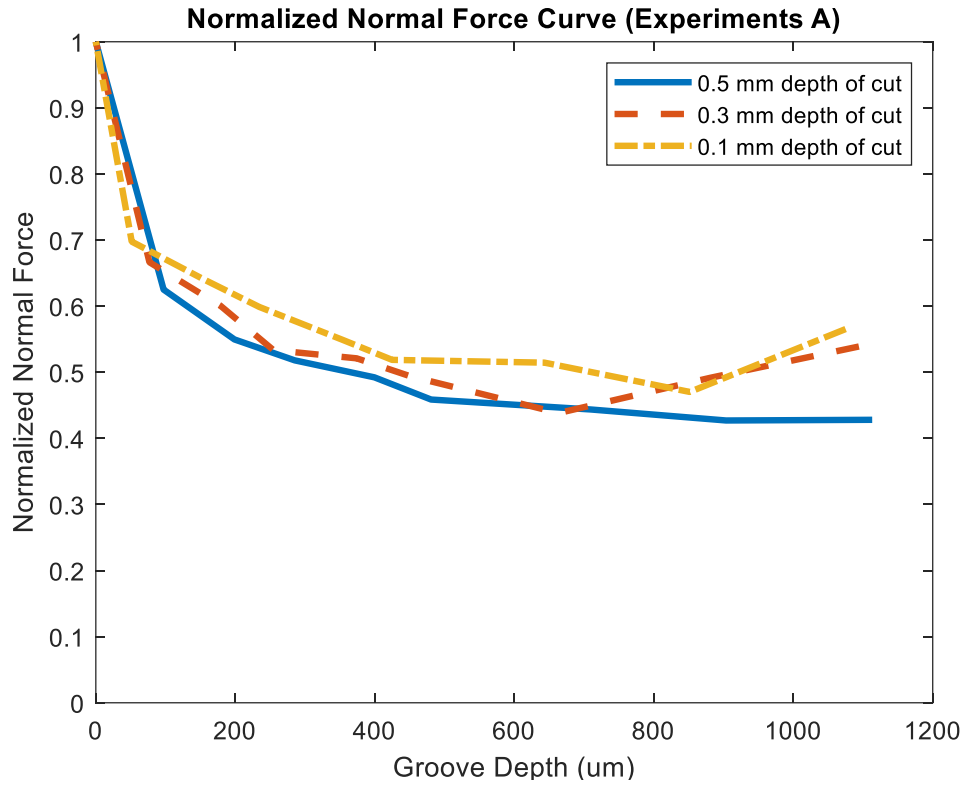
Figure 6.16: Normalized normal force curve for experiment series A
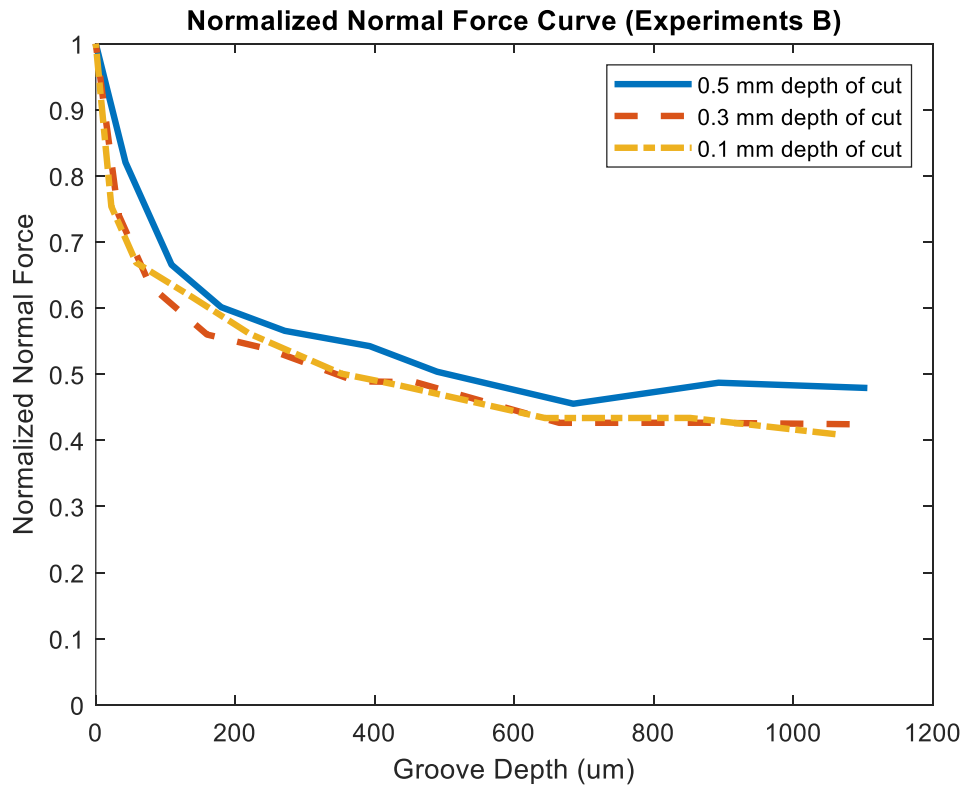
Figure 6.17: Normalized normal force curve for experiment series B

It can be seen from Figure 6.14, Figure 6.15, Figure 6.16, and Figure 6.17 that, for every depth of cut, the normalized power and normal force curves are nearly identical. This finding holds true for the results from both experiments series A and B. This outcome indicates that there is not a significant relationship between groove depth and depth of cut. It is worth pointing out that the change in magnitude for power and forces at various groove depths for different depths of cut is quite different, however, the percentage changes are very similar. For instance, at a groove depth between 600 – 700 μm, the power reductions obtained for depths of cut of 0.5 mm and 0.1 mm are ~1.4 kW and ~0.6 kW, respectively. However, both of these power reductions correspond to percentage power reductions of about 45%. Therefore, it could be said that grooved grinding wheels are best suited for high material removal rate grinding operations, since the reduction in magnitude for power and forces increases with respect to depth of cut, although the percentage reduction in power and forces is the same for every depth of cut. Note that the slight increase in normalized results for the highest groove depths in experiment series A is likely due to some source of experimental error.

The normalized power curves show that, when using a grooved wheel with a grooved depth of about 700 μm, the spindle power reaches a maximum reduction of approximately 45% compared to a non-grooved wheel for every depth of cut. Similarly, the normalized normal force curves show that the normal force reaches a maximum reduction of approximately 55% compared to a non-grooved wheel for every depth of cut. It is also worth noting that the tangential force reached a maximum reduction of approximately 45% compared to a non-grooved wheel for every depth of cut.

The percentage power reductions at each groove depth were averaged for all six sets of experiments to show how the spindle power changes, on average, with respect to groove depth. The results are presented as a bar graph in Figure 6.18. The blue bars show the overall percentage power reduction for each range of groove depths compared to a non-grooved wheel, and the orange bars show the percentage power reduction for subsequent groove depths. For instance, the orange bar for the groove depth range of 50 – 100 μm in Figure 6.18 indicates that groove depths in the range of 50 – 100 μm reduce the spindle power by an additional ~10% compared to groove depths in the range of 0 – 50 μm.
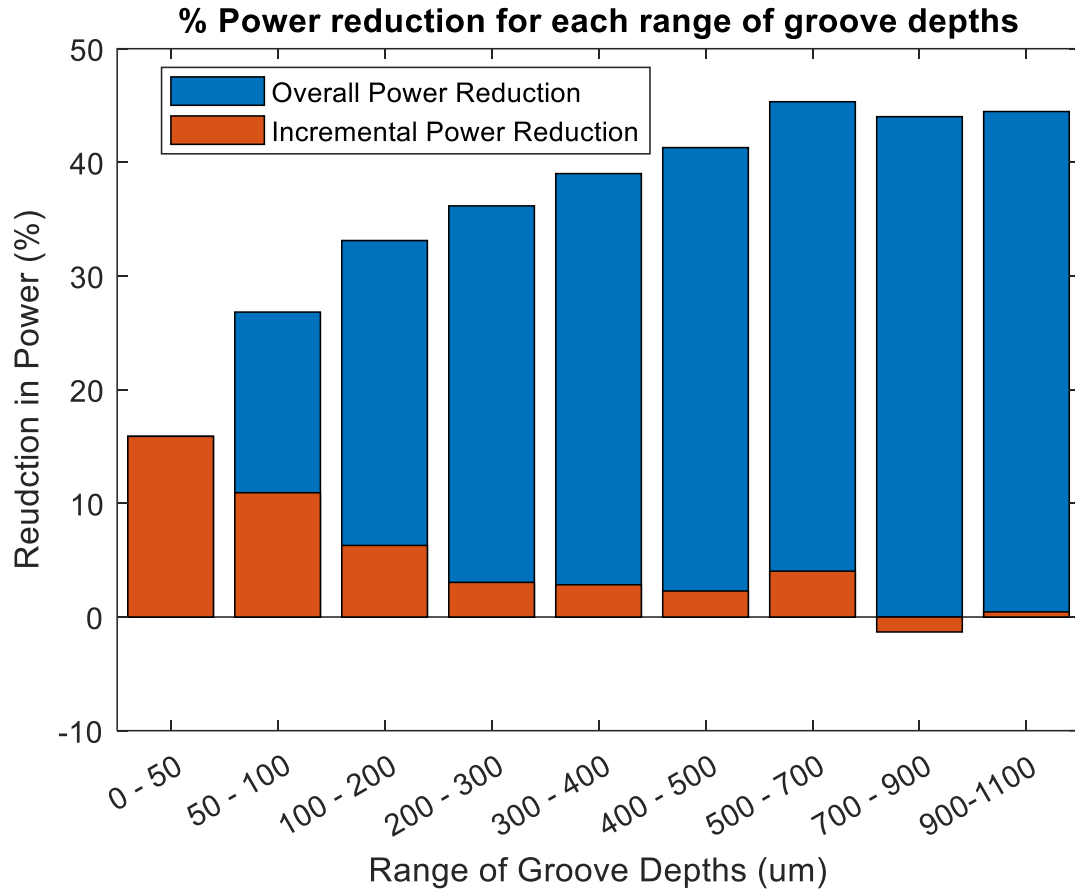
Figure 6.18: Average percentage power reductions for each range of groove depths

As can be seen in Figure 6.18, groove depths between 0 – 50 μm tend to reduce the spindle power by ~15%, whereas groove depths between 50 – 100 μm tend to reduce the spindle power by an additional ~10% for an overall power reduction of ~25%. Next, the power is reduced by an additional ~6% for groove depths in the range of 100 – 200 μm. For the next four ranges of groove depths, the power increases by about 3% each time until a maximum overall power reduction of ~45% is achieved for a groove depth range of 500 – 700 μm. It is worth pointing out that one can achieve a power reduction of over 30% by using a groove depth in the range of 100 – 200 μm. Compared to a groove depth greater than 400 μm, grooving to a depth in the range of 100 – 200 μm would take at least 3x less time to create the groove, but would only result in 1.5x less power reduction. Therefore, the most desirable groove depth depends on how the user of the grooved grinding wheel values time versus savings in power and reduced grinding forces. Future grooving systems may be

capable of grooving a grinding wheel during a grinding operation, similarly to current systems that are capable of continuously dressing a grinding wheel. In this case, the grooves would be made to always be greater than 400 μm deep since grooving time would no longer have to be taken into consideration.

6.4.3   Workpiece Surface Roughness

The results for workpiece surface roughness for the AISI 4140 steel workpieces for experiment series A and B are illustrated in Figure 6.19 and Figure 6.20, respectively.
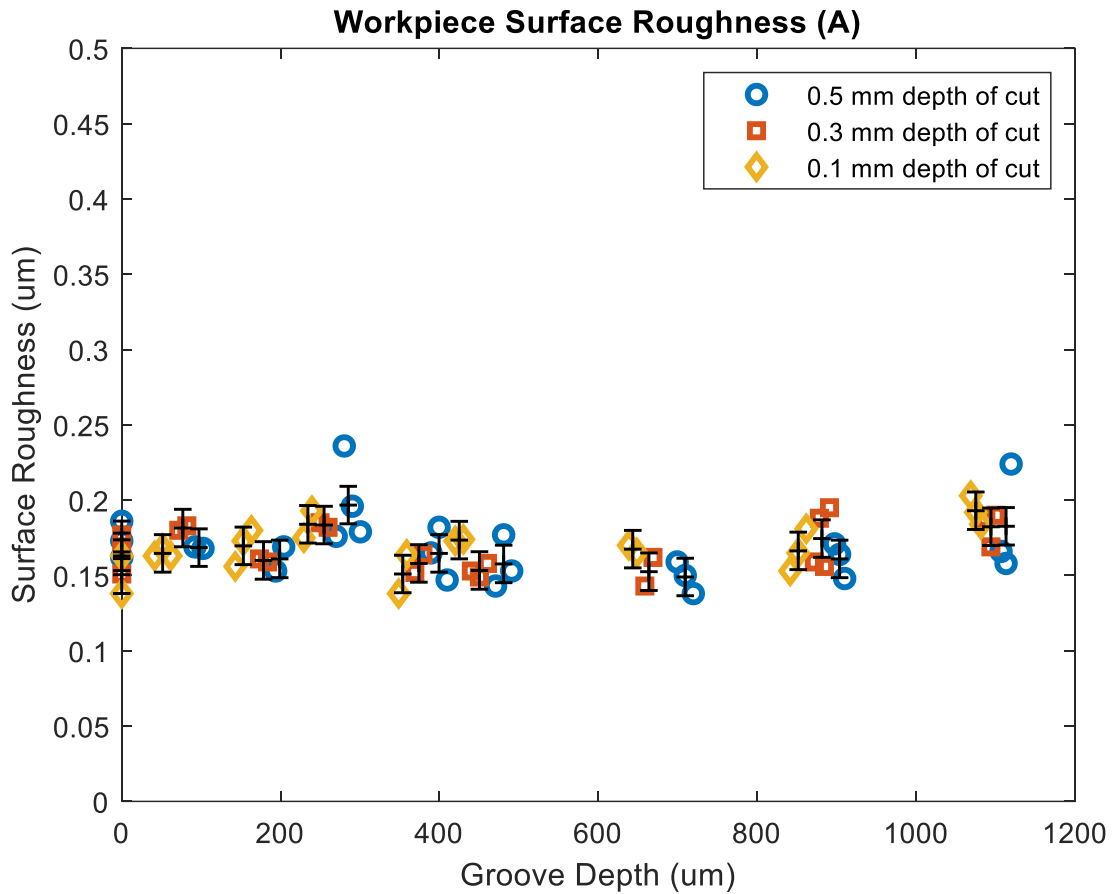
Figure 6.19: AISI 4140 workpiece surface roughness vs groove depth (experiments A)
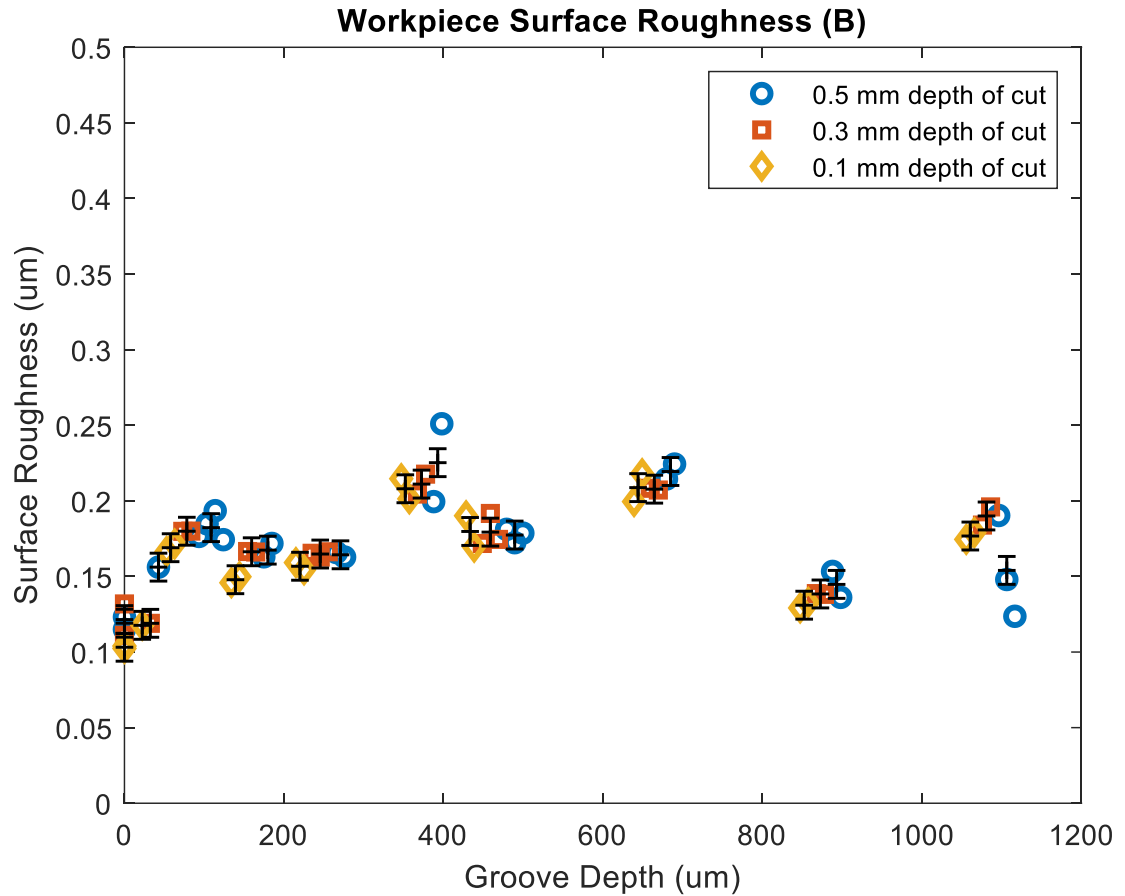
Figure 6.20: AISI 4140 workpiece surface roughness vs groove depth (experiments B)

Figure 6.19 shows that the arithmetic mean surface roughness values for experiment series A lie within 0.14 – 0.21 μm with a standard deviation over the whole data set of 0.0125 μm. Figure 6.20 shows that the arithmetic mean surface roughness values for experiment series B lie within 0.11 – 0.23 μm with a standard deviation over the whole data set of 0.01 μm. These surface roughness values fall under the "polish" classification of machined surface finishes [45]. This classification is a very good surface finish and is the second highest classification of machined surface finishes behind "super finish". This finding shows that grooved grinding wheels can produce very high-quality surface finishes in creep-feed grinding.

The surface roughness values for every groove depth are quite consistent so it does not appear as though groove depth has any influence on workpiece surface roughness for creep-feed grinding AISI 4140 steel. This finding makes sense because, as discussed in Chapter 2, the parameters that affect surface roughness the most are cutting edge density, grit size, feed rate, and wheel speed. None of these parameters change with respect to groove depth if groove width remains constant. For experiment series A, there is no difference in surface roughness between the grooved wheel and the non-grooved wheel. For experiment series B, however, the non-grooved wheel provided a finer surface finish than the grooved wheel. One would expect the non-grooved wheel to provide a better surface finish than a grooved wheel because a non-grooved wheel has a much higher cutting edge density than a grooved wheel. The most plausible explanation is that wider grooves have less of a detrimental effect on surface finish than narrower grooves. Mohamed *et al.* [18] also found that, when comparing surface finish results for grinding wheels having two different groove widths, the wheel with the wider groove produced the finer surface finish. However, a more extensive investigation is needed to determine whether wider grooves produce better surface finish results.

6.4.4   Specific Energy & Force Ratio

Figure 6.21 shows the results for specific energy plotted against groove depth for both experiment series A and B. Recall from Chapter 2 that specific energy represents the amount of energy required to remove a unit volume of material. It is a measure of the efficiency of the grinding process, where a lower specific energy signifies more efficient grinding. The data presented in Figure 6.21 was obtained by dividing the spindle power results by the material removal rate for each depth of cut so the curves are identical in shape to the spindle power results presented previously in Figure 6.11.
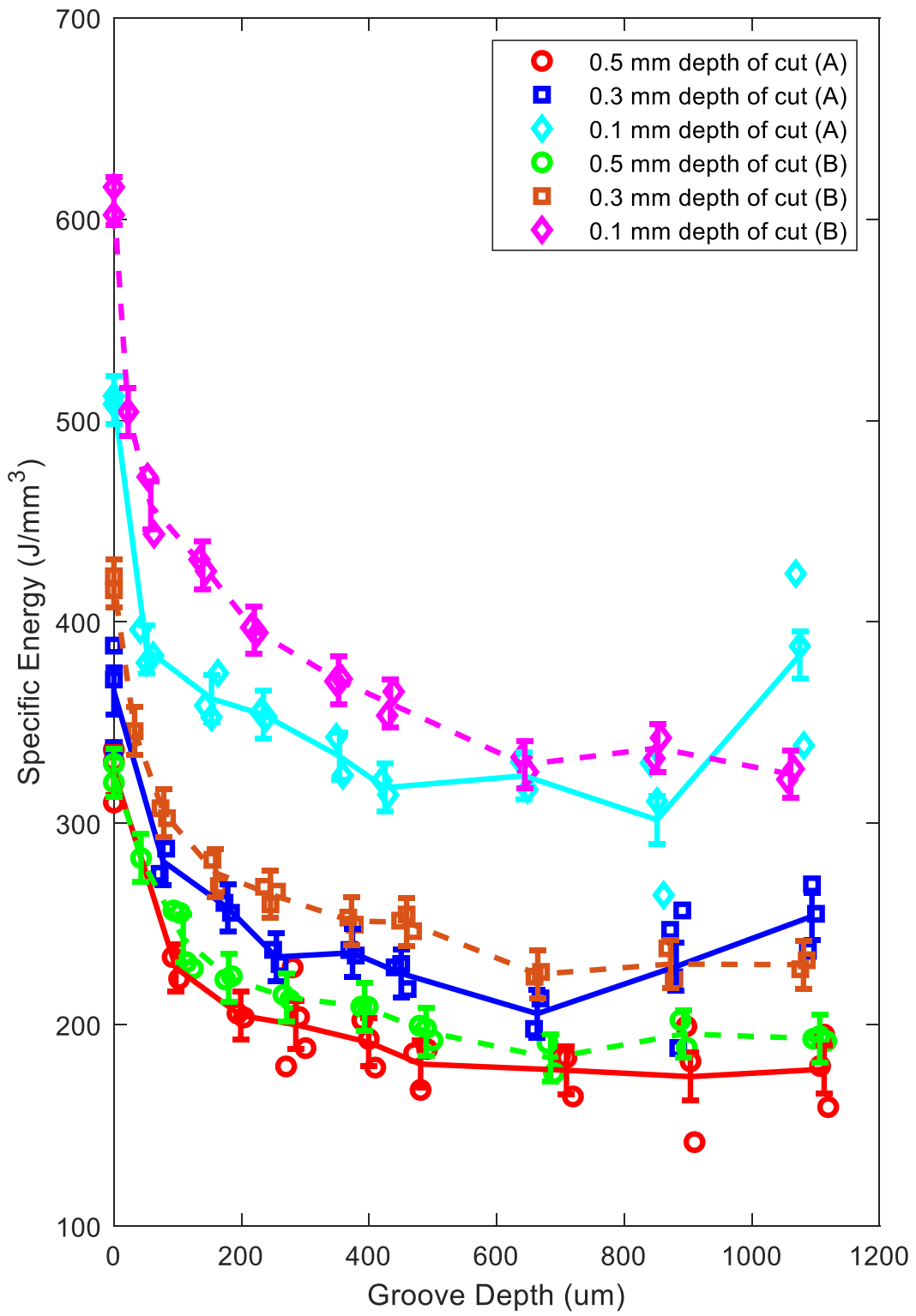
Figure 6.21: Specific energy vs groove depth

It can be seen from Figure 6.21 that the higher depths of cut have lower values of specific energy. This finding is expected because it has been shown from Equation 2.3 that chip thickness is proportional to depth of cut, and it has also been discussed in Chapter 2 that specific energy is inversely proportional to chip thickness as per the size effect. Therefore, there are really no surprises in Figure 6.21; specific energy decreases with groove depth until a groove depth of around 400 μm, similar to the spindle power results from Figure 6.11, and specific energy decreases as depth of cut increases.

The force ratio results for experiments series A and B are listed in Figure 6.22 and Figure 6.23, respectively. Force ratio is tangential force divided by normal force and it is thought to indicate how much of the applied force is being used in cutting versus how much is being used for overcoming friction [18]. For instance, a higher force ratio would indicate that more of the applied force is being used for cutting rather than for overcoming friction. Anderson *et al.* [46] stated that lower force ratios indicate that a higher proportion of grains are rubbing rather than plowing or cutting, and that, as force ratio increases, the proportion of grains that are cutting increases. Therefore, similar to specific energy, force ratio is thought to be an indicator of the efficiency of the grinding process, where a higher force ratio signifies increased grinding efficiency.
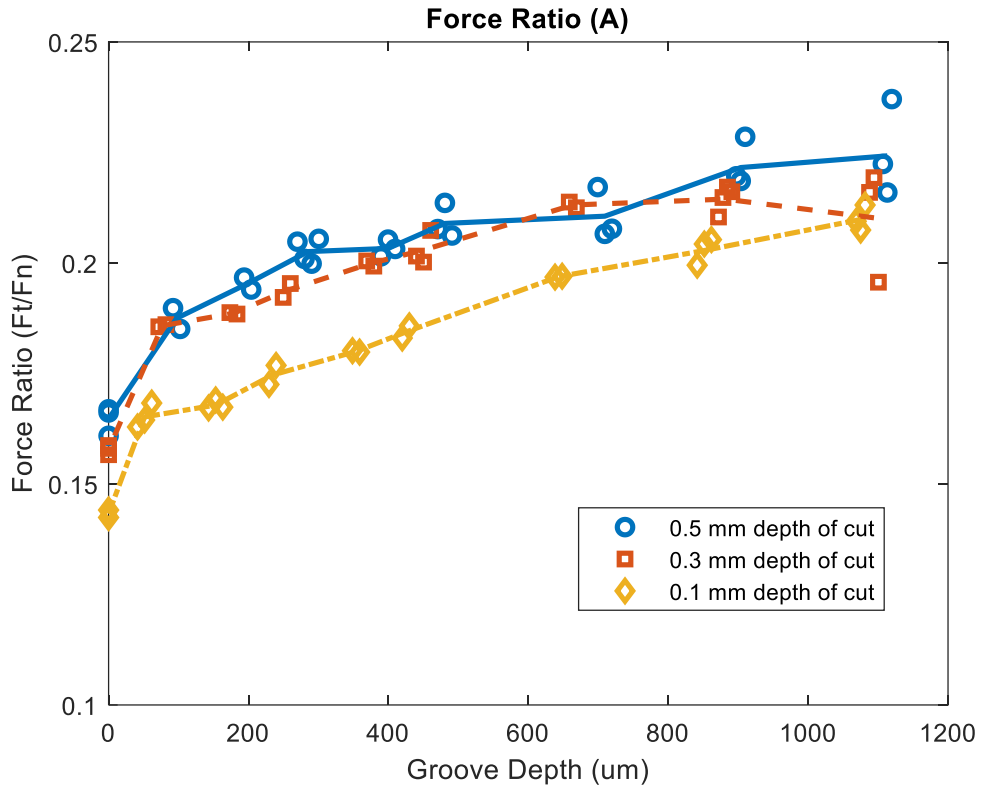
Figure 6.22: Force ratio vs groove depth for experiment series A
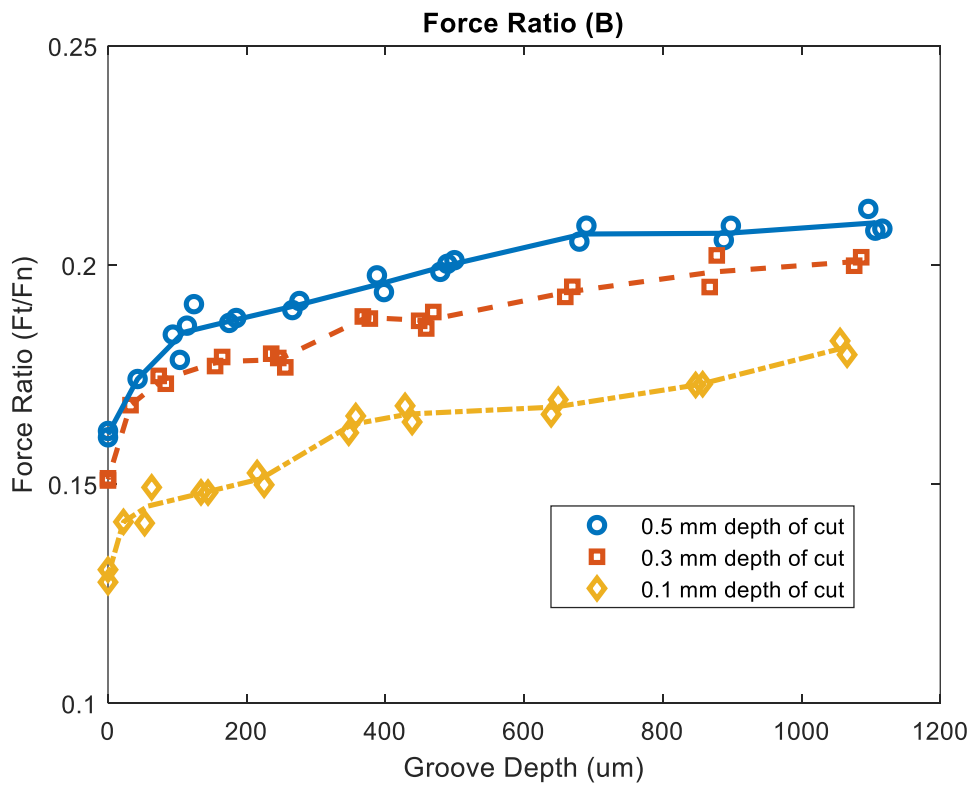
Figure 6.23: Force ratio vs groove depth for experiment series B

Figure 6.22 and Figure 6.23 show that the force ratio has a sharp initial slope until about 100 μm. Beyond this point, force ratio increases linearly with respect to groove depth. Force ratio also increases with depth of cut which implies that higher depths of cut lead to increased grinding efficiency. This result is consistent with the specific energy results shown in Figure 6.21. The force ratio results also show that the 0.5 mm depth of cut data for experiment series A has the highest force ratio, and that the 0.1 mm depth of cut data for experiment series B has the lowest force ratio. This observation is consistent with the specific energy results as well, where these same sets of experiments experience the lowest and highest specific energies, respectively. Thus, force ratio indeed appears to quite a good indicator of grinding efficiency.

There is one inconsistency between the results for force ratio and specific energy; For groove depths greater than ~400 μm, groove depth does not appear to affect the specific energy results. Force ratio, however, appears to increase for every groove depth, including those greater than ~400 μm. Recall that in section 6.4.2, it was said that the normal and tangential forces measured when using a grooved wheel compared to a non-groove wheel were reduced by a maximum of ~55% and ~45%, respectively. Since the normal force is being reduced by more than the tangential force is being reduced, the force ratio increases. It is unclear at this point why the normal force experiences a greater reduction than the tangential force. However, this result indicates that something about the grinding dynamics is changing with respect to groove depth. The cause of this change in grinding dynamics will be discussed in the next chapter which will explore the reasons behind why different groove depths yield different results.

6.5 SUMMARY

This section consists of a summary of the results presented throughout this chapter. Two grooved grinding wheels having groove widths of 3.2 mm and 1.7 mm but otherwise similar groove geometries and groove factors were used in a series of creep-feed grinding experiments. The grinding wheels were initially grooved to a groove depth of ~1100 μm and the groove depth was gradually reduced throughout the experiments by dressing the

grinding wheels. The initial groove depth was obtained by analyzing a topography scan of the grinding wheels and subsequent groove depths were estimated by subtracting the dressing amounts from the initial groove depth. Groove depths ranging from 0 – 1100 μm were tested in creep-feed grinding experiments for depths of cut of 0.5 mm, 0.3 mm, and 0.1 mm during which power and force data were collected. Workpiece surface roughness was measured afterwards. The following findings were made:

- From analyzing the initial and intermediate topography scans, it was determined that the changes in groove width with respect to groove depth are negligible.
- The power and forces during grinding for both grinding wheels decrease with respect to groove depth until a groove depth of ~400 μm. Grooves deeper than this value do not appear to significantly reduce power and force results.
- The results for power and forces are very similar for both grinding wheels. Therefore, it does not appear as though different groove widths ranging from 1.7 – 3.2 mm have much of an impact on grinding performance.
- Upon normalizing the power and forces, the power and forces are reduced by the same percentage for every depth of cut when comparing a grooved wheel with a groove depth greater than ~400 μm to a non-grooved wheel. However, the magnitude of power of forces reduction is greater for higher depths of cut.
- The workpiece surface finish obtained throughout these experiments for AISI 4140 steel is very good and is classified as a "polish". Surface roughness values ranging from 0.11 – 0.23 μm were obtained. It did not appear as though groove depth or groove width has any influence on workpiece surface roughness
- Force ratio and specific energy both indicate that grinding efficiency increases with respect to groove depth and depth of cut. Specific energy does not change significantly for groove depths greater than ~400 μm, however, force ratio seems to increase for every groove depth.

The next chapter will explore the reasons behind why different groove depths provide different results by looking at the kinematics of chip removal with a grooved grinding wheel, and by discussing fluid flow in grooved grinding wheels.

CHAPTER 7: DISCUSSION OF RESULTS

This chapter will further explore and help explain the experimental results presented in Chapter 6 for various groove depths. Recall from Chapter 3 that the two main mechanisms through which grooved grinding wheels improve grinding performance compared to non-grooved wheels are 1) a reduced number of cutting edges (which leads to increased uncut chip thickness), and 2) improved coolant flow. As stated previously, increased uncut chip thickness and increased coolant flow result in increased grinding efficiency. The following sections will investigate how changes in groove depth relate to both of these mechanisms.

7.1 GROOVE DEPTH & UNCUT CHIP THICKNESS

The formula for uncut chip thickness was presented in Equation 2.3 in Chapter 2. This equation assumes that the cutting edge spacing is constant and that the protrusion heights of the cutting edges are constant which is not true in reality; the protrusion heights and spacing of the cutting edges are random meaning that, in reality, the chips in grinding will have a range of thicknesses. However, Equation 2.3 provides a good method of estimating the average chip size based on the kinematics of the grinding process. This equation shows that uncut chip thickness is related to cutting edge spacing, wheel speed, workpiece feed rate, depth of cut, and wheel diameter. None of these parameters are affected by changes in groove depth. Therefore, it does not seem as though changes in groove depth would affect the uncut chip thickness at all based on the kinematics of the process. However, there is certainly a difference in cutting edge spacing between a non-grooved wheel and a grooved wheel. Therefore, there must exist a groove depth at which the maximum cutting edge spacing is achieved. This would be the groove depth at which no points within the groove are coming into contact with the workpiece. To help illustrate this concept, a 2D slice taken along the width of a grinding wheel is shown in Figure 7.1. The cross-section in Figure 7.1 corresponds to a grinding wheel having a single groove and a groove factor of 50%, similar to the ones used in the groove depth experiments presented in Chapter 6.
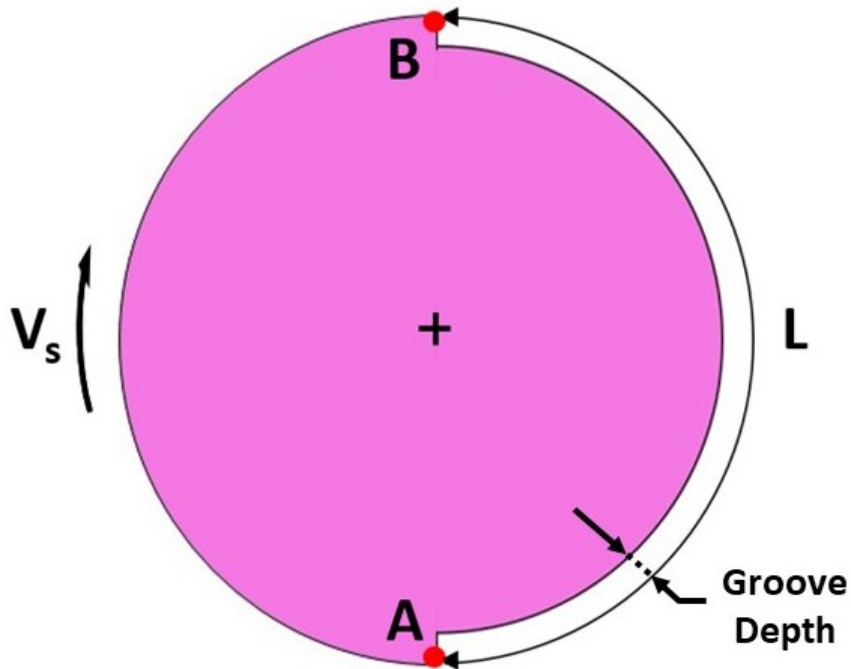
Figure 7.1: 2D cross-section of grooved grinding wheel

Given the grinding wheel in Figure 7.1, the maximum uncut chip thickness formula was used to find the minimum groove depth at which no points within the groove between points A and B interact with the workpiece. A diagram of the workpiece in the X-Y plane is shown below in Figure 7.2.
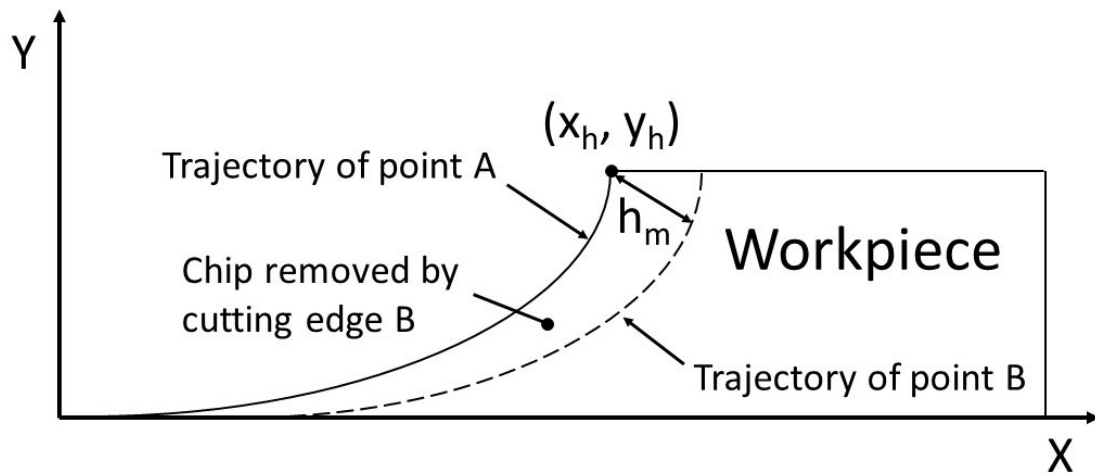
Figure 7.2: Workpiece diagram

Figure 7.2 illustrates the trajectories of points A and B from Figure 7.1 as well as the chip that is removed by cutting edge B. This chip will have a maximum chip thickness h_m that can be calculated using the formula shown in Equation 7.1:

$$h_m = 2L(\frac{v_w}{v_s})\sqrt{\frac{a}{d_s}} \qquad (7.1)$$

In Equation 7.1, L corresponds to the maximum cutting edge spacing which depends on the circumference of the grinding wheel, the groove factor, and the number of grooves, as shown below in Equation 7.2:

$$L = \frac{\pi d_s \eta}{N_g} \qquad (7.2)$$

Since the grinding wheel shown in Figure 7.1 has only one groove and a groove factor of 50%, L is simply half of the circumference of the grinding wheel. In order for no points within the groove to be interacting with the workpiece, the groove must be deeper than the maximum uncut chip thickness h_m since the point (x_h, y_h) is the point that protrudes the furthest into the groove during cutting. Therefore, the minimum groove depth at which the maximum uncut chip thickness is achieved is equal to the value of h_m.

The next step is to use Equation 7.1 to calculate the theoretical minimum groove depth to achieve the maximum uncut chip thickness for the creep-feed grinding experiments that were presented in Chapter 6. The experimental parameters and the groove geometry parameters from the creep-feed grinding experiments were substituted into Equation 7.1 to calculate the groove depth. Depth of cut is the only parameter that changed throughout the experiments that affects the minimum groove depth for maximum uncut chip thickness. Wheel diameter also affects the minimum groove depth values, however, the changes in wheel diameter due to dressing were negligible throughout the experiments. Therefore, the wheel diameter at the beginning of the experiments from Chapter 6 was used to calculate the values for minimum groove depth. Table 7.1 lists the minimum groove depth for maximum uncut chip thickness values for each depth of cut used in the creep-feed grinding experiments.

Table 7.1: Minimum groove depth for maximum uncut chip thickness

Depth of cut a	Groove depth d
0.5 mm	3.3 µm
0.3 mm	2.6 µm
0.1 mm	1.5 µm

It can be seen from Table 7.1 that the maximum uncut chip thickness is achieved at groove depths that are much shallower than the ones used for the creep-feed grinding experiments. Even for a depth of cut of 0.5 mm, the minimum groove depth required is 3.3 µm which is well below the shallowest groove depth of ~30 µm tested during the creep-feed grinding experiments. Based on these findings, it can be said that the differences in the results for power and forces for different groove depths (excluding 0 groove depth) presented in section 6.4.1 cannot be attributed to changes in uncut chip thickness. Furthermore, it is well known that the surface roughness is proportional to the uncut chip thickness. Therefore, if the uncut chip thickness was changing, then one would expect these changes to be apparent in the results for workpiece surface roughness. However, it was shown in section 6.4.3 that the workpiece surface roughness is unaffected by changes in groove depth which reinforces the argument that the uncut chip thickness is unchanging.

7.2 GROOVE DEPTH & COOLANT FLOW

In the previous section, it was determined that the groove depths used in the creep-feed grinding experiments did not affect the uncut chip thickness. At very shallow groove depths, much shallower than the ones used for the experiments performed for this research, the uncut chip thickness reaches its maximum value and then is unaffected by any further increases in groove depth. Therefore, the changes in results observed for different groove depths in Chapter 6 must be attributed to changes in coolant flow.

Recall from Chapter 2 that the grinding fluid is responsible for three things: 1) cooling, 2) lubrication, and 3) transport of debris from the grinding zone. Cooling refers to the removal of heat from the grinding zone. Higher temperatures in the grinding zone

are not responsible for creating higher spindle power and grinding forces [1]. Rather, higher spindle power and grinding forces result in creating higher grinding temperatures. Thus, it does not appear as though cooling in itself is responsible for the decreased spindle power and grinding forces that are observed at deeper groove depths.

Lubrication via the grinding fluid lowers friction between the grinding wheel and the workpiece which reduces grinding forces, spindle power, and grinding temperatures [6]. In addition, an increased ability to transport debris from the grinding zone would mean a decreased buildup of discarded chips and fractured grits in the grinding zone. This buildup leads to what is known as "wheel loading" [47]. This term is used to describe the tendency of workpiece material to weld itself to the abrasive grains, or to be forced into the pores of the grinding wheel. Wheel loading reduces the cutting ability of the wheel which leads to increased grinding forces, spindle power, grinding temperatures, and wheel wear [47]. Based on the foregoing analysis, it appears as though the decreased power and forces observed for larger groove depths are the result of increased lubrication and/or an increased ability to transport debris from the grinding zone. The following section will look further into the fluid dynamics of grinding with grooved wheels to determine whether this notion is accurate.

To better understand the fluid dynamics of the cutting fluid in grinding, a review of many publications pertaining to the effects of coolant on the grinding process was performed. There are very few publications that discuss fluid flow with grooved grinding wheels specifically; however, there were a few relevant publications on general fluid dynamics in grinding. It is widely agreed upon that a large portion of the coolant flow in grinding bypasses the grinding zone and is therefore not useful. The term "useful flow rate" has been used to describe the flowrate that succeeds in passing through the grinding zone [48]. Multiple researchers have found that more porous grinding wheels have higher useful flow rates [49-52]. The reason that more porous grinding wheels experience higher useful flow rates is that the grinding wheel can be thought of as a positive displacement pump, where the fluid within the pores is being pumped through the grinding zone by the wheel [48,51]. Therefore, by increasing the wheel porosity, the volume of coolant that can be pumped into the grinding zone via the pores is increased. This concept is applicable to

grooved grinding wheels since pores are defined as "air gaps" and grooves are essentially large air gaps. By increasing the groove depth of a grinding wheel, the volume of air gaps in the grinding wheel is being increased, which should lead to an increase in useful flow rate.

It has also been shown that the wedging effect of the coolant between the wheel and the workpiece creates a hydrodynamic pressure in the grinding zone [6]. This pressure is responsible for a percentage of the normal force during grinding which is known as the "coolant-induced force". The effect of this coolant-induced force is that it can cause deflections in the workpiece and grinding spindle which lead to reduced grinding efficiency and machining accuracy [53,54]. Furthermore, a paper by Gviniashvili *et al.* [55] stated that a lower hydrodynamic pressure would indicate less coolant being rejected from the grinding zone, thereby increasing the useful flow rate. The reason for this reduction in rejected coolant is that the hydrodynamic pressure is an indicator of how constrained the coolant flow is in the grinding zone [52]. Therefore, a lower hydrodynamic pressure signifies that there is more space in the grinding zone for coolant flow than with a higher hydrodynamic pressure. When there is more space for coolant flow in the grinding zone, the coolant delivered by the coolant jet can more easily be successfully delivered into the grinding zone which results in less coolant rejection. The same paper by Gviniashvili *et al.* [55] also stated that a higher hydrodynamic pressure would increase the penetration of the cutting fluid into the pores of the grinding wheel which could enhance lubrication. Another effect of hydrodynamic pressure discussed by Aurich and Kirsch [56] is that a higher pressure would increase the boiling point of the coolant and delay the occurrence of film-boiling which greatly deteriorates cooling efficiency.

Several publications have shown that if a gap is introduced between the workpiece and the grinding wheel, the hydrodynamic pressure is reduced as the height of the gap increases up to a certain point beyond which increases in gap height have no effect [57-59]. Similarly, Vesali and Tawakoli [53] found that grinding wheels with higher porosity lead to reduced hydrodynamic pressure. The most relevant publication here is the one by Aurich and Kirsch [56] who found that grinding with a slotted wheel leads to reduced coolant pressure in the contact zone. Another relevant publication by Hwang *et al.* [54]

found that using a toothed wheel was very effective in reducing the hydrodynamic pressure in ultraprecision mirror grinding. Based on this review, the following generalization can be made: hydrodynamic pressure decreases as the average space between the wheel and the workpiece increases. Pores, grooves, and gaps are simply different ways of creating space between the wheel and the workpiece. From this analysis, one could deduce that as groove depth increases, hydrodynamic pressure decreases since the average space between the wheel and the workpiece is being increased. Furthermore, it was just said that as hydrodynamic pressure decreases, useful coolant flow rate increases. Therefore, intuitively it would appear as though increasing groove depth reduces hydrodynamic pressure which increases the useful flow rate.

To test this hypothesis, a series of experiments were performed to measure the coolant-induced force for various groove depths. The coolant-induced force is directly related to hydrodynamic pressure so these experiments will reveal how the hydrodynamic pressure changes relative to groove depth. However, it is not possible to derive absolute values for hydrodynamic pressure in the grinding zone given the coolant-induced force. Measuring the hydrodynamic pressure would require the installation of a pressure transducer under the workpiece [53]. A method that has been proven to be effective in measuring the coolant-induced force is to perform a surface grinding cut followed by a spark out pass and then to collect the forces for a third pass at the same height as the previous two passes [6,53]. Since there is no cutting happening for the third pass, the cutting forces are eliminated and the normal force that is recorded corresponds to the coolant-induced force resulting from the hydrodynamic pressure generated between the wheel and the workpiece. An illustration of this setup is shown in Figure 7.3.
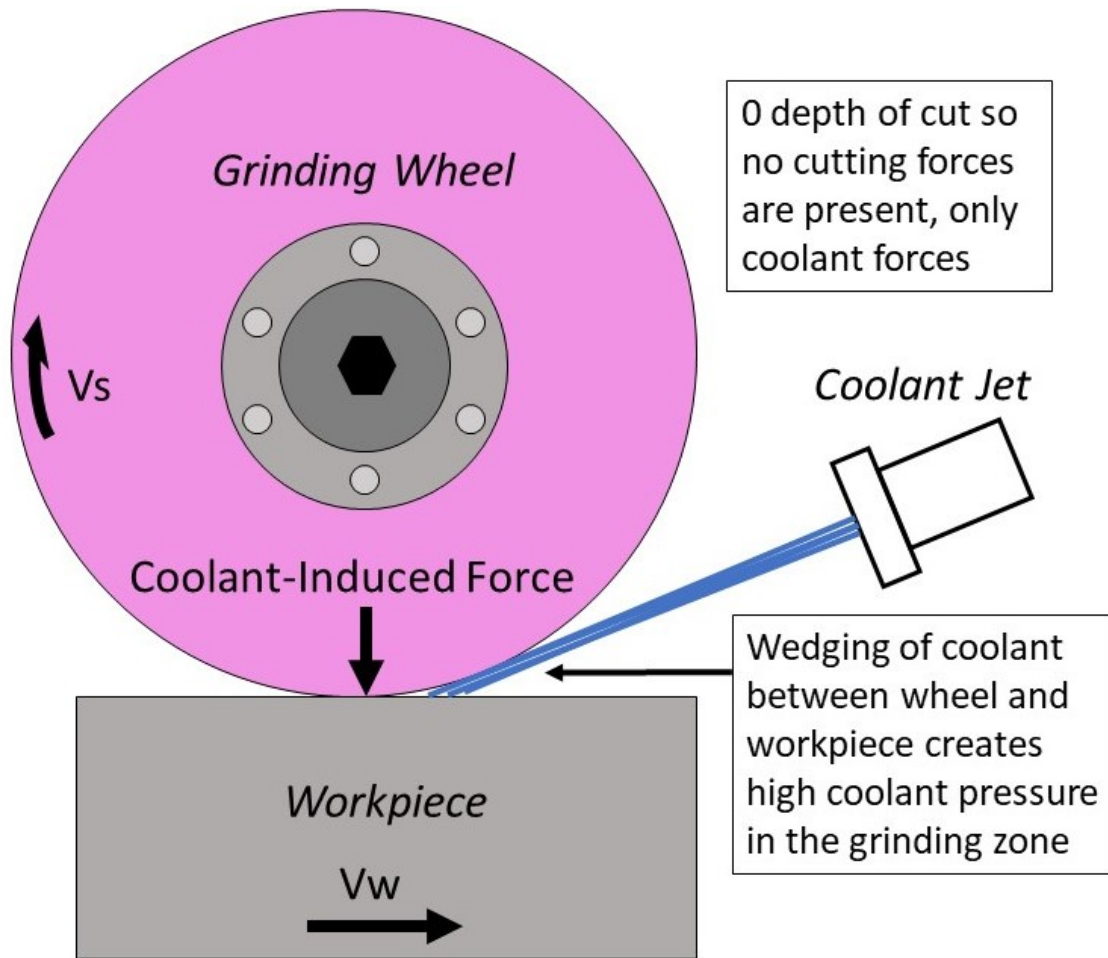
Figure 7.3: Illustration of coolant-induced force experiments

A grinding wheel was then grooved to a groove depth of 800 μm using the 1.7 mm grooving tool. The rest of the grooving parameters are the same as those listed in Table 6.3. The groove geometry parameters, besides groove depth, are similar to those listed in Table 6.4. The coolant-induced force was then measured for multiple groove depths ranging from 0 – 800 μm. The grinding parameters and dressing parameters used for these experiments are the same as those listed in Table 6.2 except that the depth of cut was 0. The results for these experiments are shown in Figure 7.4.
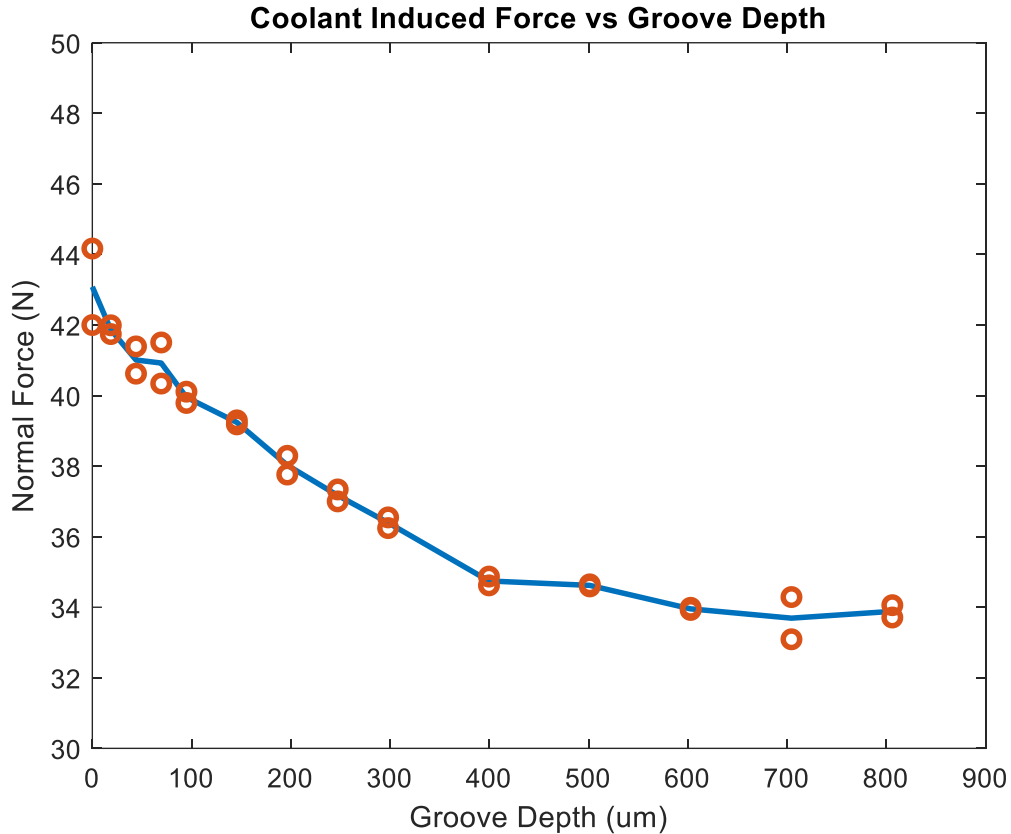
Figure 7.4: Coolant-induced force vs groove depth

It can be seen from Figure 7.4 that the coolant-induced force decreases steadily for groove depths ranging from 0 – 400 μm and then levels off around 400 μm and is fairly constant for groove depths ranging from 400 – 800 μm. The coolant-induced force is reduced by a maximum of ~22% when comparing a non-grooved wheel (0 groove depth) to a wheel with a groove depth of 700 μm. The results from Figure 7.4 are practically identical in shape to the results observed for power and forces in Chapter 6 which showed that power and forces decrease until a groove depth of about 400 μm and then level off around this depth.

Based on these results, it can be said that between groove depths of 0 – 400 μm the hydrodynamic pressure decreases which in turn decreases the amount of coolant rejected from the grinding zone and increases the useful flow rate. Unfortunately, it is not possible to directly quantify how the useful flow rate changes according to changes in coolant-induced force; there are formulas in the literature that relate hydrodynamic pressure and useful flow rate [55], however, there are no formulas that relate coolant-induced force and

useful flow rate. This increase in useful flow rate means increased cooling, lubrication, and transport of debris from the grinding zone. The result of increased lubrication and transport of debris from the grinding zone is a decrease in spindle power and grinding forces due to reduced friction and wheel loading which is believed to be responsible for the results presented in Chapter 6.

The coolant-induced force results shown in Figure 7.4 also help to explain the force ratio results from section 6.4.4. The coolant-induced force only results in a change in normal force and does not have a significant effect on the tangential force. Tangential force data was also collected during the coolant-induced force experiments and it was found that the tangential force did not vary with respect to groove depth for these experiments. Recall that the normal forces and tangential forces for creep-feed grinding with a grooved wheel were ~55% and ~45% less than those measured during grinding with a non-grooved wheel. The greater reduction in normal force observed can be attributed to the grooved wheel significantly reducing the coolant-induced normal force.

The results from Figure 7.4 show how the coolant-induced force changes with respect to groove depth for a grooved grinding wheel whose surface consists of both grooved and non-grooved areas. However, it would be interesting to know how the coolant-induced force changes with respect to groove depth in the grooved areas exclusively. Thus, to imitate the coolant flow through a single groove, another series of experiments were performed. In these experiments, a single 3.2 mm wide groove was cut into a grinding wheel and a workpiece with a width of 3.2 mm was used such that the edges of the groove slightly overlap the edges of the workpiece. Experiments were performed such that the gap between the bottom of the groove and the surface of the workpiece was gradually reduced until the minimum gap at which no points within the groove are in contact with the workpiece. This minimum height was found by gradually lowering the grinding wheel until the real-time normal force reading from the dynamometer changed. The coolant-induced force data was then collected to simulate how the coolant-induced force changes at different groove depths for a single groove. The workpiece and grinding wheel used for these experiments are shown in Figure 7.5. The results for these experiments are shown in Figure 7.6.

Figure 7.5: Setup for coolant flow groove depth experiments
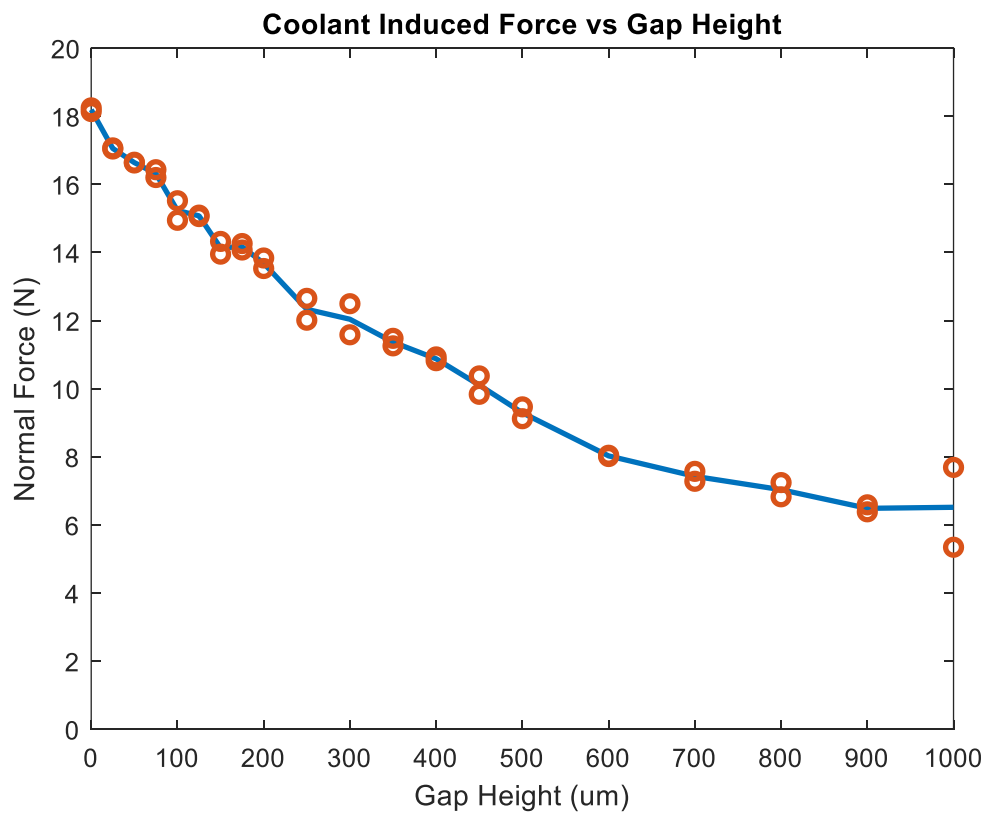
Figure 7.6: Coolant-induced force vs gap height for a single groove

Similar to the results from Figure 7.4, the results from Figure 7.6 indicate that the coolant-induced force, and therefore, the hydrodynamic pressure, decrease with respect to groove depth. It is believed that at a certain groove depth, which appears to be at about 600 μm for the results from Figure 7.6, there is no longer a wedging effect between the wheel and the workpiece since the groove provides enough space for all the coolant to flow through it without significantly pressurizing the coolant.

Therefore, a grooved grinding wheel can be considered to have high coolant pressure and low coolant pressure areas, where the high coolant pressure occurs in the non-grooved areas, and the low coolant pressure occurs in the grooved areas. The coolant pressure in the non-grooved areas remains constant and the coolant pressure in the grooved areas decreases with respect to increasing groove depth until it reaches a minimum when it is no longer being wedged. The overall hydrodynamic pressure experienced by a grooved grinding wheel can then be thought of as the sum of these high pressure and low pressure areas. This concept is illustrated in Figure 7.7. The blue curve in Figure 7.7 is similar to the results from Figure 7.4 since it represents the overall hydrodynamic pressure in the grinding zone for a grooved wheel. The green curve in Figure 7.7 is similar to the results from Figure 7.6 since it represents the pressure in the grooved half of the wheel only. The drop in pressure results in the benefits mentioned earlier; namely, increases in useful flow rate which improves lubrication and transport of debris from the grinding zone.

However, a consequence of having high pressure and low pressure areas on the surface of the grinding wheel is that the coolant may be more inclined to flow through the low pressure areas (the grooves) and less likely to flow through the high pressure areas to fill the pores at the surface of the grinding wheel. Therefore, although coolant flow through the grinding zone is increased by using a grooved wheel, it is possible that transport of coolant into the grinding zone via the pores of the grinding wheel is reduced. It is unclear what effect this reduction of coolant in the pores would have and more research is needed to validate this hypothesis.
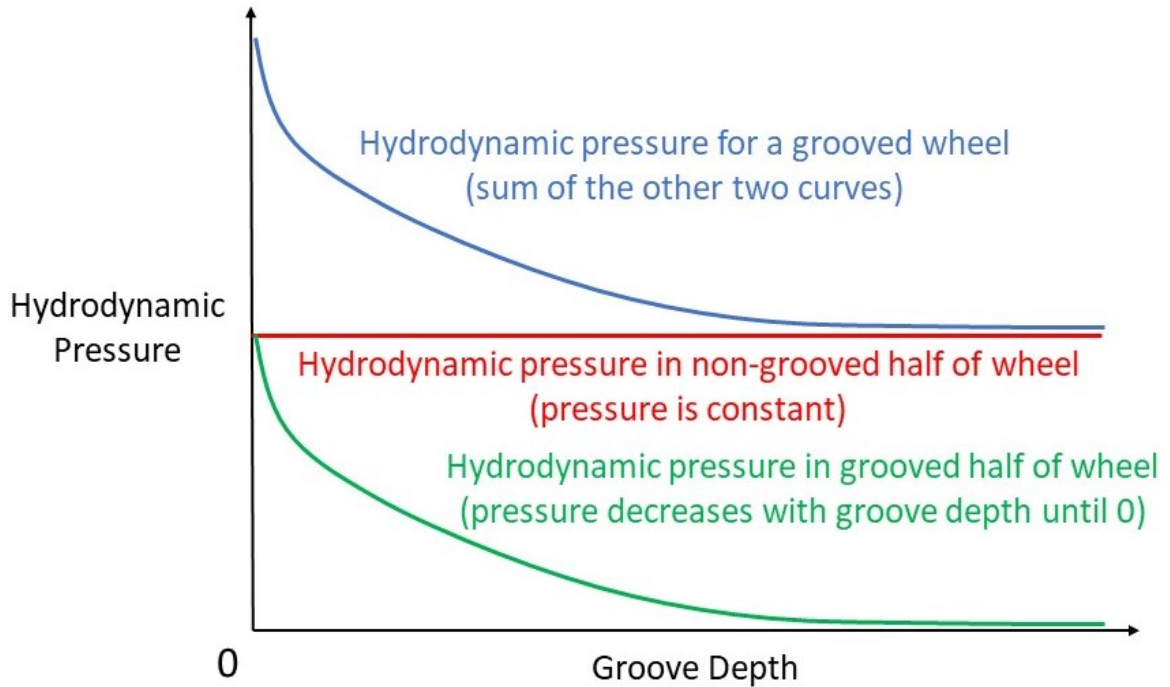
Figure 7.7: Hydrodynamic pressure for a grooved grinding wheel

7.3 SUMMARY

This chapter presented an analysis of how changes in groove depth relate to the two mechanisms responsible for the improvements in grinding performance observed when using grooved grinding wheels. These two mechanisms are 1) increases in uncut chip thickness caused by increased average cutting edge spacing and 2) improved coolant flow. It was found that, for the creep-feed grinding experiments presented in Chapter 6, the uncut chip thickness is constant for every groove depth excluding 0 groove depth (non-grooved wheel). At groove depths <5 μm, the maximum cutting edge spacing, and therefore, the maximum uncut chip thickness is achieved and is then unaffected by further increases in groove depth. Thus, it was concluded that the changes in results observed at different groove depths cannot be attributed to changes in uncut chip thickness.

This chapter proceeded by concluding that the changes in results observed at different groove depths can be attributed to changes in useful flow rate. A literature review

on cutting fluid application in the grinding process was performed and it was found that more porous wheels have higher useful flow rates. Pores and grooves are both types of "air gaps". By increasing the depth of a groove, the volume of air gap is increasing which would result in an increase in useful flow rate. It was also discussed how the wedging of the coolant between the grinding wheel and the workpiece results in the generation of a hydrodynamic pressure in the grinding zone. Higher hydrodynamic pressures indicate that higher volumes of coolant are being rejected from the grinding zone, thereby reducing the useful flow rate.

A series of experiments were performed to measure the coolant-induced force resulting from the hydrodynamic pressure generated for different groove depths. It was found that the coolant-induced force decreases with respect to groove depth until a groove depth of about 400 μm and that deeper groove depths do not influence the coolant-induced force significantly. This result indicates that the useful flow rate increases with respect to groove depth until about 400 μm. This means that cooling, lubrication, and transport of debris from the grinding zone increases up until 400 μm which results in reduced power and forces which is consistent with the power and forces results observed in Chapter 6.

Another series of experiments were performed to measure the coolant-induced force through a single groove. This set of experiments once again found that coolant-induced force decreases with respect to groove depth. It was then suggested that the hydrodynamic pressure resulting from using a grooved grinding wheel is the sum of the pressure in the grooved areas and the non-grooved areas. The pressure in the non-grooved areas is constant since the air gap volume in these areas is constant whereas the pressure in the grooved areas decreases with respect to groove depth since the air gap volume in these areas is increasing. It is possible that the coolant is more likely to flow through the low pressure grooved areas and less likely to flow through the high pressure areas between the surface of the grinding wheel and the workpiece which would mean a reduced ability to fill the pores at the surface of the grinding wheel. To summarize the findings of this chapter in a single sentence: the useful flow rate increases with respect to groove depth up to a certain depth, and the coolant-induced force is an indicator of this increase in useful flow rate, but the coolant may be less likely to fill the pores of the grinding wheel.

CHAPTER 8: CONCLUSION

This concluding chapter provides a summary of how the research presented in this thesis satisfies the objectives outlined in the introductory chapter and identifies gaps in the research that should be subject to future investigation.

8.1 OBJECTIVES

The first objective of this thesis was to determine whether it is possible to cut a groove into a grinding wheel whose width does not change relative to depth. This objective was accomplished by using two grooving tools whose widths do not change relative to depth. One of the tools was in the shape of a cylinder having a 3.2 mm diameter and the other tool was in the shape of a rectangular prism having a 1.7 mm wide cutting surface. The resulting grooved grinding wheels were scanned using a grinding wheel topography scanning system. Upon analysing the scans, it was found that the changes in groove width with respect to groove depth were negligible. A method of computing the groove depth based on the wheel topography scan data was introduced. This method took the value of the 95th percentile of points at the surface of the wheel and the 95th percentile of points within the groove. The difference between these two values was taken as the groove depth.

The second objective of this thesis was to experimentally investigate the effect of various groove depths on grinding performance. A series of creep-feed grinding experiments were performed for both the wheel having the 3.2 mm wide groove and the wheel having the 1.7 mm wide groove. Grinding forces and spindle power decreased with respect to groove depth with diminishing reductions in forces and power as groove depth increases. It was found that groove depths greater than ~400 μm do not provide any further significant reductions in forces and power. Upon normalizing the forces and power results, it was found that for every depth of cut, the spindle power, normal force, and tangential force were reduced by a maximum of ~45%, ~55%, and ~45%, respectively, compared to a non-grooved wheel. This finding indicates that the effect of groove depth is not related to the depth of cut. However, although the percentage reductions in grinding forces and power are similar for every depth of cut, the reductions in magnitude for grinding forces

and power are greater for higher depths of cut. The workpiece surface roughness were found to equate to an excellent "polish" finish with values ranging from 0.11 – 0.23 µm and it was determined that groove depth does not influence surface roughness for AISI 4140 steel. The specific energy values indicated that grinding efficiency increases with respect to groove depth until about a groove depth of ~400 µm. The force ratio values increased continuously with respect to groove depth.

The third objective was to investigate the effect of different groove widths on grinding performance while keeping the groove factor constant. For the two groove widths of 3.2 mm and 1.7 mm that were compared, there were almost no significant differences in grinding results observed. The only difference in results was that, for the groove width of 1.7 mm, the workpiece surface roughness was increased compared to the non-grooved wheel. For the groove width of 3.2 mm, on the other hand, the workpiece surface roughness achieved by the grooved wheel and the non-grooved wheel were similar. These findings indicate that similar results can be obtained for groove widths in the range of 1.7 – 3.2 mm, and that it is possible that larger groove widths lead to better workpiece surface roughness.

The fourth and final objective was to provide explanations on why different groove geometries produce different results. There are two mechanisms through which grooved grinding wheels increase grinding performance: 1) increased cutting edge spacing and uncut chip thickness and 2) improved coolant flow. It was determined that at groove depths much shallower than the ones used in the experiments performed for this research, the maximum benefits of the increased uncut chip thickness are achieved. Improved coolant flow must then be responsible for the changes in grinding performance observed at different groove depths. A series of experiments found that the coolant-induced force, and thus the hydrodynamic pressure, decreases with respect to groove depth up until a depth of about ~400 µm. A reduction in hydrodynamic pressure indicates that less coolant is rejected from entering the grinding zone. Therefore, the useful flow rate through the grinding zone increases with respect to groove depth which explains the changes in grinding forces and spindle power observed at different groove depths. However, a reduction in hydrodynamic pressure may also indicate a reduced ability of the coolant to fill the pores at the surface of the grinding wheel.

8.2 RECOMMENDATIONS FOR FUTURE WORK

There are practically an infinite number of different possible groove geometries, so there remains plenty of opportunity for further investigations on this subject. In terms of groove width and groove depth, the following areas could be further explored:

- The effect of groove widths outside the range of 1.7 – 3.2 mm. It would be especially interesting to study very small groove widths (<10 µm) and the largest possible groove widths. For instance, the largest possible groove width for a wheel having a groove factor of 50% would be half of the wheel width. This would be especially helpful to verify whether larger groove widths have less of a harmful effect on workpiece surface roughness.

- The effect of the ratio of groove width to groove depth. For instance, if the groove depth is several times greater than the groove width, would this compromise the structural integrity of the grinding wheel?

- The effect of groove depth in the presence of different cooling conditions. For grinding experiments with a reduced coolant flow rate, would the grinding forces and spindle power stop decreasing at a groove depth of 400 µm or would they level off before this depth?

APPENDIX A: PROGRAM FLOWCHARTS
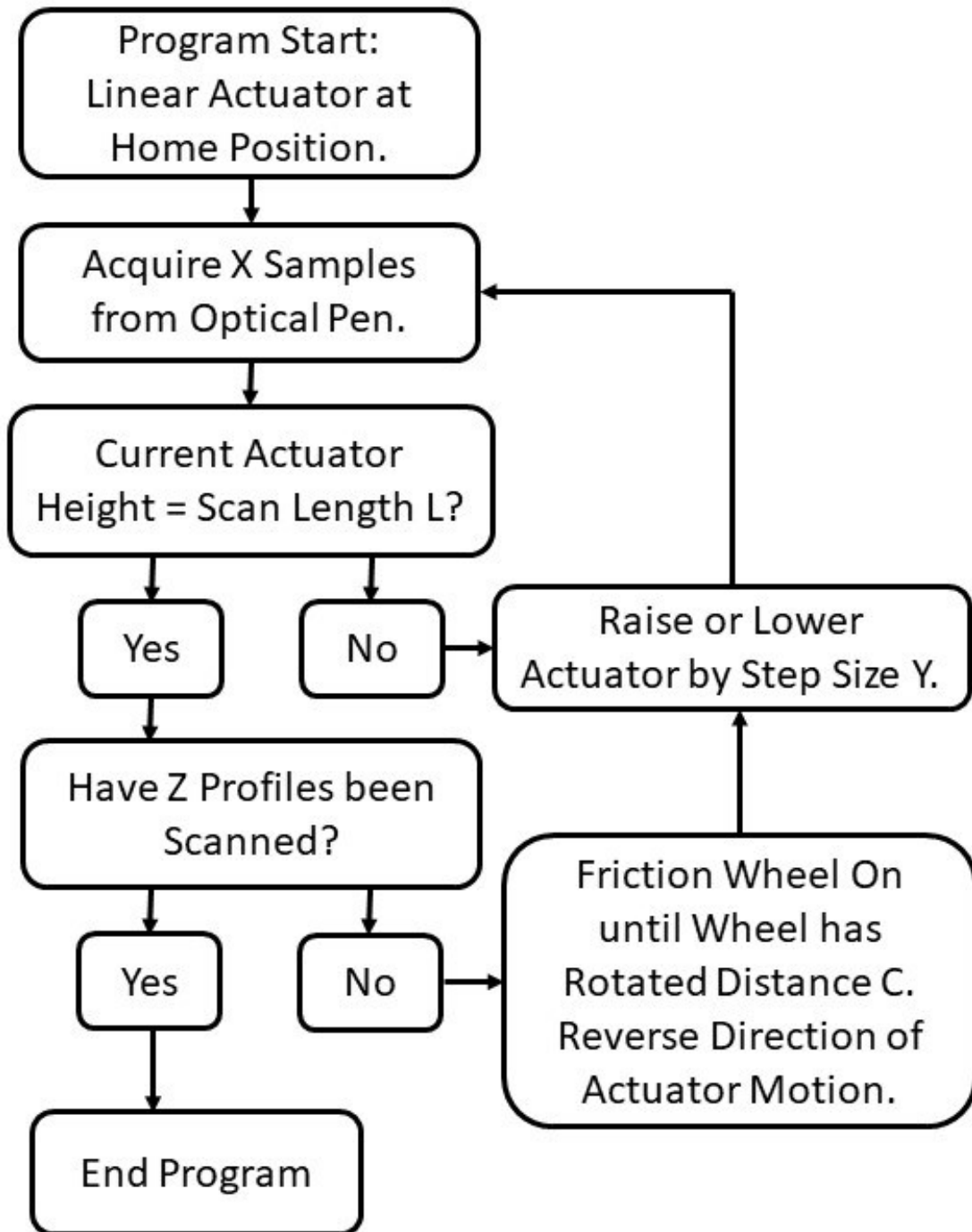
Figure A.1: Wheel scannner program flowchart
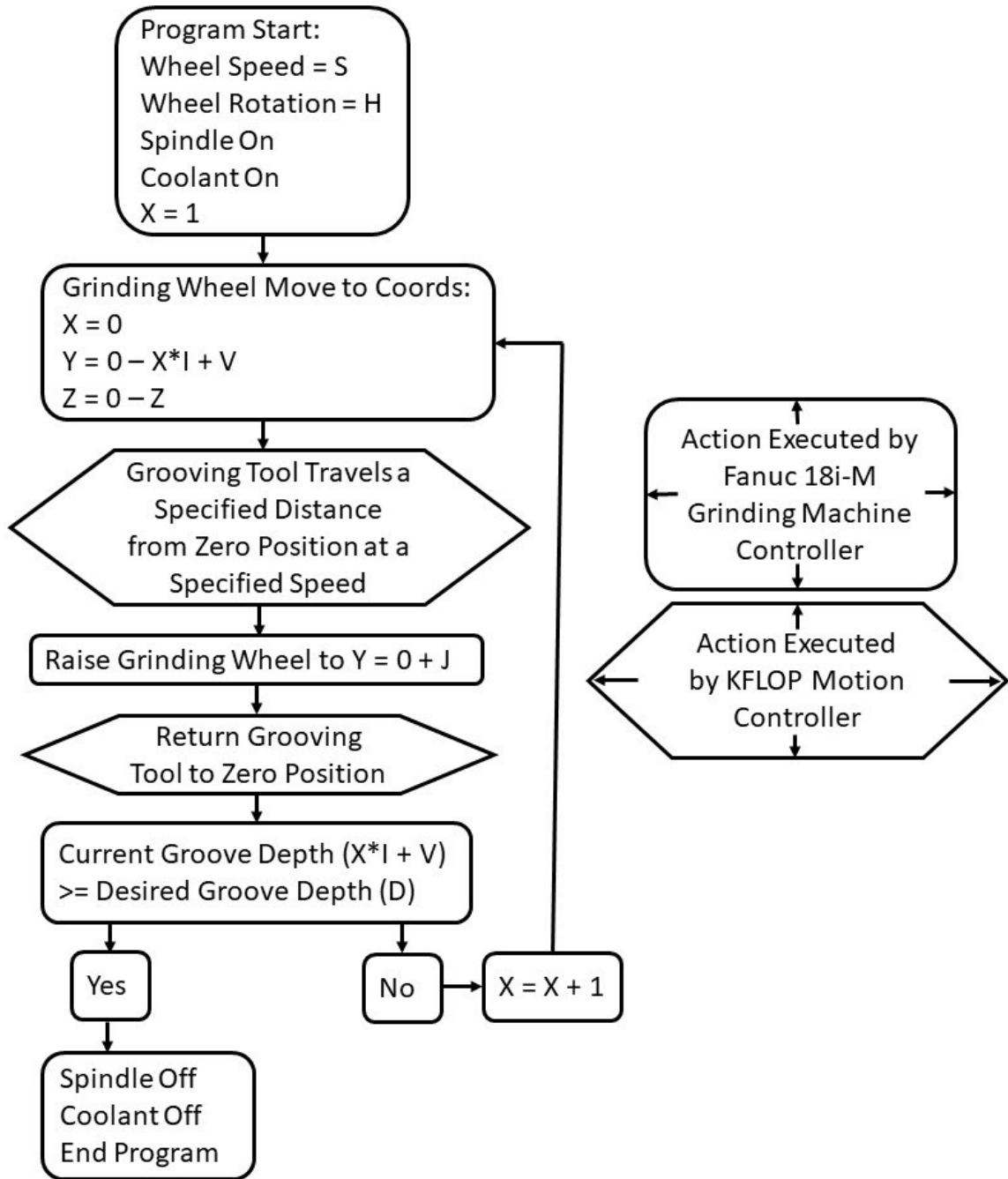
Figure A.2: Grooving program flowchart

Table A.1: Wheel scanner program variables

Variable	Meaning	Value
X	Number of measurements to acquire at each point	1
Y	Linear actuator step size (um)	4
L	Length of each profile to be scanned (um)	28000
C	Distance between profiles on wheel circumference (um)	5
Z	Number of profiles to scan	50

Table A.2: Grooving program variables

Variable	Meaning	Typical Value
S	Wheel speed (ft/min)	Changes with diameter to maintain 150 RPM
H	Direction of wheel rotation	Clockwise
D	Final groove depth (in)	0.04" (1016 um)
I	Infeed per cut (in)	0.00025" (6.35 um)
J	Height to raise wheel after tool pass (in)	0.5"
K	Number of retracing passes at final depth	0-5
V	Starting groove depth (in)	Always 0 unless the wheel is already grooved
Z	Z-axis offset from zero position (in)	0.3"

APPENDIX B: INITIAL WHEEL SCANS
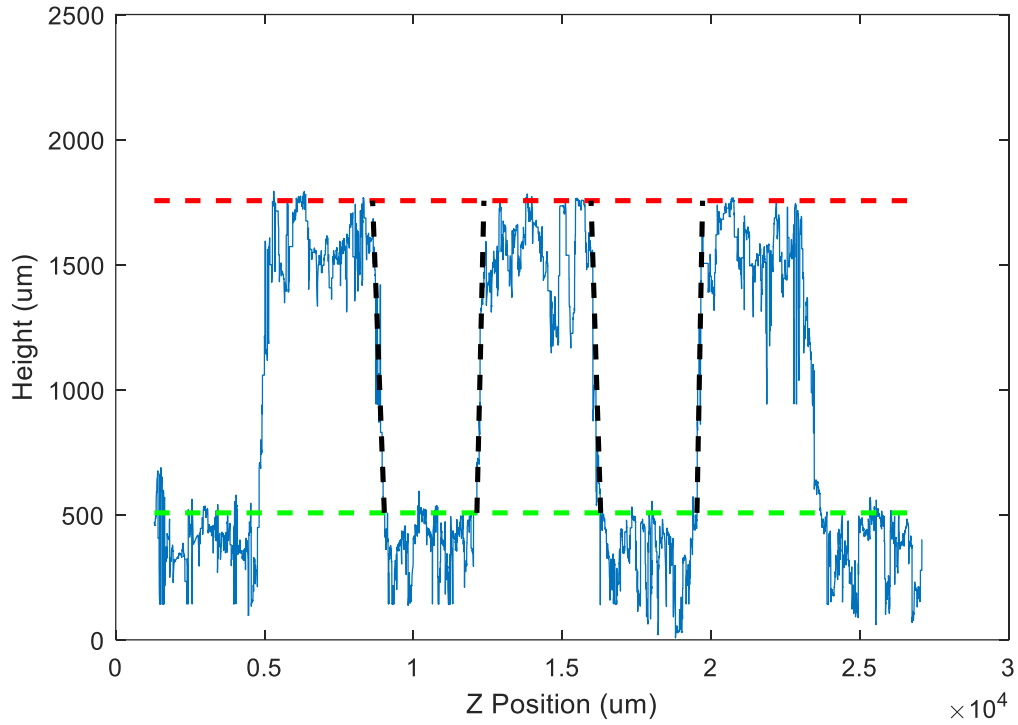
Figure B.1: Initial topography scan of grinding wheel A (2/3)
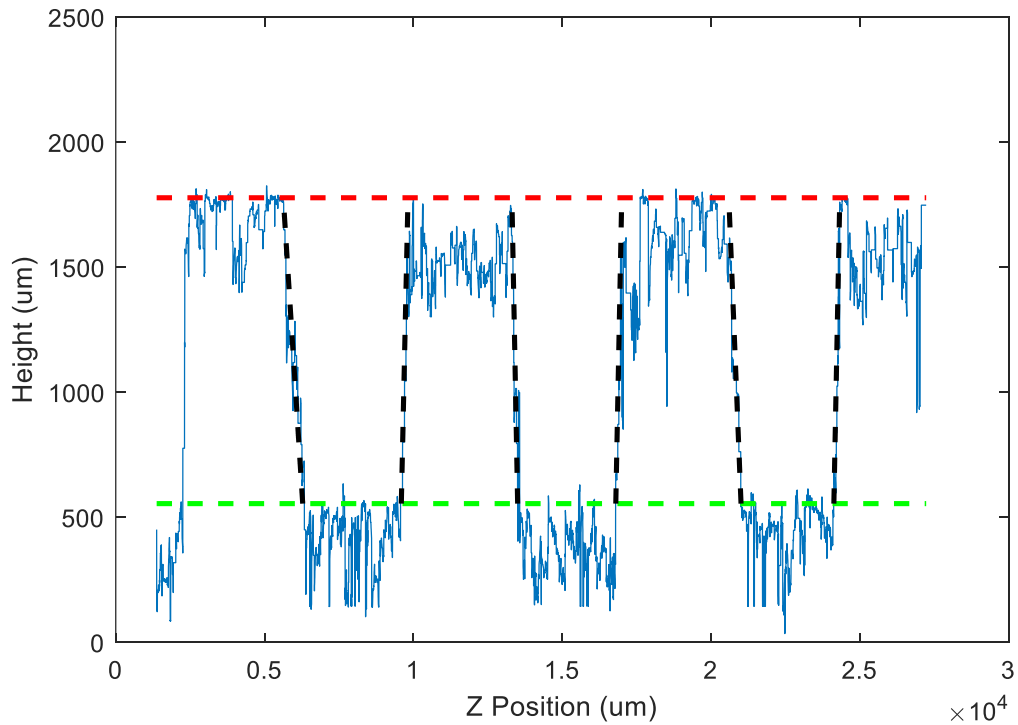
Figure B.2: Initial topography scan of grinding wheel A (3/3)
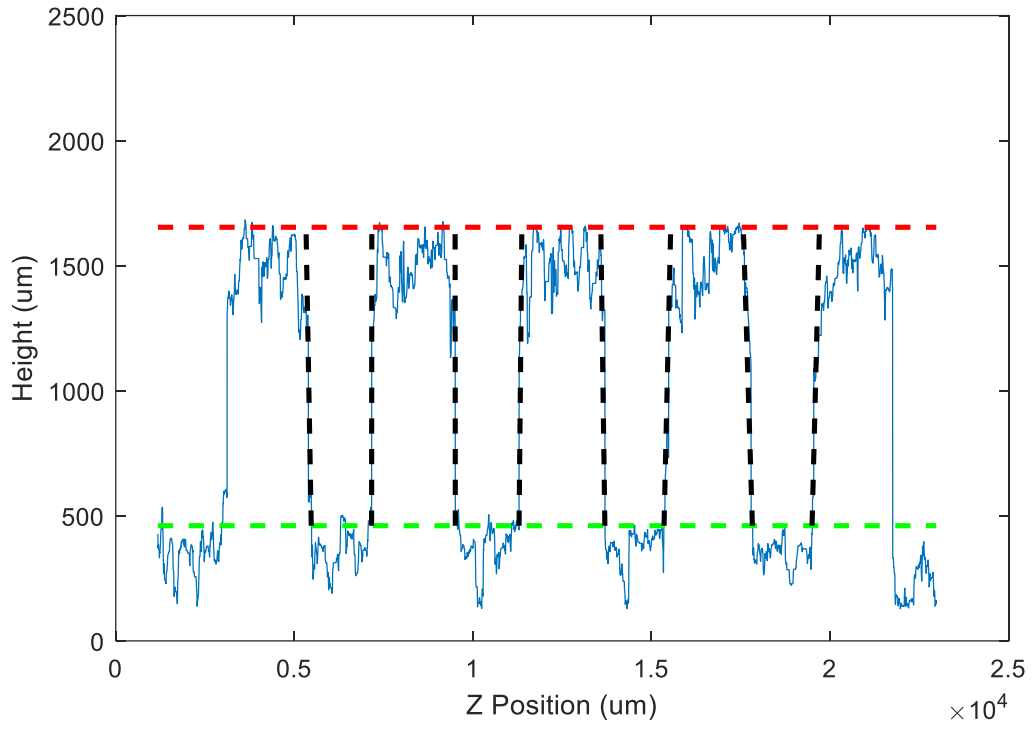
Figure B.3: Initial topography scan of grinding wheel B (2/3)
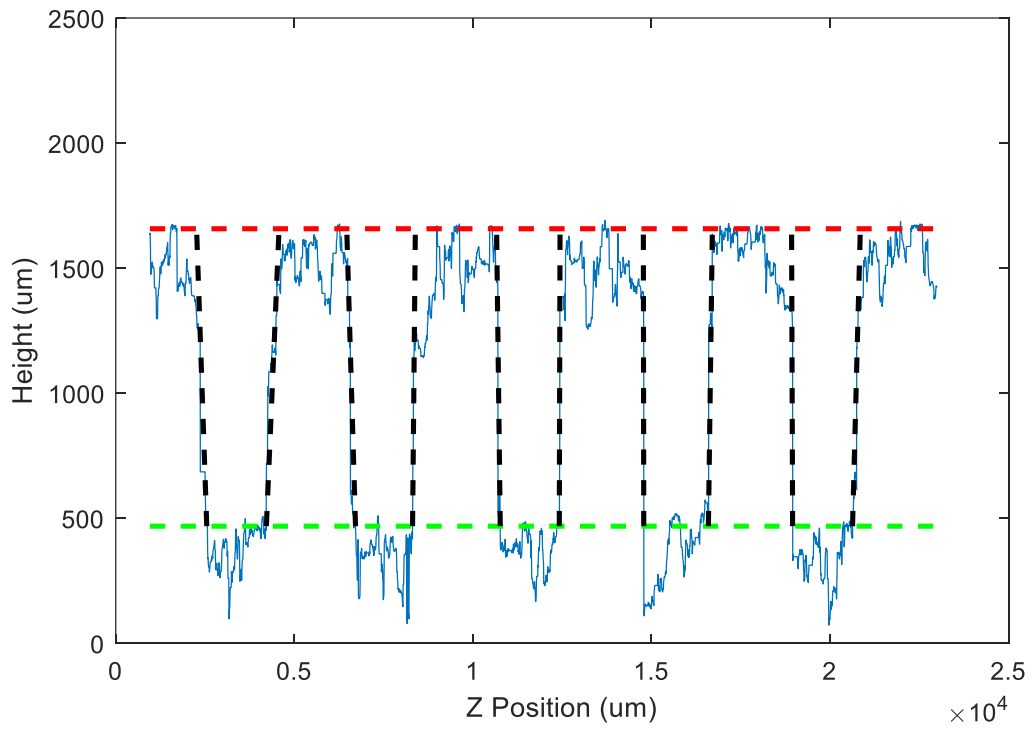
Figure B.4: Initial topography scan of grinding wheel B (3/3)

APPENDIX C: INTERMEDIATE WHEEL SCANS
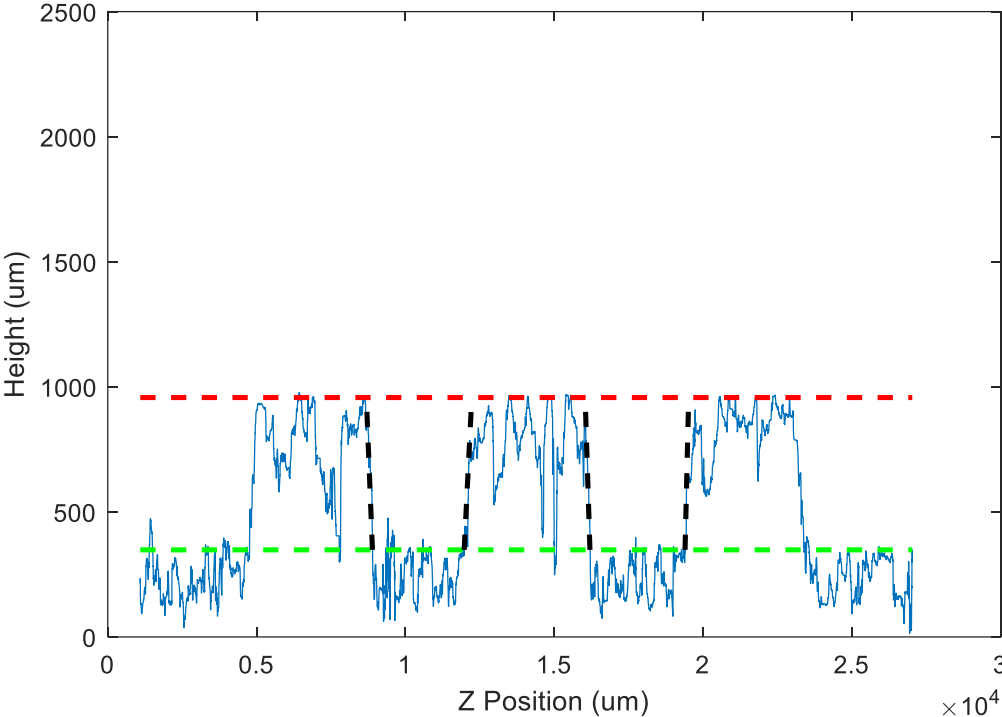
Figure C.1: Intermediate topography scan of grinding wheel A (2/3)
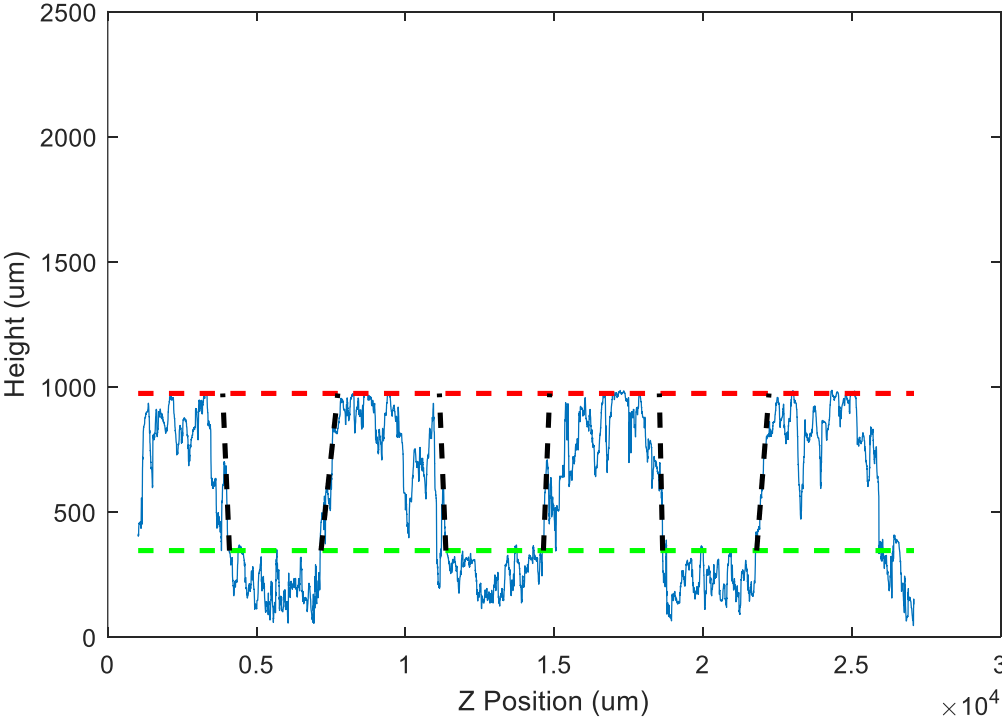
Figure C.2: Intermediate topography scan of grinding wheel A (3/3)
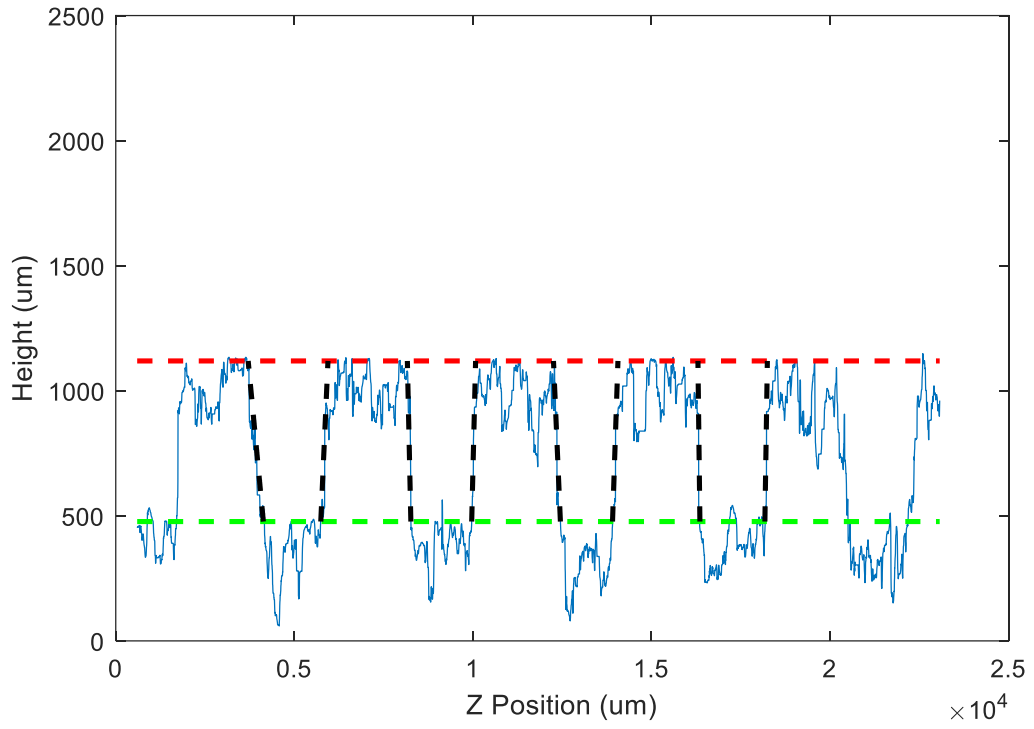
Figure C.3: Intermediate topography scan of grinding wheel B (2/3)
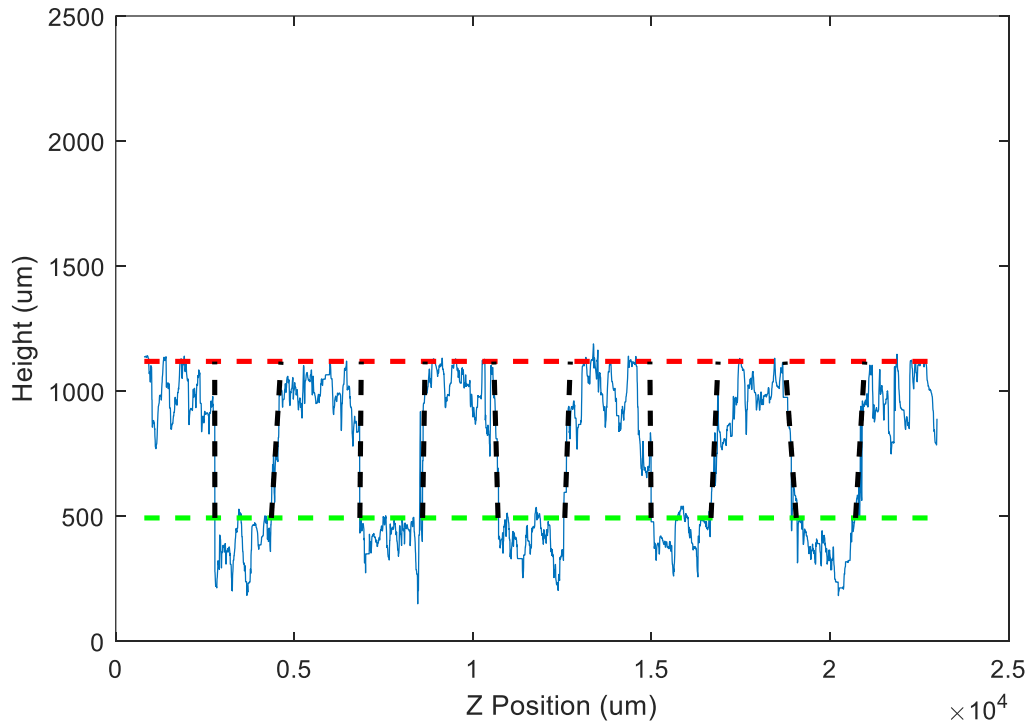
Figure C.4: Intermediate topography scan of grinding wheel B (3/3)

APPENDIX D: RESULTS FIGURES
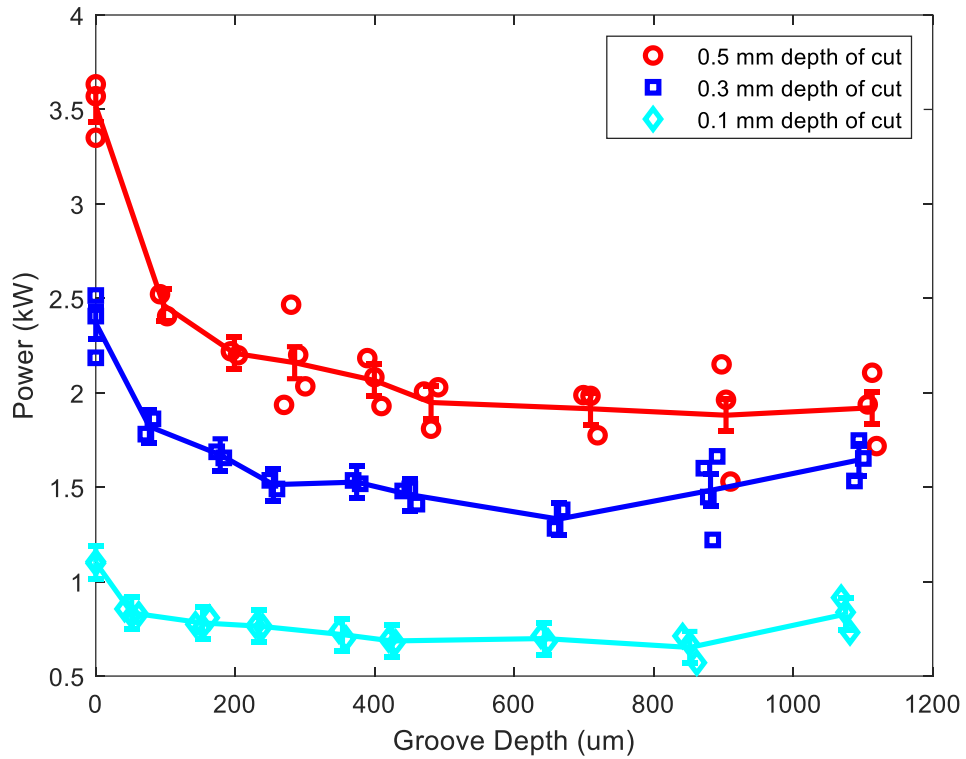
Figure D.1: Spindle power vs groove depth for experiment series A
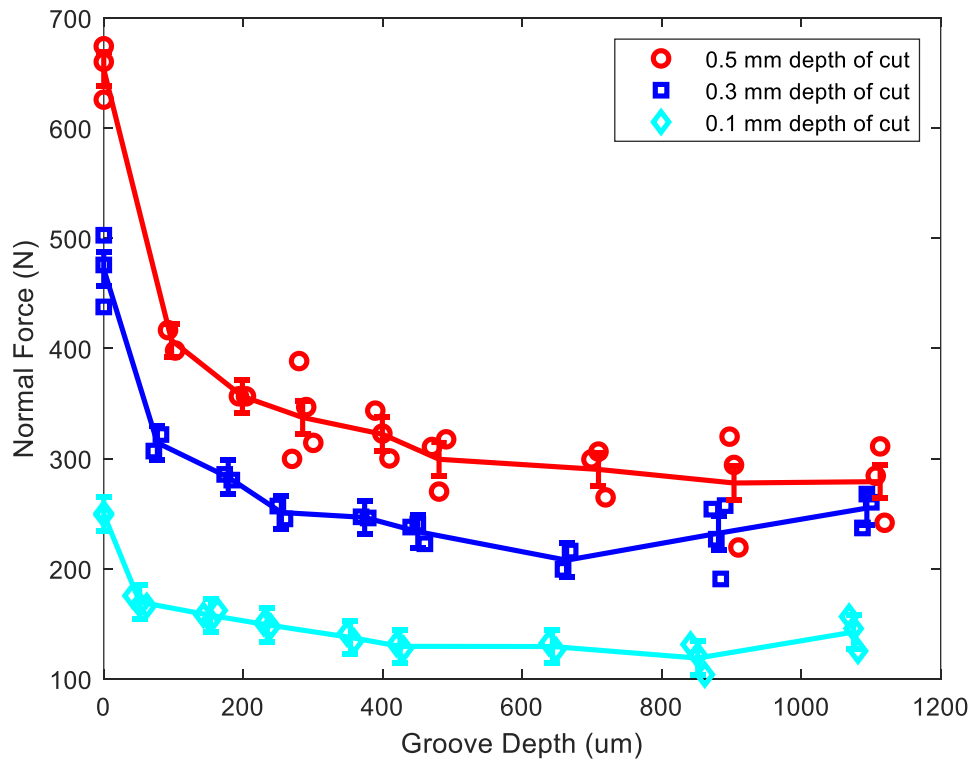
Figure D.2: Normal force vs groove depth for experiment series A
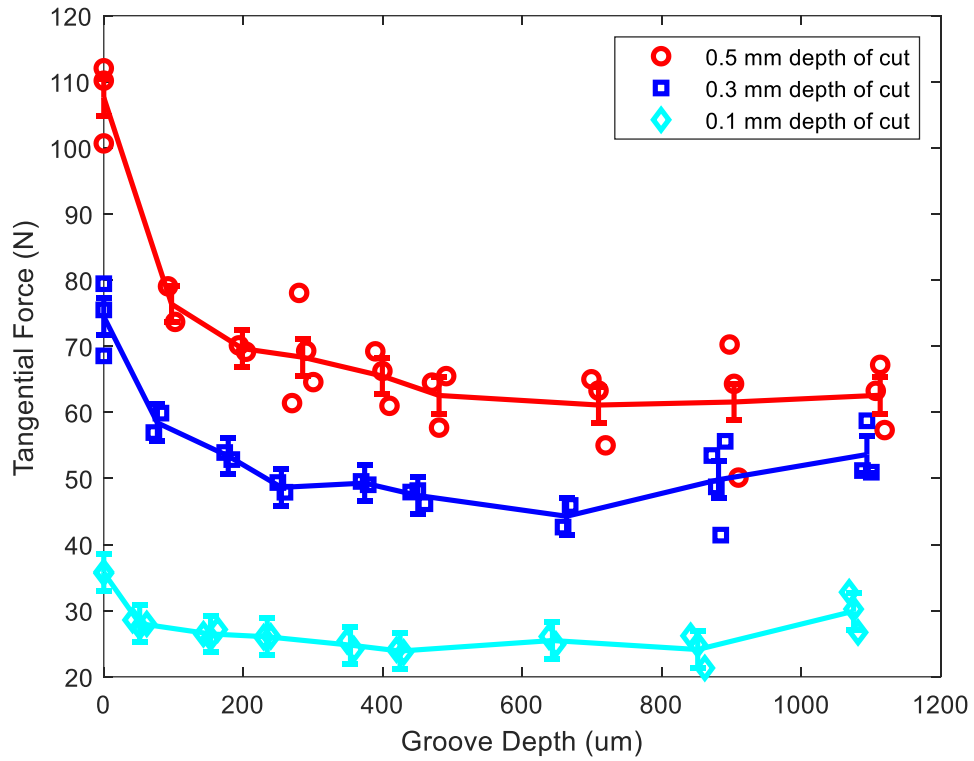
Figure D.3: Tangential force vs groove depth experiment series A
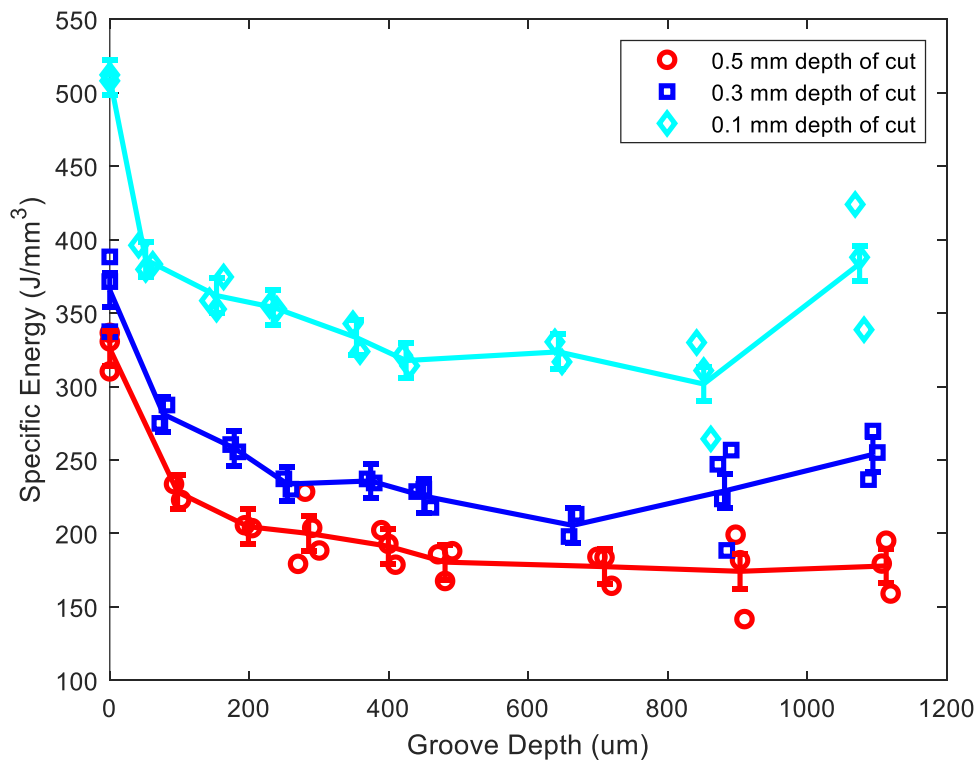
Figure D.4: Specific energy vs groove depth for experiment series A
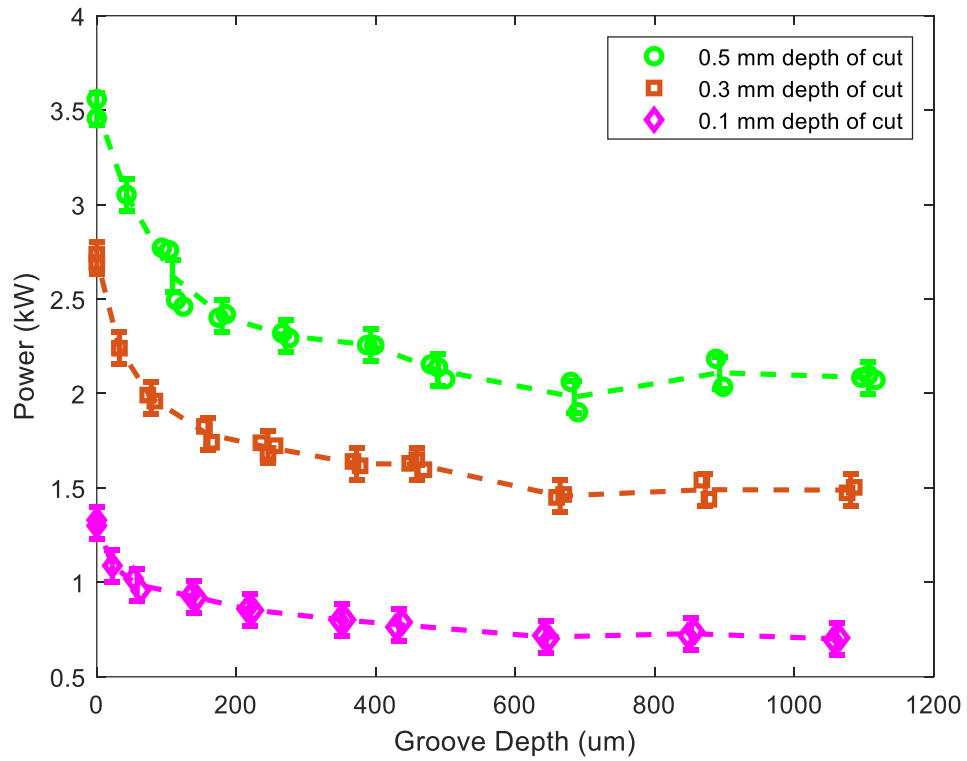
Figure D.5: Spindle power vs groove depth for experiment series B
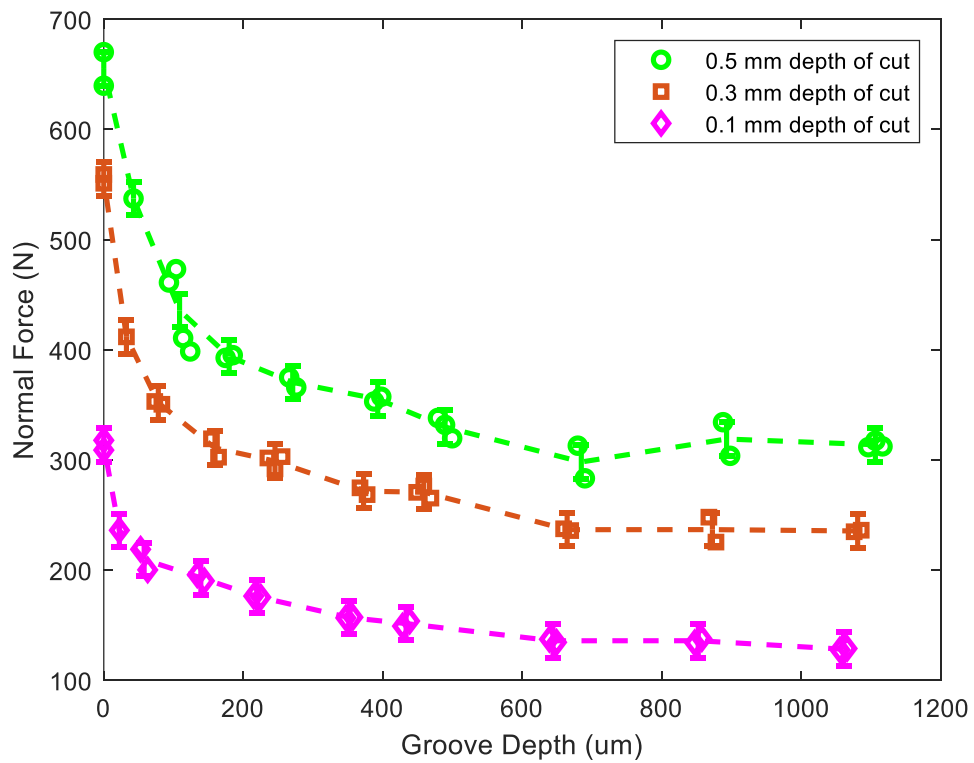
Figure D.6: Normal force vs groove depth for experiment series B

110
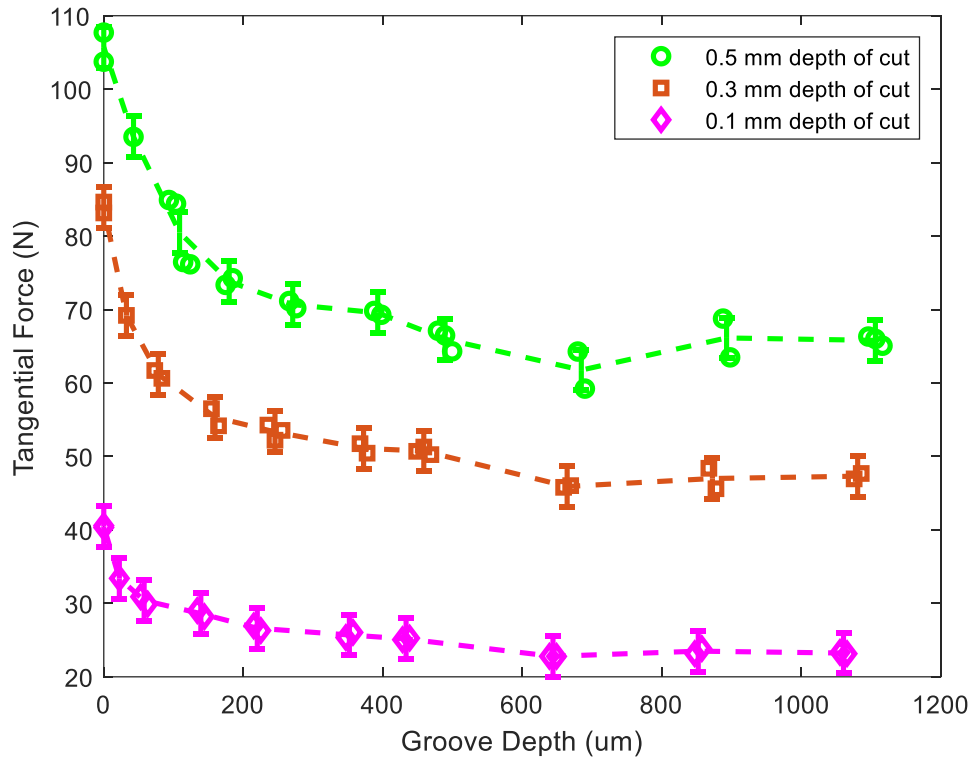
Figure D.7: Tangential force vs groove depth for experiment series B
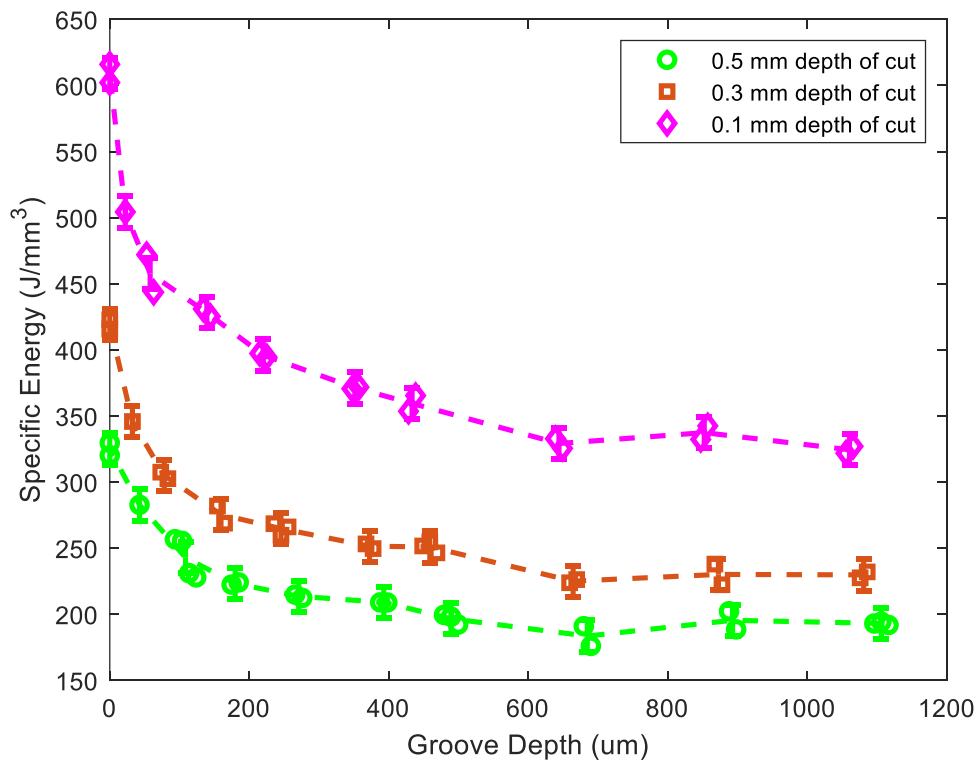
Figure D.8: Specific energy vs groove depth for experiment series B

111

APPENDIX E: RESULTS TABLES

Table E.1: Experiment series A results (1/2)

| Exp #	a (mm)	d (µm)	b_g (µm)	η (%)	P (kW)	F_n (N)	F_t (N)	e_c (J/mm³)	µ	R_a (µm)
1	0.5	1119.6	3687.1	48.8	1.72	241.8	57.3	159.1	0.24	0.22
2	0.5	1113.2	3684.4	48.8	2.11	311.1	67.2	195.1	0.22	0.16
3	0.5	1106.9	3681.7	48.9	1.94	284.5	63.3	179.5	0.22	0.17
4	0.3	1100.5	3678.9	48.9	1.65	260.4	50.9	255.1	0.20	0.19
5	0.3	1094.2	3676.2	48.9	1.75	267.8	58.7	269.7	0.22	0.17
6	0.3	1087.8	3673.5	49.0	1.53	237.1	51.2	236.7	0.22	0.19
7	0.1	1081.5	3670.8	49.0	0.73	125.4	26.7	338.7	0.21	0.18
8	0.1	1075.1	3668.1	49.1	0.84	145.8	30.2	388	0.21	0.19
9	0.1	1068.8	3665.4	49.1	0.92	156.6	32.8	424	0.21	0.20
10	0.5	910.0	3597.7	50.0	1.53	219.4	50.1	141.7	0.23	0.15
11	0.5	903.7	3595.0	50.1	1.96	294.3	64.3	181.8	0.22	0.16
12	0.5	897.3	3592.3	50.1	2.15	320.0	70.3	199.2	0.22	0.17
13	0.3	891.0	3589.6	50.1	1.66	257.4	55.6	256.8	0.22	0.20
14	0.3	884.6	3586.9	50.2	1.22	190.8	41.4	188.5	0.22	0.16
15	0.3	878.3	3584.2	50.2	1.45	226.9	48.7	223.6	0.21	0.19
16	0.3	871.9	3581.5	50.3	1.60	254.1	53.5	247.1	0.21	0.16
17	0.1	861.7	3577.2	50.3	0.57	103.9	21.3	264.4	0.21	0.18
18	0.1	851.6	3572.8	50.4	0.67	121.6	24.8	310.9	0.20	0.17
19	0.1	841.4	3568.5	50.4	0.71	131.3	26.2	330	0.20	0.15
20	0.5	719.5	3516.5	51.2	1.77	264.8	55.0	164.4	0.21	0.14
21	0.5	709.3	3512.2	51.2	1.98	306.4	63.3	183.7	0.21	0.15
22	0.5	699.2	3507.9	51.3	1.99	299.4	65.0	184.1	0.22	0.16
23	0.3	668.7	3494.9	51.5	1.38	216.1	45.9	213.1	0.21	0.16
24	0.3	658.5	3490.5	51.5	1.28	199.5	42.7	197.9	0.21	0.14
25	0.1	648.4	3486.2	51.6	0.68	126.3	24.9	316.8	0.20	0.17
26	0.1	638.2	3481.9	51.6	0.71	132.6	26.1	330.4	0.20	0.17
27	0.5	490.9	3419.1	52.5	2.03	317.6	65.5	188	0.21	0.15
28	0.5	480.7	3414.7	52.6	1.81	270.1	57.7	167.6	0.21	0.18
29	0.5	470.6	3410.4	52.6	2.01	310.6	64.5	185.9	0.21	0.14
30	0.3	460.4	3406.1	52.7	1.41	222.7	46.2	217.7	0.21	0.16
31	0.3	450.3	3401.7	52.8	1.49	240.6	48.2	230.2	0.20	0.15
32	0.3	440.1	3397.4	52.8	1.48	237.9	47.9	228.5	0.20	0.15
33	0.1	429.9	3393.1	52.9	0.68	127.5	23.7	314.1	0.19	0.17
34	0.1	419.8	3388.8	52.9	0.69	131.7	24.1	321.3	0.18	0.17
35	0.5	409.6	3384.4	53.0	1.93	300.2	61.0	178.8	0.20	0.15
36	0.5	399.5	3380.1	53.1	2.08	322.8	66.3	192.9	0.21	0.18

Table E.2: Experiment series A results (2/2)

Exp #	a (mm)	d (μm)	b_g (μm)	η (%)	P (kW)	F_n (N)	F_t (N)	e_c (J/mm³)	μ	R_a (μm)
37	0.5	389.3	3375.8	53.1	2.18	343.6	69.2	202.3	0.20	0.17
38	0.3	379.1	3371.4	53.2	1.52	246.1	49.1	234.4	0.20	0.16
39	0.3	369.0	3367.1	53.2	1.54	247.2	49.6	237.1	0.20	0.15
40	0.1	358.8	3362.8	53.3	0.70	134.3	24.1	323.8	0.18	0.16
41	0.1	348.7	3358.4	53.4	0.74	141.2	25.4	342.8	0.18	0.14
42	0.5	300.4	3337.9	53.6	2.03	314.3	64.6	188.4	0.21	0.18
43	0.5	290.2	3333.5	53.7	2.20	346.8	69.3	203.9	0.20	0.20
44	0.5	280.1	3329.2	53.8	2.47	388.6	78.1	228.5	0.20	0.24
45	0.5	269.9	3324.9	53.8	1.94	299.8	61.4	179.3	0.20	0.18
46	0.3	259.8	3320.5	53.9	1.49	245.3	47.9	230.2	0.20	0.18
47	0.3	249.6	3316.2	53.9	1.54	257.0	49.4	237.2	0.19	0.19
48	0.1	239.4	3311.9	54.0	0.76	147.7	26.1	352.7	0.18	0.19
49	0.1	229.3	3307.5	54.1	0.77	150.7	26.0	355.2	0.17	0.18
50	0.5	203.9	3296.7	54.2	2.20	356.6	69.2	203.6	0.19	0.17
51	0.5	193.7	3292.4	54.3	2.22	356.6	70.1	205.6	0.20	0.15
52	0.3	183.6	3288.1	54.3	1.66	280.5	52.9	255.6	0.19	0.16
53	0.3	173.4	3283.7	54.4	1.69	285.7	53.9	260.5	0.19	0.16
54	0.1	163.2	3279.4	54.5	0.81	162.2	27.2	374.6	0.17	0.18
55	0.1	153.1	3275.1	54.5	0.76	153.0	25.9	352.7	0.17	0.17
56	0.1	142.9	3270.7	54.6	0.77	158.2	26.4	358.5	0.17	0.16
57	0.5	102.3	3253.4	54.8	2.41	398.2	73.7	222.8	0.19	0.17
58	0.5	92.1	3249.1	54.9	2.52	416.7	79.1	233.6	0.19	0.17
59	0.3	82.0	3244.7	54.9	1.86	321.9	59.9	287.4	0.19	0.18
60	0.3	71.8	3240.4	55.0	1.78	306.9	56.9	274.9	0.19	0.18
61	0.1	61.6	3236.1	55.1	0.83	166.4	28.0	383.3	0.17	0.16
62	0.1	51.5	3231.7	55.1	0.82	167.5	27.5	379.7	0.16	0.17
63	0.1	41.3	3227.4	55.2	0.86	175.6	28.6	396.2	0.16	0.16
64	0.5	0.0	0.0	100.0	3.35	625.8	100.7	310.3	0.16	0.16
65	0.5	0.0	0.0	100.0	3.63	674.3	112.1	336.6	0.17	0.19
66	0.5	0.0	0.0	100.0	3.57	660.2	110.2	330.7	0.17	0.17
67	0.3	0.0	0.0	100.0	2.51	502.8	79.5	388.3	0.16	0.18
68	0.3	0.0	0.0	100.0	2.19	437.7	68.6	337.4	0.16	0.15
69	0.3	0.0	0.0	100.0	2.41	475.8	75.5	371.5	0.16	0.17
70	0.1	0.0	0.0	100.0	1.10	250.4	35.7	508.1	0.14	0.16
71	0.1	0.0	0.0	100.0	1.11	248.9	35.9	512.2	0.14	0.14

Table E.3: Experiment series B results (1/2)

Exp #	a (mm)	d (μm)	b_g (μm)	η (%)	P (kW)	F_n (N)	F_t (N)	e_c (J/mm³)	μ	R_a (μm)
1	0.5	1116.5	1938.9	52.1	2.07	312.4	65.1	191.9	0.21	0.12
2	0.5	1106.3	1936.8	52.2	2.10	317.5	66.0	194.4	0.21	0.15
3	0.5	1096.2	1934.7	52.2	2.08	311.7	66.3	193.0	0.21	0.19
4	0.3	1086.0	1932.6	52.3	1.50	236.3	47.7	232.0	0.20	0.20
5	0.3	1075.9	1930.5	52.3	1.47	234.9	46.9	227.6	0.20	0.18
6	0.1	1065.7	1928.4	52.4	0.71	128.9	23.2	327.0	0.18	0.18
7	0.1	1055.5	1926.3	52.4	0.69	127.6	23.3	321.8	0.18	0.17
8	0.5	898.1	1893.8	53.2	2.04	303.8	63.5	188.6	0.21	0.14
9	0.5	887.9	1891.7	53.3	2.18	334.3	68.8	202.3	0.21	0.15
10	0.3	877.7	1889.6	53.3	1.44	225.5	45.6	222.3	0.20	0.14
11	0.3	867.6	1887.5	53.4	1.54	248.2	48.4	238.0	0.19	0.14
12	0.1	857.4	1885.4	53.4	0.74	137.9	23.8	342.5	0.17	0.13
13	0.1	847.3	1883.3	53.5	0.72	134.1	23.1	332.3	0.17	0.13
14	0.5	689.8	1850.7	54.3	1.90	283.4	59.2	176.1	0.21	0.22
15	0.5	679.6	1848.6	54.4	2.06	313.0	64.3	191.0	0.21	0.21
16	0.3	669.5	1846.5	54.4	1.47	236.0	46.0	226.2	0.20	0.21
17	0.3	659.3	1844.4	54.5	1.45	237.6	45.8	223.8	0.19	0.21
18	0.1	649.1	1842.3	54.5	0.70	134.6	22.8	325.5	0.17	0.22
19	0.1	639.0	1840.2	54.6	0.72	137.3	22.8	332.8	0.17	0.20
20	0.5	499.5	1811.4	55.3	2.08	319.8	64.3	192.2	0.20	0.18
21	0.5	489.3	1809.3	55.3	2.14	331.9	66.5	198.2	0.20	0.17
22	0.5	479.2	1807.2	55.4	2.15	338.2	67.1	199.6	0.20	0.18
23	0.3	469.0	1805.1	55.4	1.60	265.5	50.2	246.5	0.19	0.17
24	0.3	458.8	1803.0	55.5	1.65	276.4	51.3	254.7	0.19	0.19
25	0.3	448.7	1800.9	55.5	1.63	270.7	50.7	251.7	0.19	0.17
26	0.1	438.5	1798.8	55.6	0.79	153.9	25.3	365.4	0.16	0.17
27	0.1	428.4	1796.7	55.6	0.76	149.3	25.1	353.5	0.17	0.19
28	0.5	397.9	1790.4	55.8	2.26	357.4	69.3	209.0	0.19	0.25
29	0.5	387.7	1788.3	55.8	2.26	353.2	69.8	209.0	0.20	0.20
30	0.3	377.6	1786.2	55.9	1.62	268.6	50.4	249.7	0.19	0.22
31	0.3	367.4	1784.1	55.9	1.64	274.8	51.7	253.2	0.19	0.20
32	0.1	357.2	1782.0	56.0	0.80	157.3	26.0	371.8	0.17	0.20
33	0.1	347.1	1779.9	56.1	0.80	156.7	25.3	370.6	0.16	0.21
34	0.5	276.0	1765.2	56.4	2.29	365.9	70.2	212.4	0.19	0.16
35	0.5	265.8	1763.1	56.5	2.32	375.0	71.2	214.9	0.19	0.17
36	0.3	255.6	1761.0	56.5	1.72	303.1	53.5	266.1	0.18	0.17

Table E.4: Experiment series B results (2/2)

Exp #	a (mm)	d (μm)	b_g (μm)	η (%)	P (kW)	F_n (N)	F_t (N)	e_c (J/mm³)	μ	R_a (μm)
37	0.3	245.5	1758.9	56.6	1.68	292.0	52.2	259.8	0.18	0.16
38	0.3	235.3	1756.8	56.6	1.74	301.9	54.3	268.5	0.18	0.17
39	0.1	225.2	1754.7	56.7	0.85	175.5	26.3	394.7	0.15	0.15
40	0.1	215.0	1752.6	56.7	0.86	176.5	26.9	397.3	0.15	0.16
41	0.5	184.9	1746.4	56.9	2.42	395.2	74.3	224.1	0.19	0.17
42	0.5	174.7	1744.3	56.9	2.40	392.7	73.4	222.4	0.19	0.16
43	0.3	164.6	1742.2	57.0	1.74	302.6	54.2	268.9	0.18	0.17
44	0.3	154.4	1740.1	57.0	1.83	319.2	56.5	281.9	0.18	0.17
45	0.1	144.2	1738.0	57.1	0.92	190.3	28.2	425.2	0.15	0.15
46	0.1	134.1	1735.9	57.1	0.93	195.9	29.0	430.9	0.15	0.15
47	0.5	123.9	1733.8	57.2	2.46	398.5	76.2	227.9	0.19	0.17
48	0.5	113.8	1731.7	57.2	2.49	410.7	76.5	231.1	0.19	0.19
49	0.5	103.6	1729.6	57.3	2.76	473.2	84.4	255.6	0.18	0.18
50	0.5	93.4	1727.5	57.3	2.77	461.1	84.9	256.8	0.18	0.18
51	0.3	83.3	1725.4	57.4	1.96	350.6	60.6	302.6	0.17	0.18
52	0.3	73.1	1723.3	57.4	1.99	353.1	61.7	307.5	0.17	0.18
53	0.1	63.0	1721.2	57.5	0.96	200.3	29.9	443.5	0.15	0.17
54	0.1	52.8	1719.1	57.6	1.02	219.0	30.9	472.0	0.14	0.17
55	0.5	42.6	1717.0	57.6	3.05	537.3	93.5	282.8	0.17	0.16
56	0.3	32.5	1714.9	57.7	2.24	411.8	69.2	345.8	0.17	0.12
57	0.1	22.3	1712.8	57.7	1.09	236.2	33.4	504.3	0.14	0.12
58	0.5	0.0	0.0	100.0	3.46	639.7	103.7	320.3	0.16	0.12
59	0.5	0.0	0.0	100.0	3.56	670.2	107.7	329.7	0.16	0.12
60	0.3	0.0	0.0	100.0	2.69	551.2	83.2	415.7	0.15	0.11
61	0.3	0.0	0.0	100.0	2.74	559.2	84.6	422.7	0.15	0.13
62	0.1	0.0	0.0	100.0	1.30	309.0	40.3	602.1	0.13	0.10
63	0.1	0.0	0.0	100.0	1.33	317.9	40.6	616.0	0.13	0.10

REFERENCES

1. Malkin, S. (1989). *Grinding technology: Theory and applications of machining with abrasives*. Chichester: Ellis Horwood. Print.

2. Groover, M. P. (2007). *Fundamentals of modern manufacturing materials, processes, and systems*. New York: Wiley. Print.

3. Li, H. N., & Axinte, D. (2016). Textured grinding wheels: A review. *International Journal of Machine Tools and Manufacture*, *109*, 8–35.

4. Forbrigger, C., Bauer, R., & Warkentin, A. (2017). A review of state-of-the-art vitrified bond grinding wheel grooving processes. *The International Journal of Advanced Manufacturing Technology*, *90*(5–8), 2207–2216.

5. Jiang, J., Ge, P., & Hong, J. (2013). Study on micro-interacting mechanism modeling in grinding process and ground surface roughness prediction. *International Journal of Advanced Manufacturing Technology*, *67*, 1035–1052.

6. Brinksmeier, E., Heinzel, C., & Wittmann, M. (1999). Friction, Cooling and Lubrication in Grinding. *CIRP Annals - Manufacturing Technology*, *48*(2), 581–598.

7. Irani, R. A., Bauer, R., & Warkentin, A. (2005). A review of cutting fluid application in the grinding process. *International Journal of Machine Tools and Manufacture*, *45*(15), 1696–1705.

8. Rowe, B. W (2014). *Principles of modern grinding technology.* William Andrew. Print.

9. Kim, J., Kang, Y., Jini, D., & Lee, Y. (1997). Development of discontinuous grinding wheel with multi-porous grooves. *International Journal of Machine Tools and Manufacture*, *37*(11), 1611–1624.

10. Kwak, J. S., & Ha, M. K. (2001). Force modeling and machining characteristics of the intermittent grinding wheels. *KSME International Journal*, *15*(3), 351–356.

11. Koklu, U. (2014). Grinding with helically grooved wheels. *Proceedings of the Institution of Mechanical Engineers, Part E: Journal of Process Mechanical Engineering*, *228*(1), 33–42.

116

12. Uhlmann, E., & Hochschild, L. (2013). Tool optimization for high speed grinding. *Production Engineering*, *7*(2–3), 185–193.

13. Nakayama, K., Takagi, J., & Abe, T. (1977). Grinding wheel with helical grooves - an attempt to improve the grinding performance, *26*(1), 133–138.

14. Zheng, H. W., & Gao, H. (1994). A general thermal model for grinding with slotted or segmented wheel, *43*(l), 287–290.

15. Tawakoli, T., & Daneshi, A. (2013). New kinematic in dressing of grinding wheels. *Proceedings of the ASME 2013 Mechanical Engineering Congress and Exposition*, 15–21.

16. Silva, E. J. Da, Oliveira, J. F. G. De, Salles, B. B., Cardoso, R. S., & Reis, V. R. A. (2013). Strategies for production of parts textured by grinding using patterned wheels. *CIRP Annals - Manufacturing Technology*, *62*(1), 355–358.

17. Oliveira, J. F. G., Bottene, A. C., & França, T. V. (2010). A novel dressing technique for texturing of ground surfaces. *CIRP Annals - Manufacturing Technology*, *59*(1), 361–364.

18. Mohamed, A. M. O., Bauer, R., & Warkentin, A. (2013). Application of shallow circumferential grooved wheels to creep-feed grinding. *Journal of Materials Processing Technology*, *213*(5), 700–706.

19. Mohamed, A. M. O., Bauer, R., & Warkentin, A. (2014). A novel method for grooving and re-grooving aluminum oxide grinding wheels. *International Journal of Advanced Manufacturing Technology*, *73*(5–8), 715–725.

20. Aslan, D., & Budak, E. (2015). Surface roughness and thermo-mechanical force modeling for grinding operations with regular and circumferentially grooved wheels. *Journal of Materials Processing Technology*, *223*, 75–90.

21. Mohamed, A. M. O., Bauer, R., & Warkentin, A. (2016). Uncut chip thickness and coolant delivery effects on the performance of circumferentially grooved grinding wheels. *International Journal of Advanced Manufacturing Technology*, *85*(5–8), 1429–1438.

22. Walter, C., Komischke, T., Kuster, F., & Wegener, K. (2014). Laser-structured grinding tools - Generation of prototype patterns and performance evaluation. *Journal of Materials Processing Technology*, *214*(4), 951–961.

23. Deng, H., & He, J. (2017). A study of the grinding performance of laser micro-structured coarse-grained diamond grinding wheels. *The International Journal of Advanced Manufacturing Technology*, *93*(5–8), 1989–1997.

24. Zhang, X. H., Kang, Z. X., Li, S., Wu, Q. P., & Zhang, Z. C. (2018). Experimental investigations on the impact of different laser macro-structured diamond grinding wheels on alumina ceramic. *International Journal of Advanced Manufacturing Technology*, *96*(5–8), 1959–1969.

25. Zhang, X., Zhang, Z., Deng, Z., Li, S., Wu, Q., & Kang, Z. (2019). Precision grinding of silicon nitride ceramic with laser macro-structured diamond wheels. *Optics & Laser Technology*, *109*, 418–428.

26. Li, H. N., & Axinte, D. (2018). On the inverse design of discontinuous abrasive surface to lower friction-induced temperature in grinding: An example of engineered abrasive tools. *International Journal of Machine Tools and Manufacture*, *132*(February), 50–63.

27. Verkerk, J. (1979). Slotted wheels to avoid cracks in precision grinding. *1979 Proceedings: Sixteenth Annual Abrasive Engineering Society Conference/Exhibition*, 75–81.

28. Suto, T., Waida, T., Hosei, N., & Hideo, I. (1990). High performance creep feed grinding of difficult-to-machine materials with new-type wheels. *Japan Society of Precision Engineering*, *24*(1), 39–44.

29. Lee, K. W., Wong, P. K., & Zhang, J. H. (2000). Study on the grinding of advanced ceramics with slotted diamond wheels. *Journal of Materials Processing Technology*, *100*(1), 230–235.

30. Tawakoli, T., Westkaemper, E., & Rabiey, M. (2007). Dry grinding by special conditioning. *International Journal of Advanced Manufacturing Technology*, *33*(3–4), 419–424.

31. Stepień, P. (2007). Grinding forces in regular surface texture generation. *International Journal of Machine Tools and Manufacture*, *47*(14), 2098–2110.

32. Nguyen, T., & Zhang, L. C. (2009). Performance of a new segmented grinding wheel system. *International Journal of Machine Tools and Manufacture*, *49*(3–4), 291–296.

33. Gavas, M., Karacan, Ä., & Kaya, E. (2011). A novel method to improve surface quality in cylindrical grinding. *Experimental Techniques*, *35*(1), 26–32.

34. Denkena, B., Grove, T., & Göttsching, T. (2015). Grinding with patterned grinding wheels. *CIRP Journal of Manufacturing Science and Technology*, *8*, 12–21.

35. Denkena, B., Grove, T., Göttsching, T., da Silva, E. J., Coelho, R. T., & Filleti, R. (2015). Enhanced grinding performance by means of patterned grinding wheels. *International Journal of Advanced Manufacturing Technology*, *77*(9–12), 1935–1941.

36. Azarhoushang, B., Daneshi, A., & Lee, D. H. (2017). Evaluation of thermal damages and residual stresses in dry grinding by structured wheels. *Journal of Cleaner Production*, *142*, 1922–1930.

37. Dewar, S., Bauer, R., & Warkentin, A. (2018). Application of high-angle helical-grooved vitrified wheels to cylindrical plunge grinding. *International Journal of Advanced Manufacturing Technology*, *96*(5–8), 2443–2453.

38. Forbrigger, C., Warkentin, · Andrew, & Bauer, · Robert. (2018). Improving the performance of profile grinding wheels with helical grooves. *The International Journal of Advanced Manufacturing Technology*, *97*, 2331–2340.

39. Vesali, A., & Tawakoli, T. (2014). Study on hydrodynamic pressure in grinding contact zone considering grinding parameters and grinding wheel specifications. *Procedia CIRP*, *14*, 13–18.

40. Mohamed, A. M. O., Warkentin, A., & Bauer, R. (2017). Prediction of workpiece surface texture using circumferentially grooved grinding wheels. *International Journal of Advanced Manufacturing Technology*, *89*(1–4), 1149–1160.

41. Zahedi, A., & Azarhoushang, B. (2017). Microstructuring strategies of cBN grinding wheels. *International Journal of Advanced Manufacturing Technology*, *91*(9–12), 3925–3932.

42. Fu, Y. C., Xu, H. J., & Xu, J. H. (2002). Optimization design of grinding wheel topography for high efficiency grinding. *Journal of Materials Processing Technology*, *129*, 118–122.

43. Aurich, J. C., & Kirsch, B. (2013). Improved coolant supply through slotted grinding wheel. *CIRP Annals - Manufacturing Technology*, *62*(1), 363–366.

44. McDonald, A., Bauer, R., & Warkentin, A. (2016). Design and validation of a grinding wheel optical scanner system to repeatedly measure and characterize wheel surface topography. *Measurement: Journal of the International Measurement Confederation*, *93*, 541–551.

45. Davis, J. R. ASM International Handbook Committee (2010), *ASM Handbook, Volume 16 – Machining*, ASM International.

46. Anderson, D., Warkentin, A., & Bauer, R. (2012). Development of an experimentally validated abrasive-grain cutting model using a hybrid Euler-Lagrange finite element formulation. *Finite Elements in Analysis and Design*, *53*, 1–12.

47. Agarwal, S. (2019). On the mechanism and mechanics of wheel loading in grinding. *Journal of Manufacturing Processes*, *41*(January), 36–47.

48. Gviniashvili, V. K., Woolley, N. H., & Rowe, W. B. (2004). Useful coolant flowrate in grinding. *International Journal of Machine Tools & Manufacture*, *44*, 629–636.

49. Guo C, Malkin S (1992) Analysis of Fluid Flow Through the Grinding Zone. Journal of Engineering for Industry 114:427–434.

50. Engineer F, Guo C, Malkin S (1992) Experimental Measurement of Fluid Flow Through the Grinding Zone. ASME Journal of Engineering for Industry 114:61–66.

51. Morgan, M. N., Jackson, A. R., Wu, H., Baines-Jones, V., Batako, A., & Rowe, W. B. (2008). Optimisation of fluid application in grinding. *CIRP Annals - Manufacturing Technology*, *57*(1), 363–366.

52. Chong-Ching, C. (1997). An application of lubrication theory to predict useful flow-rate of coolants on grinding porous media. *Tribology International*, *30*(8), 575–581.

53. Vesali, A., & Tawakoli, T. (2014). Study on hydrodynamic pressure in grinding contact zone considering grinding parameters and grinding wheel specifications. *Procedia CIRP*, *14*, 13–18.

54. Hwang, Y., Ha Kim, G., Kim, Y. B., Kim, J. H., & Lee, S. K. (2016). Suppression of the inflection pattern in ultraprecision grinding through the minimization of the hydrodynamic force using a toothed wheel. *International Journal of Machine Tools and Manufacture*, *100*, 105–115.

55. Gviniashvili, V. K., Webster, J., & Rowe, W. B. (2005). Fluid flow and pressure in the grinding wheel-workpiece interface. *Journal of Manufacturing Science and Engineering, 127(1),* 198-205.

56. Kirsch, B., & Aurich, J. C. (2014). Influence of the macro-topography of grinding wheels on the cooling efficiency and the surface integrity. *Procedia CIRP*, *13*, 8–12.

57. Ebbrell, S., Woolley, N. H., Tridimas, Y. D., Allanson, D. R., & Rowe, W. B. (2000). Effects of cutting fluid application methods on the grinding process. *International Journal of Machine Tools and Manufacture*, *40*(2), 209–223.

58. Klocke, F., Baus, A., & Beck, T. (2000). Coolant induced forces in CBN high speed grinding with shoe nozzles. *CIRP Annals - Manufacturing Technology*, *49*(1), 241–244.

59. Zhao, Z., Xu, J., & Fu, Y. (2016). Study on coolant-induced hydrodynamic pressure in contact zone while deep grinding with CBN wheels. *Machining Science and Technology*, *20*(4), 547–566.